The role of cGMP/PKG1 signaling in osteogenic differentiation

Dissertation

zur

Erlangung des Doktorgrades (Dr. rer. nat.)

der

Mathematisch - Naturwissenschaftlichen Fakultät

der

Rheinischen Friedrich - Wilhelms Universität Bonn

vorgelegt von

Nadine Schall

aus Würselen

Bonn, 2021

Angefertigt mit Genehmigung der Mathematisch-Naturwissenschaftlichen Fakultät der Rheinischen Friedrich-Wilhelms-Universität Bonn.

1. Gutachter: Prof. Dr. Alexander Pfeifer

2. Gutachterin: Prof. Dr. Evi Kostenis

Tag der Promotion: 25. Januar 2022

Erscheinungsjahr: 2022

Publishment

Parts of this thesis have been published in JCI Insight.

Schall N, Garcia JJ, Kalyanaraman H, Pal China S, Lee JJ, Sah RL, Pfeifer A, Pilz RB. Protein Kinase G1 regulates bone regeneration and rescues diabetic fracture healing. *JCI Insight, 2020 May 07.* DOI: 10.1172/jci.insight.135355

ABSTRACT

Nitric oxide has important effects on bone cell function. NO stimulates cGMP synthesis, activation of protein kinase G (PKGs) and improves proliferation, differentiation, and survival of bone forming cells. In bone resorbing osteoclasts, NO regulates their differentiation and activity (effects are only partly cGMP-independent). Mice deficient in NO synthesis show severe deficiencies in bone repair, but the mechanism(s) whereby NO affects fracture healing are unknown. Mice with osteoblast-specific knockout of type 1 PKG (Prkg1 OB-KO) were generated to investigate the role of PKG in healing of a bone defect. Skeletal phenotypes in NO synthase- and PKG-deficient mice as well as NO/cGMP effects on bone remodelling were reviewed.

Prkg1 OB-KO mice have normal osteoblast and osteoclast numbers, and PKG1 deficient osteoblasts proliferate normally *in vitro*. Despite evidence of reduced osteoblast activity *in vivo*, by decreased bone formation rates and osteoblastic marker gene expression, Prkg1 OB-KO mice showed normal bone micro-architecture under basal conditions. However, bone regeneration in a mono-cortical defect model was severely reduced in Prkg1 OB-KO mice compared to control litter mates, and the knockout mice exhibit decreased capillary density and evidence of reduced BMP signaling in the region of the bone defect. Primary osteoblasts and tibiae from Prkg1 OB-KO mice contained less transcripts encoding bone morphogenic protein (BMP)-2/4, vascular endothelial growth factor (VEGF)-A, and their receptors BMPR2 and VEGFR1 than bone samples and cells from control littermates. PKG1 was required for cGMP-stimulated expression of these genes, and for BMP-induced Smad phosphorylation in osteoblasts. Since osteoblast-derived BMP-2 and VEGF are essential for fracture healing, these data suggest that PKG1 controls bone regeneration by regulating BMP and VEGF production in osteoblasts.

TABLE OF CONTENTS

INTRODUCTION

1.1 Bone biology and remodelling process

Throughout the lifespan of an organism, bone remodelling is a regulated process where old bone gets replaced via endochondral ossification through sequential osteoclastic mineralized matrix resorption and osteoblastic bone formation to maintain skeletal homeostasis and strength (Fig. 1) (1). Imbalances in bone remodelling due to accelerated bone turnover, are caused by excess bone resorption or decreased bone formation relative to resorption. The result in loss of bone mass and qualitative changes in skeletal architecture is leading to osteoporosis and an increased risk of bone fractures (2).

Bone resorption is carried out by osteoclasts, which originate from hematopoietic precursors of the monocyte/macrophage lineage (2). The dominating pathway regulating osteoclastic differentiation and function is the RANKL/OPG pathway, based on osteoblasts promoting osteoclast differentiation by receptor activated nuclear factor kappa-B ligand (RANKL) and its inhibition by osteoprotegerin (OPG) (2). New bone is formed by osteoblasts, mesenchymal cells derived from mesodermal progenitor cells, differentiated into proliferating (pre)osteoblasts and matrix-producing osteoblasts to form mature bone (2). At the end of their lifespan, osteoblasts transform into osteocytes or lining cells, embedded in the mineralized matrix. The rate of bone remodelling is regulated by networks of systemic hormones, such as estrogens and parathyroid hormone, by cytokines, such as RANKL/OPG and Wnts/sclerostin, and by small signaling molecules such as nitric oxide (NO) and prostaglandins (2, 3).

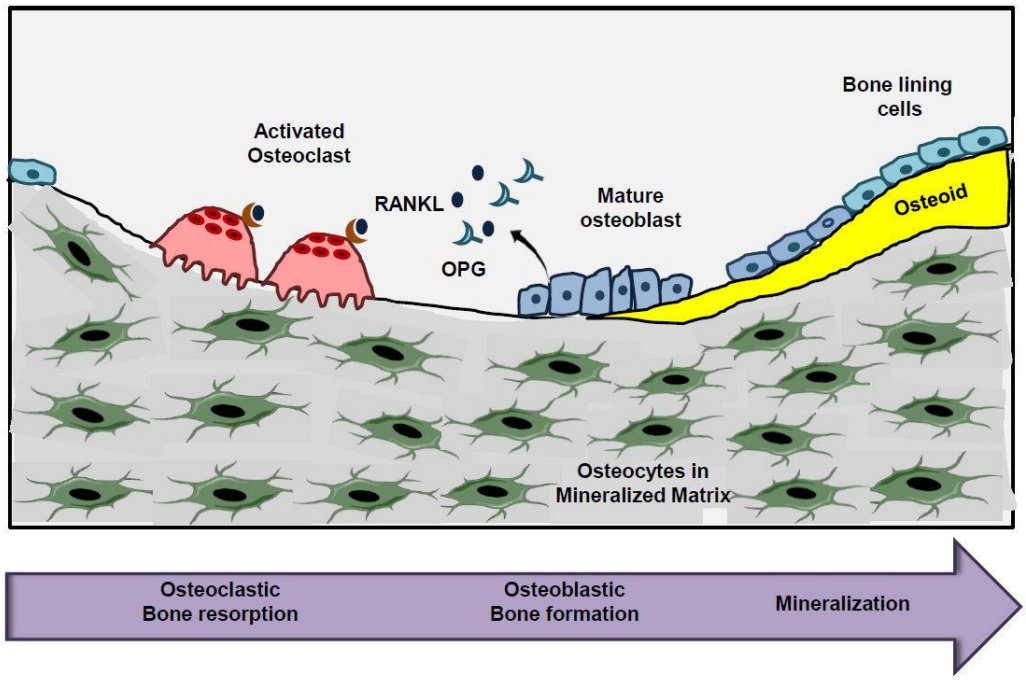

Fig. 1: Bone remodelling process by osteoblasts and osteoclasts (modified after Kalyanaraman et al. 2018, 117). Remodelling begins with the production of cytokines from osteoblasts leading to recruitment of osteoclasts attached to the endosteal bone surface. Osteoclasts resorb mineralized matrix and recruit osteoblasts to secrete extracellular matrix to form osteoid.

1.2 Osteoporosis

Osteoporosis is a major health problem – back in 2011 almost 44 million of men and women aged 50+ were affected in the U.S. (2) and according to recent statistics from the International Osteoporosis Foundation, 20 million individuals in Europe suffer from osteoporosis, with 5.3 million reported cases only in Germany and a 3-times higher prevalence in women. Osteoporosis is manifested by fractures and enhanced skeletal fragility due to loss of bone mass and strength - the osteoporosis foundation estimated an increase in fragility fracture incidence in Europe by around 25% until the year 2030 (2). Risk factors for osteoporosis include unchangeable risks (e.g. aging, sex and family history), hormone levels (e.g. sex hormone deficiency), dietary factors and lifestyle choices (e.g. decreased physical activity (2, 54).

Recent treatment options for Osteoporosis were limited to agents that reduce bone resorption, e.g. estrogens, selective estrogen receptor modules, bisphosphonates, calcitonin and denosumab. The only FDA-approved anabolic agent that stimulates bone formation is a recombinant form of human parathyroid hormone (2). Nitric oxide has anabolic and anti-resorptive effects in bone, and (pre)clinical data support an important role of NO in bone health (5, 7, 40). New bone-anabolic agents are needed that are safe for long-term use (40).

NO/cGMP/PKG signaling in metabolic bone diseases with effects on bone in human studies

The role of the NO/cGMP/PKG signaling pathway is relevant in bone diseases associated with estrogen deficiency-induced osteoporosis, hypothyroidism and type 1 diabetes. Thyroid diseases have widespread systemic manifestations including their effect on bone metabolism (e.g. low bone turnover condition) characterized by low numbers of bone cells and decreased bone formation parameters (16). Cinaciguat, a sGC activator, increases osteoblast numbers and stimulates bone formation in hypothyroid mice (16). Furthermore, the NO/cGMP/PKG pathway plays a central role in osteoporosis with low bone turnover caused by type 1 diabetes. Insulin normally has a pro-proliferative and survival promoting effect in osteoblasts (56). In type 1 diabetes, the effects of insulin deficiency lead to NOS-3 and sGC inactivation and PKG1 and 2 down-regulation in

osteoblasts (56). Here, Cinaciguat increases cGMP synthesis, restore proliferation, differentiation and survival of osteoblasts under diabetic conditions (56).

Balanced cGMP signaling is essential for normal bone development and skeletal homeostasis in adults (27). Phenotypes observed in humans are consistent with these observed in mice and can carry the following genetic alterations: (i) polymorphisms in the NOS-3 gene may be associated with a low bone volume phenotype in some populations (57, 58), (ii) loss-of-function mutations of the human GC-B gene lead to a rare form of dwarfism (35), (iii) heterozygous PKG2 deficiency is associated with severe growth restriction in humans (35, 59-61) and in contrast, (iv) gain-of-function mutations in human GC-B by constitutive activation result in bone overgrowth (26, 62).

Estrogens induce NO production in humans - plasma concentrations of stable nitric oxide derivatives correlate with estrogen concentrations in humans, are decreased in post-menopausal women and increased with estrogen supplementation (50, 51). The following positive effects of nitrates on bone were reported: (i) nitroglycerin, was shown to be effective in preventing bone loss in young women after ovariectomy (52) and (ii) isosorbide mononitrate treatment in post-menopausal women with established osteoporosis, showed improvement in bone mineral density as compared to bisphosphonates (53). However, organic nitrates are suboptimal NO donors, because of tolerance development and oxidative stress (47, 48). Estrogen-deficiency and aging cause excess oxidative stress, which may affect NO bioavailability (54). A newer NO-independent sGC activator, Cinaciguat, may represent a new paradigm for the treatment of osteoporosis (40, 55).

1.3 NO/cGMP/PKG signaling cascade

Nitric oxide is synthesized in response to estrogen treatment by nitric oxide synthase (NOS), which oxidizes a guanidine nitrogen of L-arginine. Soluble guanylyl cyclase (sGC) is produced by the enzyme NOS and can be stimulated by cinaciguat independently of NO (40). The activation of PKG (cGMP-dependent protein kinase) by cGMP mediates its action to phosphorylate multiple target proteins with direct impact on bone formation (e.g. stimulate genes associated with osteoblast differentiation, promote survival of osteoblasts and osteocytes).

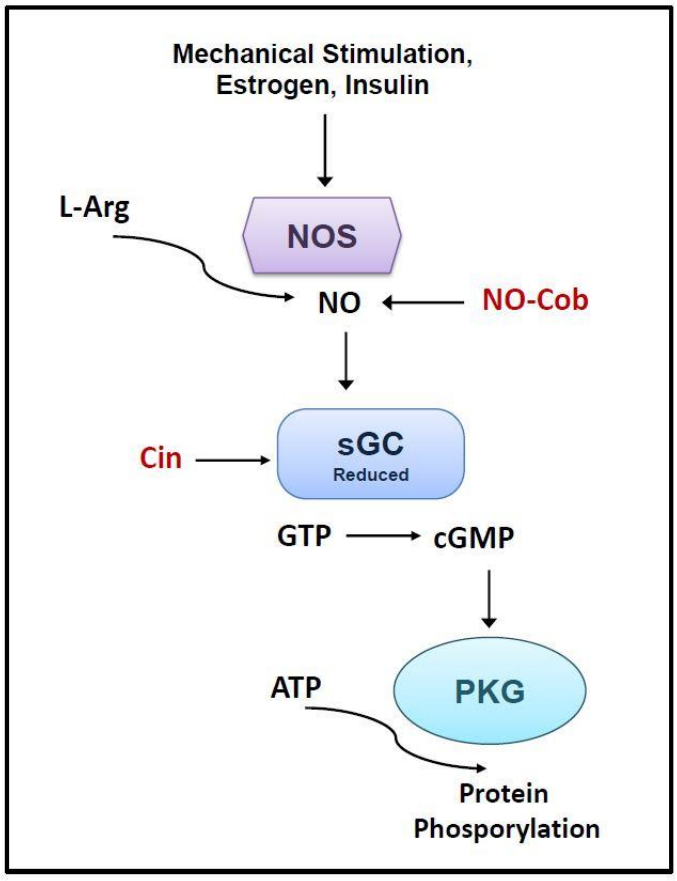

Fig. 2: NO/cGMP/PKG pathway in bone (modified after Joshua et al. 2014, 40). NO is generated from arginine via NO synthases. NO-Cob, nitrosyl-cobinamide; Cin, cinaciguat.

NO synthases expression and bone phenotypes

Three forms of NO synthase (NOS) have been identified in bone, in isolated osteoblasts and osteoclasts: endothelial (eNOS or NOS-3), neuronal (nNOS or NOS-1) and inducible (iNOS or NOS-2) (8, 9, 11). Estrogens stimulate NOS-3 activity and mRNA levels in endothelial cells and osteoblasts, associated with an increase in intracellular calcium and Akt phosphorylation of NOS-3, raising the possibility that NO derived from the NOS-3 pathway plays a role in mediating the effect of sex hormones in bone (13, 14, 15).

NOS knockout mice have been used to examine the role of NO in bone homeostasis. Mice with NOS-1 deficiency exhibit increased bone mass with decreased osteoclast and osteoblast numbers *in vivo*. However, *in vitro* assays have shown that more osteoclasts are formed, suggesting a non-cell-autonomous mechanism (17). NOS-2-deficient mice have no obvious bone abnormalities, with normal bone formation rate, and osteoclast surface area (19). NOS-3-deficient mice demonstrate decreased bone mass due to reduced osteoblast activity and decreased mineralisation causing abnormal prenatal and postnatal bone development (e.g. fetal growth restriction, limb malformations, reduced longitudinal bone growth and increased perinatal death) (20, 21). Together, murine models that globally lack NOS isoforms exhibit contrasting bone phenotypes.

Cyclic GMP targets in bone: PKG1 and 2

Two important cGMP effector proteins in bone are cGMP-dependent protein kinases, PKG1 and PKG2. The PRKG1 gene on human chromosome 10 encodes the soluble two isoforms (PKG1α and 1β), which are generated by alternative transcript splicing of the first exon. The membrane-bound isoform, PKG2 is located on a separate gene on human chromosome 4. Isoforms PKG1α and 1β have identical cGMP-binding and catalytic domains, but differ in their N-terminal domain which mediates their dimerization and kinase enzyme activity (28). (Pre)osteoblasts and osteocytes express both PKG1 isoforms and PKG2 including different functions: (i) pro-proliferative effects of cGMP in osteoblasts require PKG2 activation of Src and Erk-1/2 and (ii) anti-apoptotic effects of cGMP in osteocytes are mediated by PKG1α and PKG2 via various mechanisms (Fig. 3) (12, 15, 29). Osteoclasts express primarily PKG1α and 1β (30, 31).

Mice globally deficient in PKG1 have a short life span due to severe gastrointestinal motility dysfunction and growth retardation due to malnutrition (32). PKG1 knockout mice with smooth muscle-specific re-expression of either PKG1α or 1β have improved life expectancy (33). Globally deficient PKG2 mice develop dwarfism caused by severe defects in endochondral ossification at the growth plates (34).

NO/cGMP effects in cells of osteoblastic lineage and in osteoclasts

Nitric oxide appears to have dose-dependent effects on osteoblast activity. Low concentrations of NO promote proliferation, differentiation, and survival, while high NO concentrations have inhibitory effects (22, 36). Positive effects of low NO doses on osteoblast proliferation as well as anti-apoptotic effects in bone marrow stromal cells are mediated by cGMP and require either PKG1 or PKG2 (22, 29). Low doses of NO donors improve osteogenic differentiation, by stimulating mRNA expression of osteoblastic genes and increasing bone matrix synthesis (23, 38, 39). These NO effects are prevented by pharmacological inhibition, imitated by cell-permeable cGMP analogs or NO-independent stimulators of sGC, suggesting that NO works via cGMP (25, 40). In summary, NO activation affects the osteoblastic lineage at all differential stages (Fig. 3).

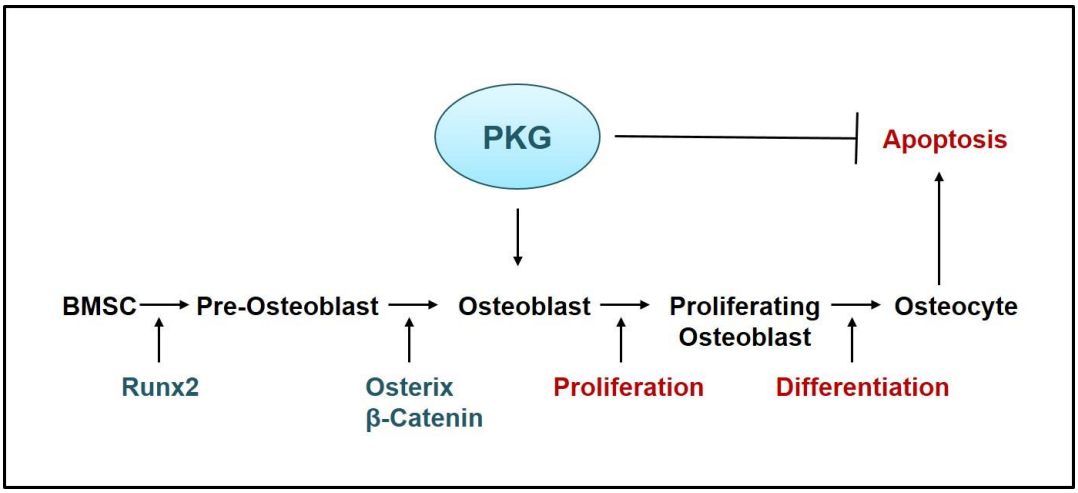

Fig. 3: NO/cGMP regulation of osteoblastic cells (modified after Kalyanaraman et al. 2018, 117). After cGMP-dependent protein kinases activation via NO/cGMP - PKG regulates different stages in the osteoblastic lineage, promotes proliferation and differentiation, and inhibits apoptosis.

Effects of NO concentrations are similar in osteoclasts - low levels of NO promote, while high levels inhibit osteoclast differentiation and survival (17, 22). Mice with NOS-1 deficiency have decreased osteoclast numbers and bone resorption surfaces confirmed by poorly-functioning osteoclasts *in vitro* (17, 18). RANKL induces NOS-2 expression in osteoclasts with high NO concentrations leading to inhibition of osteoclastic differentiation and bone resorption (Fig. 4) (10). NO stimulates detachment of osteoclasts via PKG1 phosphorylation of the vasodilator-stimulated protein (VASP) and the inositol-1,4,5-triphosphate receptor-associated protein (IRAG) and downregulates their acid secretion (Fig. 4) (24, 30, 31). The effects of NO and cGMP on osteoclast differentiation and function are mostly inhibitory.

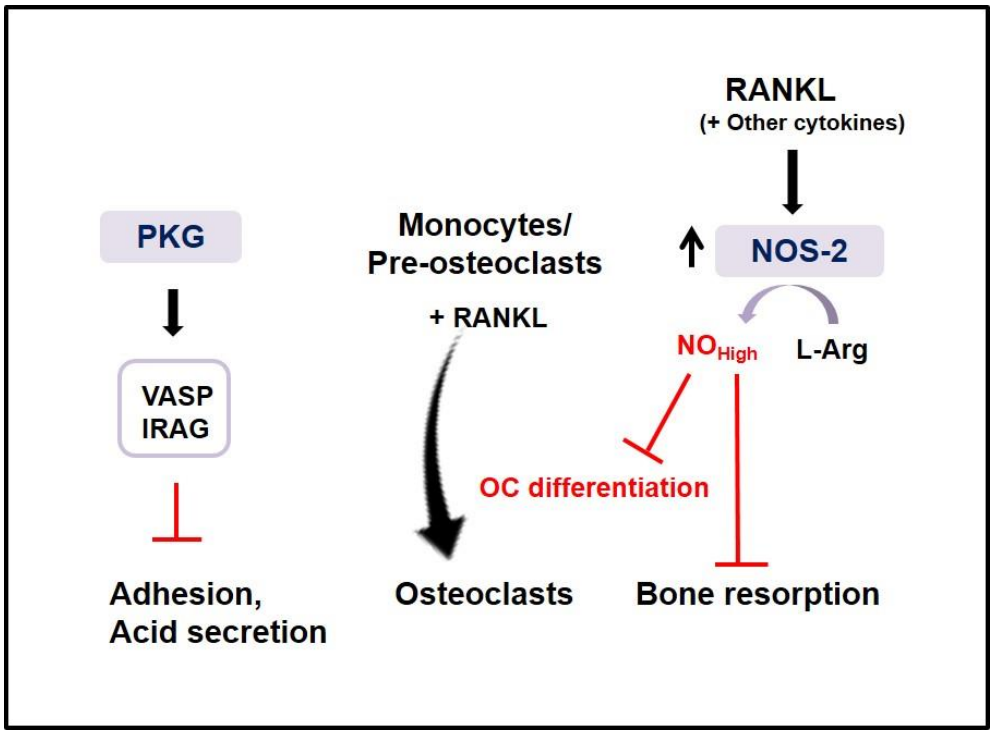

Fig. 4: NO/cGMP regulation of osteoclasts (modified after Ramdani et al. 2018, 89). RANKL induces NOS-2 expression in osteoclasts with high NO concentrations, leading to inhibition of osteoclast differentiation. NO/cGMP signaling via PKG activation downregulates osteoclast adhesion and acid secretion, whereby bone resorption is inhibited.

NO/cGMP effects on bone formation and resorption *in vivo*

The defects in endochondral bone formation of NOS-3-deficient mice suggest that NOS-3-derived NO is important for osteoblast differentiation and function *in vivo* (21). Administration of the NOS inhibitor, L-NAME, leads to a significant decrease in bone metabolism with suppression of bone formation, suggesting that basal NO production is required for skeletal homeostasis (41). In contrast, administration of the NO donor, nitrosyl-cobinamide (NO-Cbi), increases bone formation rates and bone mineral density (22). Administration of sGC-stimulants increase bone turnover including bone formation and resorption with increased numbers of osteoblasts and osteoclasts (42), whereas administration of the sGC activator cinaciguat, is lacking a significant influence on osteoclast numbers (40).

NO/sGC signaling is a major regulator in blood vessel growth and angiogenesis plays an important role in endochondral ossification and bone repair. NO-donors and cGMP-inhibitors improve fracture healing and bone regeneration in rodents (43).

1.4 Animal models

Bone fracture repair –NO/cGMP interaction in defect models

Facture healing is characterized by overlapping stages: an inflammation phase, soft callus phase, cartilage turnover phase, and bone remodelling phase (66). Fractures normally heal by the combination of both intramembranous and endochondral ossification (63). Fracture repair starts with the formation of a hematoma after an injury with generation of growth factors and cytokines. The inflammatory response is necessary for mesenchymal stem cell recruitment, cell proliferation, initiation of chondrogenesis, followed by vascular growth and neo-angiogenesis (63, 65). Cells differentiate into chondrocytes to form cartilage, which mineralizes and mechanically stabilizes the fracture site, and is later removed by osteoclasts and replaced by osteoblasts to form new bone. The biological processes driving these stages are regulated by the following cell signaling molecules: (i) pro-inflammatory cytokines, (ii) transforming growth factor-beta superfamily (TGF-β) members, and (iii) angiogenic factors (63). Interleukins-1 and 6 (IL-1 and IL-6) play a role in initiating the repair cascade. Tumor-derived growth factor (TGF-β) and bone morphogenic protein (BMP-2) expression increase to initiate callus formation (67). The transition from cartilage to bone is associated with increased angiogenesis and requires vascular endothelial growth factor (VEGF) produced by osteoblasts (66). Growth factors most important for fracture healing include Wnts, BMPs, and VEGF. Osteoblast production of these factors is increased by cGMP, and signaling downstream of the corresponding receptors involves NO/cGMP directly or indirectly, through positive cross-talk with NO/cGMP/PKG (4).

Importance of NO/cGMP signaling for normal fracture healing was shown by a study using a different NO donor (chitosan-NONOate), indicating improved fracture healing in normal rats (30% increase in callus cross-sectional area), while inhibition of NO synthase with L-NAME severely impaired fracture healing (43). In addition, experiments in transgenic mice with increased production of C-type natriuretic peptide using an open transverse femur fracture healing model showed increased bone remodelling and accelerated fracture healing (70).

NO/cGMP effects in estrogen-deficient rodents

Ovariectomy-induced estrogen deficiency in rodents results in significant bone loss with changes in bone architecture and turnover including increased bone resorption, inadequate bone formation response, and enhanced osteocyte apoptosis (44). Estrogens promote bone health by increasing osteoblast and osteocyte survival via NO/cGMP-dependent phosphorylation of BAD (directly by PKG1) and activation of Erk and Akt (indirectly by PKG2) (14, 15).

Bone formation induced by high doses of estrogens, requiring NOS-3 coupled estrogen membrane receptor activation, is blocked by administration of the NOS inhibitor L-NAME (45), while NO-generating agents can partially replace bone protective effects *in vivo* (22). Treatment of ovariectomized rats with nitroglycerin prevents loss of bone mineral density and improves mechanical bone properties (46). Novel NO donors, like Nitrosy-cobinamide (NO-Cbi), circumvent the problem of organic nitrate limitations in tolerance development and oxidative stress induction, and release NO directly (49). NO-Cbi increases trabecular bone mass in intact and ovariectomized mice, increases intracellular cGMP concentrations, proliferation, and osteoblastic gene expression, prevents the ovariectomy- induced increase in osteoclasts (partly cGMP-dependent) and protects cells from apoptosis (22). Treatment of ovariectomized mice with the NO-independent sGC activator cinaciguat improves trabecular bone microarchitecture and enhances osteocyte survival similar to estrogen replacement therapy (40). However, compared to 17β-estradiol or NO-Cbi, cinaciguat has a lower effect on osteoclasts (22, 40). In summary, the bone protective effects of NO appear to be mediated by cGMP with NO donors and sGC activators showing anabolic effects in (pre)clinical models of estrogen-deficiency osteoporosis.

1.5 Aim of PhD thesis

The overall goal of this study was to investigate the role of PKG1 in osteogenesis under physiological and pathophysiological conditions *in vitro* and *in vivo*. Preliminary data (generated in the group of A. Pfeifer, Bonn) indicated that the osteogenic differentiation of murine cells can be modulated by cGMP/PKG1 *in vitro*. Thus, detailed analysis of the exact role of cGMP/PKG1 in osteogenic differentiation of MSCs and primary osteoblasts was supposed to help in better understanding of PKG1 function during development as well as in disease.

The aim of this project is to elucidate the exact role of PKG1 in osteoblast differentiation and function. Using *in vitro* and *in vivo* models, this work will investigate cellular mechanisms of actions, signal transduction and interactions among key factors regulating bone metabolism. The exact role of PKG1 for bone development and regeneration *in vivo* has never been investigated due to severity of the phenotype of global PKG1 knockout mice. Therefore, the use of a novel mice model with an osteoblast specific deletion of PKG1 was one important goal of this study. This work will investigate whether cGMP signaling modulation in disease models (e.g. Tibial monocortical defect mice model) could lead to developing novel treatments in regenerative medicine.

MATERIALS AND METHODS

2.1 Chemicals and Kits

Antibodies against PKG1, Smad 1/5/8 (pSer 463/465/426/428), Smad 1/5/9 (pSer 463/465/467), SAPK/JNK (pThr183 /pTyr185), CD-31 (PECAM-1), and cleaved caspase-3 were from Cell Signaling Technology (Danvers, MA). Antibodies against BMP-2/ BMP-4, α-tubulin and β-actin were from Santa Cruz Biotechnology (Santa Cruz, CA). Antibodies against PKG2 and FITC-labelled secondary antibodies were from Invitrogen (Carlsbad, CA).

Bromodeoxyuridine (BrdU), deoxyribonuclease 1 (DNase 1), hydrogen peroxide solution (H_2O_2), anti-BrdU antibody, acid phosphatase, leucocyte (TRAP) kit and the soluble guanylyl cyclase (sGC) activator cinaciguat (BAY 58-2667) was from Sigma. The cyclic GMP agonist 8-(4-chlorophenylthio)-cGMP (8-pCPT-cGMP) was from BioLog, Inc., Bremen, Germany. Recombinant human BMP-2 (Bone morphogenetic protein 2) was from HumanZyme Inc., USA. Alizarin red S staining kit was from ScienCell, Research Laboratories, Inc.

2.2 *In vitro* Experiments

Culture of murine primary osteoblasts (mPOBs)

POBs were isolated from the femurs and tibiae of 8-12 week-old Prkg1 fl/fl (Prkg1 Control) and Prkg1 OB-KO mice, and were grown in Dulbecco's modified Eagle's medium (DMEM, 25 mM glucose) supplemented with 10% fetal bovine serum (FBS). Briefly, bones were transferred into a petri dish with sterile PBS, soft tissues were removed and the cleaned bone was chopped into small fragments of approximately 1-2 mm^2. Fragments were incubated in a two-step 0.5% Worthington Collagenase 2 in PBS solution first for 10 min. and second for 1 hour at 37°C in a shaking water bath. Bone pieces were rinsed three times in PBS and transferred to 100-mm diameter dishes. On average the cell monolayer growing from the bone fragments reached confluency after 13-15 days, upon which the monolayer was trypsinized by incubating the cells with 0.5 ml 0.25% trypsin/ 0.02% EDTA solution at 37°C for 3-5 min (12, 22, 40, 89). Each batch of POBs was tested for their ability to mineralize; cells were used at passages 1-5. To delete exon 2 of Prkg1, cells from Prkg1 fl/fl mice were infected with adenovirus encoding Cre recombinase (or control virus, GFP) at an MOI of 10 and were used 48 hours later. In some cases, confluent mPOB cultures were induced to differentiate using 50 μg/mL (0.3 mM) L-ascorbic acid (AA) and 10 mM β-glycerophosphate (ß-GP); experimental drugs were added when cells were switched to differentiation medium, and medium with drugs was changed twice a week (40, 89). Alkaline phosphatase (ALP) activity was assessed after 14 days by colorimetric assay (16).

For alkaline phosphatase staining, cells were fixed with 3.7% formaldehyde in PBS and washed two times with PBS. Cells were stained using the staining solution for 30 min. in the dark. The reaction was stopped using the stop solution and photomicrographs were scanned using a commercial scanner in 48-bit colour and 600 dpi resolution. Staining Solution: 0.1 M Tris pH 9.5, 100 mM NaCl, 50 mM MgCl2, 0.6 mM NBT, 0.6 mM 5-Bromo- 4-Chloro-3-Indolyl Phosphate (BCIP), Stop Solution: 10 mM Tris HCl (pH 8.0) 1 mM EDTA) (Promocell).

Bone marrow stromal cell (BMSC) cultures

Primary bone marrow mononuclear cells were collected by flushing marrow from femoral and tibial bones of 8-12 week-old Prkg1 fl/fl (Prkg1 Control) and Prkg1 OB-KO mice, red blood cells were lysed in 155 mM NH_4Cl, 12 mM $NaHCO_3$, and 0.1 mM EDTA, and cells were plated at 4 x 10^5 cells/cm^2 in 12-well dishes in Dulbecco's modified Eagle's medium containing 10% FBS and 10% horse serum with 100-U/mL penicillin and 100 µg/mL streptomycin (40). After seven days, when adherent cells were still at low density, the medium was switched to α-MEM supplemented with 0.3 mM ascorbate, 10 mM β-glycerophosphate and 10 nM Dexamethasone to induce differentiation. Two or three weeks later, Alkaline phosphatase and Alizarin Red staining was performed, respectively, and stained area per well was quantified by ImageJ (40). Alkaline phosphatase staining was performed as described above.

For alizarin red staining, cells were fixed with 3.7% formaldehyde in PBS for 15 min. at room temperature and washed three times with diH_2O. Cells were stained using 1 ml of 2% Alizarin red S Stain solution for 30 min. The reaction was stopped by removing the dye, washing with diH_2O and photomicrographs were scanned using a commercial scanner in 48-bit colour and 600 dpi resolution. Alizarin Red S staining kit was purchased from ScienCell, Research Laboratories, Inc.

Mouse C57BL/6 calvaria osteoblast precursor (MC3T3-E1) cultures

Murine MC3T3-E1 (osteoblastic cells with high differentiation potential, clone 4, hereafter referred to as MC3T3 cells) were from American Tissue Culture Collection. MC3T3 cells were maintained in ascorbate-free-Minimal Essential Medium (MEM) supplemented with 10% FBS (Fetal Bovine Serum). Cells were grown in 100-mm diameter dishes and passaged 1:6 twice a week (12). Cells were simulated with different concentrations of BMP-2 (1 nM, 10 nM and 30 nM) for 48 hours.

Immunofluorescence Staining and Bromodeoxyuridine (BrdU) Incorporation

POBs isolated from Prkg1 Control (Prkg1 fl/fl) or Prkg1 OB-KO mice were plated on glass coverslips in 24 well dishes. Cells were transferred to medium containing 0.1%

BSA, and incubated in the absence or presence of 8-pCPT-cGMP for 24 hours. Cells were fixed in 3.7% paraformaldehyde in PBS for 10 min., permeabilized with 0.5% Triton-X-100 in PBS for 8 min., blocked with 2% BSA in PBS for 1 hour, and incubated with cleaved caspase-3-specific antibody (at 1:100 dilution) overnight at 4°C, followed by secondary antibody conjugated to anti-rabbit FITC (at 1:100 dilution) in 2% BSA in PBS for 1 hour (89). Nuclei were counterstained with 1 mg/ml Hoechst 33342 for 3 min., and images were analyzed with a Keyence BZ-X700 fluorescence microscope (89).

Murine primary osteoblasts were plated on glass coverslips. Cells were serum-starved in 0.5% FBS, followed by treatment with cGMP or 20% FBS for 1 h and 200 μM bromodeoxyuridine (BrdU) was added in fresh medium containing 0.5% FBS for 18 h (40). Cells were fixed and permeabilized with 3.7% formaldehyde and 0.5% Triton X-100 respectively. The cells were incubated in deoxyribonuclease I (DNase I, Sigma), blocked with 2% BSA, before staining with anti-BrdU antibody (at 1:100 dilution) and Hoechst 33342 (40). Cells were visualized with a Keyence BZ-X700 fluorescence microscope and analysed with Photoshop (Adobe). The percentage of cells staining positive for cleaved caspase-3 and BrdU were counted with >200 cells per condition (40, 89). Identical software settings were used for image acquisition of all samples in a given experiment (40).

RNA Isolation, cDNA Synthesis and Quantitative RT-qPCR

RNA was extracted using TriReagent™ (Molecular Research Center, Inc.). Briefly, RNA was extracted using 0.1 ml bromochloropropane for 10 min. RNA was precipitated by transferring the aqueous phase to a clean tube and adding 0.5 ml isopropanol for 8 min. After washing the pellet in 1 ml 75% ethanol, the pellet was air-dried for 15 min., dissolved in diH_2O and incubated at 56°C for 10 min.

1 μg of total RNA was reverse-transcribed and cDNA was synthesized using the iScript cDNA Synthesis Kit (BioRad) according to the manufacturer's instructions. PCR conditions were 30 s of denaturation at 95 ˚C, 45 s of annealing at 60 ˚C, and 1 s extension at 72 ˚C for 40 cycles (12). Quantitative RT-PCR was performed using an MX3000 real time PCR detection system (Stratagene) and Brilliant II SYBR® Green QPCR Master Mix (Agilent Technologies). Melting curves after 40 cycles confirmed a single PCR product for each primer pair. Relative changes in mRNA expression were analyzed using

the 2–ΔΔ*Ct* method, with 18S and *Hprt1* serving as an internal reference to correct for differences in RNA extraction or reverse transcription efficiencies (12, 40). Primer sequences are described in Table 1, Appendix – List of Tables.

Preparation of bone cell extracts and Western blot analysis

Protein extracts were prepared from mPOBs of Prkg1 fl/fl (Control) and Prkg1 OB-KO mice. Same cell numbers were plated in 12-well dishes and treated as indicated in results. Briefly, media was removed and cells were lyzed in 100 µl 95°C hot 1x SDS-Sample Buffer (SB) with 2-mercaptoethanol, sonicated, and boiled at 95°C for 5 min. prior to loading of 40 µl cell extract per sample (12). Whole cell lysates were separated by 10% sodium dodecyl sulfate-polyacrylamide gel electrophoresis (SDS-PAGE). After transfer, polyvinylidene difluoride (PVDF) membranes were blocked with 5% milk in Tris buffered saline containing 0.1% Tween 20 (TBST) and incubated with primary antibody, e.g. protein kinase G1 (1:2000), phosphor-JNK and phosphor-Smad1/5/8 (1:1000 dilution) followed by Horseradish peroxidase-conjugated secondary antibodies, e.g. anti-rabbit (all 1:5000 dilution). Enhanced chemiluminescence (LI-COR Biosciences) with a 700 nm - and 800 nm channel were used to generate western blots. Images were analyzed using ImageJ software.

Statistical Analysis

Graph Pad Prism 5 was used for two-tailed Student t-test (to compare two groups) or one-way ANOVA with Bonferroni post-test selected comparisons analysis against the control group (to compare more than two groups); A p value <0.05 was considered statistically significant. Bar graphs represent mean ± SEM of three independent experiments unless stated otherwise.

2.3 *In vivo* Experiments

Animal experiments

All experiments involving the genetically-modified mice and their wild type littermates were approved by the Institutional Animal Care and Use Committee of the University of California, San Diego, and mice were maintained in accordance with the Guide for the Care and Use of Laboratory Animals (2011, 8th ed, Washington, DC: National Research Council, National Academies Press). Mice were housed at 3 to 5 animals per cage in a temperature controlled environment with a 12 hour light/dark cycle and *ad libitum* access to food and water; they were fed standard Teklad Rodent Diet (Teklad #8604) (113). For the analysis of the basal phenotype, 8 week-old Prkg1 fl/fl (Control) and Prkg1 OB-KO males and females and for the bone regeneration experiments 10 week-old control and knockout mice were used.

Generation of osteoblast-specific PKG1 knockout mice

Mice carrying floxed Prkg1 alleles (Prkg1 fl/fl) were generated and provided from Prof. Alexander Pfeifer, Institute of Pharmacology and Toxicology, University Bonn, Germany. Briefly, to obtain Prkg1 fl/fl mice, a 400-base-pair-DNA fragment from the 5` region of the mouse Prkg1 complementary DNA was used to isolate genomic DNA from a 129sv cosmid library. The Prkg1-construct consisted of the 2.3-kb left arm, a single loxP site, a 0.9-kb genomic fragment, a neo-tk cassette flanked by loxP sites, and a 7.8-kb right arm (72). The osteoblast specific Prkg1 knockout mice were made by breeding floxed-Prkg1 mice that carry loxP sequences flanking exon 2 with transgenic mice (Col1a1-Cre) expressing Cre recombinase under the control of a 2.3-kb Collagen type 1, alpha 1 [Col1a1] promoter (B6.Cg-Tg(Col1a1-cre) Haak mice, RIKEN BioResource Research Center Jackson Laboratories, Japan) (113). To generate Prkg1 OB-KO mice, hemizygous Col1a1-Cre transgenic mice were crossed with Prkg1 fl/fl mice to produce heterozygous Prkg1 fl/+ offspring carrying a Cre allele (1. Generation). These mice were then crossed with Prkg1 fl/fl mice generating the following 3 genotypes: Prkg1 OB-KO, Prkg1 fl/+ Col1a1-Cre, and Prkg1 fl/fl (2. Generation). Littermates not expressing the Cre recombinase served as controls.

Genotyping and determination of tissue-specific deletion of the PKG1 gene

Genomic DNA was extracted from tail snips and other tissues (bone, kidney, lung and brain) of Prkg1 Control and Prkg1 OB-KO mice using DNeasy Blood and Tissue Kit (Qiagen, Valencia, CA, USA) for purification and KOD Hot Start PCR Kit for amplification (EMD Millipore Novagen, USA). Polymerase chain reaction (PCR) analyses of the DNA from tail snips were performed to detect floxed-Prkg1 alleles using corresponding primer sets with standard conditions (2 min at 95°C; 30 s at 94°C, 30 s at 55°C, and 30 s at 72°C for 40 cycles; 10 min at 72°C; end at 4°C). The flox allele was amplified to generate a 340-bp fragment compared with 244 bp for the wildtype allele using the following primers: 5′-GTGAAAATACTACTAGGTATCATGG-3′ (forward) and 5′-CATGTAGTAAACATTAAGGGTAGAG-3′ (reverse). The Cre transgene was detected by PCR using the primers 5′-ATCCGAAAAGAAAACGTTGA-3′ (forward) and 5′-ATCCAGGTTACGGATATAGT-3′ (reverse) with standard conditions (3 min at 94°C; 45 s at 94°C, 30 s at 56°C, and 90 s at 72°C for 40 cycles; 10 min at 72°C; end at 4°C) to amplify a 650-bp DNA product. The other primers were specific for the deleted exon 2 allele of genomic DNA in tissues (bone, kidney, lung and brain) to show homologous recombination. The deleted exon 2 allele was detected by PCR (2 min at 95°C; 10 s at 98°C, 30 s at 56°C for 40 cycles; 2 min at 68°C) using primers outside of the 5’ and 3’ arms: 5′-CAACAGAAGCAAGACACTCAG-3′ (forward) and 5′-GCAAGTGACTAAAAACATCACC-3′ (reverse), to amplify a 550-bp fragment after homologous recombination.

Tibial monocortical defect model

The tibial monocortical defect model used is a simplified stable fracture model, described previously (66, 73). Prkg1 fl/fl (Control) and Prkg1 OB-KO male and female mice at the age of 10 weeks were used for all experiments. Mice were placed under general anesthesia by intraperitoneal (i.p.) injection of 100 mg/kg ketamine and 10 mg/kg xylazine. The lateral aspect of the right tibia was exposed and carefully cleared of overlying soft tissues while preserving the periosteum (66). A monocortical osseous hole (0.8 mm diameter) was created on the anterior surface of the tibia crest using a round burr

attached to a dental drill (5000 rpm). Irrigation with saline was used to remove bone dust and fragments (66). The soft-tissue wound was closed by separately suturing the muscle and skin layers with 4-0 absorbable gut suture. After surgery, mice received subcutaneous (s.c.) injection of 0.05–0.1 mg/kg buprenorphine for 72 h for analgesia (66).

For monocortical tibial defect model experiments, a) 10 week-old wild-type and transgenic males and females and b) 10 week-old females were used and randomly divided into four groups: group 1 (Prkg1 fl/fl, n=6) and group 2 (Prkg1 OB-KO, n=5) received i.p. injections of vehicle (0.1% DMSO in 0.9% NaCl), whereas group 3 (Prkg1 fl/fl, n=6) and group 4 (Prkg1 OB-KO, n=6) were injected with Cinaciguat (10 µg/kg/day in 0.1% DMSO in 0.9% NaCl) starting one day after surgery for 8 consecutive days, all groups underwent monocortical tibial defect operation.

Fluorescent labelling for bone formation detection

Alizarin red complexone and Calcein green were used for the detection of the bone formation rate. Fluorescent dyes bind calcium in the blood and are incorporated into newly formed bone. Labelling was performed by i.p. injection of alizarin red complexone (50 mg/kg) and calcein green (25 mg/kg) at 7 and 2 d (for 8 week-old and 10 week-old mice) before euthanasia. Mice were euthanized at 8 weeks of age (basal phenotype analysis) or 12 weeks of age (monocortical tibial defect model) by CO_2 intoxication and exsanguination, and femoral and tibial bones were dissected for qRT-PCR, histology, and micro–computed tomography (micro-CT) analyses.

Gene expression analysis

Immediately after euthanasia, mice were placed on ice, and their femurs and tibiae were removed and dissected from other tissues. After flushing out bone marrow cells with ice-cold PBS, the bone shafts were flash frozen in dry ice, pulverized in liquid nitrogen using a precooled mortar and pestle, and the powder was dissolved in TRIzol reagent (Molecular Research Center, Inc) to isolate total RNA (40). One microgram of total RNA was reverse transcribed, and quantitative PCR was performed using an MX3005P real-time PCR detection system (Stratagene) with Brilliant II SYBR® Green QPCR Master Mix (Agilent Technologies) (37). PCR conditions were a) 30 s of denaturation at 95 ˚C,

45 s of annealing at 60 ˚C, and 1 s extension at 72 ˚C for 40 cycles or b) 30 s of denaturation at 95 ˚C, 30 s of annealing at 55 ˚C, and 45 s extension at 72 ˚C for 40 cycles (12). Melting curves after 40 cycles confirmed a single PCR product for each primer pair. Primer sequences are described in Table 1, Appendix - List of Tables. Relative changes in mRNA expression were analyzed using the $2^{-\Delta\Delta Ct}$ method, with hypoxanthine phosphoribosyltransferase 1 (*Hprt1*) or 18S rRNA serving as an internal reference (22, 40). The threshold cycle (Ct) indicates the cycle number at which the amount of amplified target reaches a fixed threshold.

Bone histomorphometry (static and dynamic bone formation analyses)

For static bone formation analyses, tibiae of 8 week-old Prkg1 Control and Prkg1 OB-KO mice (basal phenotype analyses) were fixed in 70% Ethanol, dehydrated in graded concentrations of ethanol and xylene, embedded in methyl-methacrylate without decalcification (40, 113) and sectioned at the University of Alabama, Birmingham, Center for Metabolic Bone Disease. Some sections were stained with Masson's trichrome for static histomorphometry. Histomorphometric measurements of trabecular bone were performed between 0.25 and 1.25 mm distal to the growth plate excluding the cortex as described (22, 40). Osteoblast and osteoclast numbers were counted on trabecular surfaces and were expressed as 2-dimensional parameters per millimeter of bone perimeter (B.Pm), as recommended by the American Society for Bone and Mineral Research Histomorphometry Nomenclature Committee (74).

Tibia of 12 week-old Prkg1 Control and Prkg1 OB-KO mice (regeneration model, bones with defect) were fixed overnight in 70% Ethanol, decalcified in 0.5 M EDTA (pH 8.0) for 7 days (113), embedded in paraffin blocks, sagittal sectioned and stained with Masson´s trichrome at the University of San Diego, Moores Histology & Sanford Consortium Histology. Briefly, the samples were de-paraffinized in xylene and rehydrated in graded ethanol and water before staining in the following solutions: Bouins Solution overnight at room temperature, Weigert's Iron Hematoxylin for 10 min., Biebrich Scarlet-Acid Fushion for 5 min., Phosphotungstic-Phosphomolybdic Acid for 5 min., Aniline Blue for 5 min. and 1% Acetic Acid for 2 min. Finally, samples were dehydrated in ethanol and xylene before mounting with coverslips. Nuclei will be stained in black, cytoplasm in red, muscle fibers in red and collagen in blue. An area of 200 µm

x 500 µm between the two cortical bone ends (CB) was analysed (a 0.1 mm^2 "region of interest" marked by the black rectangle) (113). Collagen content (hole region stained by Aniline blue divided by the whole region of interest in %) was measured using Nanozoomer Digital Pathology NDP.view2 software (40).

For dynamic bone formation analyses, left tibiae of 12 week-old Prkg1 Control and Prkg1 OB-KO mice (regeneration model, bones without defect) were fixed in 10% neutral buffered formalin for 24 hours at room temperature and transferred to 70% Ethanol for storage until further processing. Bones were placed in histology cassettes into a container containing 500 ml of 5-10% aqueous potassium hydroxide and incubated for 96 hours at room temperature with gentle shaking (40 rpm) on an orbital shaker (75, 113). Next, the bones were rinsed by running tap water for 15 min. and kept in 50% Ethanol until further processing. Samples were dehydrated in graded concentrations of ethanol and xylene, embedded in paraffin blocks and sagittal sectioned at the University of San Diego, Moores Histology & Sanford Consortium Histology. Once the entire surface of the bone was exposed the block is placed face down into a petridish containing 1% aqueous potassium hydroxide for 5-10 min. on a cold plate (75). Final sections, about 6-8 consecutive full bone sections were taken at 4 microns, placed on a charged slide and dried at 56°C (75). Unstained sections, cut parallel to the sagittal plane, were used for assessing fluorochrome labeling. Total bone surface (BS), percentage of osteoid surface (OS), percentage of single- and double-labeled BSs, and the double-calcein interlabel width were measured at endocortical surfaces (22, 40). The limited number of trabeculae after potassium hydroxide treatment prevented meaningful measure of osteoid or calcein label on trabecular surfaces. Mineralizing surface (MS) ([double-labeled BS + 1/2 single-labeled BS]/BS), mineral apposition rate (MAR) (interlabel width/labeling period), and bone formation rate (BFR) (MS × MAR) were calculated according to standard protocols (74). Slides were scanned with a Hamamatsu Nanozoomer 2.0 HT Slide Scanning System, and image analysis was performed using the Nanozoomer Digital Pathology NDP.view2 software (40).

Immunohistochemistry and TRAP staining

Tibiae were fixed overnight in 70% Ethanol, decalcified in 0.5 M EDTA (pH 8.0) for 7 days, embedded in paraffin blocks and sagittal sectioned at the University of San

Diego, Moores Histology & Sanford Consortium Histology. Sections (5 µm thick) were de-paraffinized in xylene and rehydrated in graded ethanol and water (89). For antigen retrieval, slides were placed in 10 mM sodium citrate buffer (pH 6.0) at 80–85°C, and allowed to cool to room temperature for 30 min. Endogenous peroxidase activity was quenched in 3% hydrogen peroxide for 10 min (89). Slides were blocked with 5% normal goat serum and a) 8 week-old Prkg1 Control and Prkg1 OB-KO mice (basal phenotype analyses) samples were incubated overnight at 4°C with anti-PKG1-, anti-PKG2 antibody (1:100 in blocking buffer) and anti-BMP-2/ BMP-4 antibody (1:50 in blocking buffer), followed by HRP-conjugated secondary antibody (SignalStain® Antibody diluent, Cell Signalling) for 1 h at room temperature. b) 12 week-old Prkg1 Control and Prkg1 OB-KO mice (regeneration model, bones with- and without defect) samples were incubated overnight at 4°C with anti-CD31 (PECAM-1) or anti-pSmad 1/5/9 antibody (1:100 in blocking buffer), followed by HRP-conjugated secondary antibody (Cell Signaling, SignalStain® Antibody diluent) for 1 h at room temperature. After development with 3,3-diaminobenzidine substrate (Vector Laboratories, Inc., Burlingame, CA), slides were counterstained with hematoxylin for 2 min. and dehydrated in ethanol and xylene before mounting with coverslips. Blood vessel (capillary) density was calculated based on anti-CD31 staining - Single CD31 immunoreactive endothelial cells and clusters separate from other microvessels (red arrow heads) were counted as individual capillaries. The total number of microvessels in the hole region (area 0.1 mm^2) was counted to calculate capillary density (N/mm^2). Brown cells/nuclei, indicated by red arrows, represent cells/nuclei stained with a phosphor-Smad1/5/9 (Ser 463/465/467)-specific antibody. The number of phospho-Smad1/5/9 positive cells was counted in the hole region (area 0.1 mm^2).

For Tartrate-resistent phosphatase staining (TRAP) tibiae of 12 week-old Prkg1 Control and Prkg1 OB-KO mice (regeneration model, bones with- and without defect) were fixed overnight in 70% Ethanol, decalcified in 0.5 M EDTA (pH 8.0) for 7 days, embedded in paraffin blocks and sagittal sectioned at the University of San Diego, Moores Histology & Sanford Consortium Histology. Sections (5 µm thick) were de-paraffinized in xylene and rehydrated in graded ethanol to distilled water. Slides were placed in a pre-warmed TRAP staining solution mix and incubated for 40 min. at 37°C. Staining Solution: Deionized water pre-warmed to 37°C, 7 mg/ml Fast Garnet GBC base in 0.4 mol/L hydrochloric acid with stabilizer, 12.5 mg/ml Naphthol AS-BI phosphoric

acid, 2.5 mol/L (pH 5.2) Acetate buffer, 0.335 mol/L (pH 4.9) L(+)-Tartrate buffer (Acid phosphatase Leucocyte kit, Sigma Aldrich). Samples were rinsed in diH_2O, counterstained with hematoxylin solution for 2 min., rinsed in diH_2O, dehydrated in ethanol and xylene before mounting with coverslips. Osteoclasts were defined by red/brown-stained multinucleated cells, indicated by red arrow heads, counted in the hole area (area 0.1 mm^2) and calculated as N/mm^2. Slides were scanned with a Hamamatsu Nanozoomer 2.0 HT Slide Scanning System, and image analysis was performed using the Nanozoomer Digital Pathology NDP.view2 software (40).

Micro-computed tomography (micro-CT)

Micro-CT analyses were performed on ethanol-fixed tibiae of a) 8 week-old male and female Prkg1 Control and Prkg1 OB-KO mice (basal phenotype analyses), using a Skyscan 1076 (Kontich, Belgium) scanner at 9 µm voxel size, and applying an electrical potential of 50 kVp and current of 200 µA, with a 0.5 mm aluminum filter as described (Cooperation with Prof. Robert L. Sah, UCSD Jacobs School of Engineering) (22, 89). Mineral density was determined by calibration of images against 2-mm diameter hydroxyapatite (HA) rods (0.25 and 0.75 g/cm^3). Additionally a beam hardening correction algorithm was applied prior to image reconstruction (22, 89). To visualize the sample data, Skyscan's software, Dataviewer and CTAn (Kontich, Belgium) were used. Samples were aligned vertically, and 2D orthogonal cross-sections were selected at the tip of the proximal growth plate.

Cortical bone was analyzed by automatic contouring the periosteal tissue and excluding the marrow cavity, the region of interest was 3.6 to 4.5 mm distal to the proximal growth plate, using a global threshold to identify cortical bone, and eroding one pixel to eliminate partial volume effects (113). A global threshold was used to identify cortical bone and an erosion of one pixel was performed to eliminate partial volume effects. From this region of cortical bone, the following parameters were determined: cross-sectional tissue area (T.Ar), cross-sectional cortical bone area (B.Ar), cortical bone area fraction (B.Ar/T.Ar), cross-sectional bone thickness (Cs.Th) and tissue mineral density (TMD) (113).

Trabecular bone was analysed by automatic contouring of the proximal tibial metaphysis (0.36 to 2.1 mm distal to the growth plate), using an adaptive threshold to

select the trabecular bone (113). All contours were checked to ensure they covered the desired area, otherwise they were manually adjusted. An adaptive threshold (using the mean maximum and minimum pixel intensity values of the surrounding ten pixels) was used to identify trabecular bone. From this region of trabecular bone, the following parameters were determined: tissue volume (TV), Trabecular bone volume (BV), trabecular bone volume fraction (BV/TV), trabecular thickness (Tb.Th), trabecular separation (Tb.Sp), trabecular number (Tb.N) and bone mineral density (BMD) (113). As quality control, samples that had quantitative values further from the group's median were checked for image quality, sample alignment, selection of the growth plate, contoured region, and number of slices being analyzed. The quantitative data obtained was compared to the series of axial cross-sections showing the trabecular and cortical region analyzed to make sure both visual and quantitative results were in agreement.

Micro-CT analyses were performed on ethanol-fixed tibiae of b) 12 week-old male and female Prkg1 Control and Prkg1 OB-KO mice (regeneration model), using a Skyscan 1076 (Kontich, Belgium) scanner at 9 μm voxel size, and applying an electrical potential of 50 kVp and current of 200 μA, with a 0.5 mm aluminum filter, exposure time of 1600 ms, rotation step of 0.8 deg and partial width of 70% as described (22, 69).

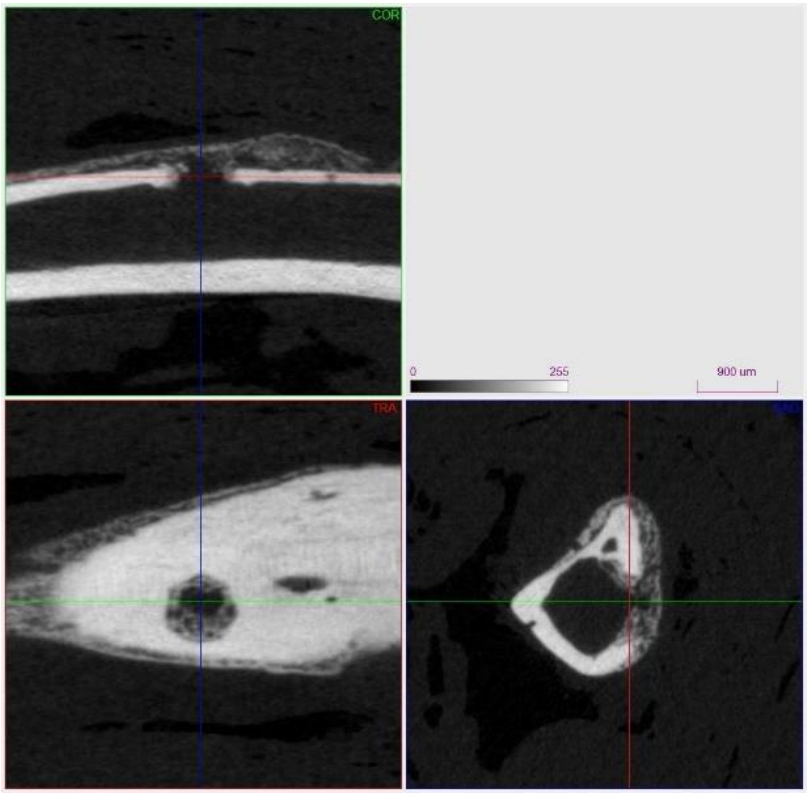

Fig. 5: 2D orthogonal views of rotated tibia in Dataviewer (modified after Schall et al. 2020 Suppl. Figure 3, 113).

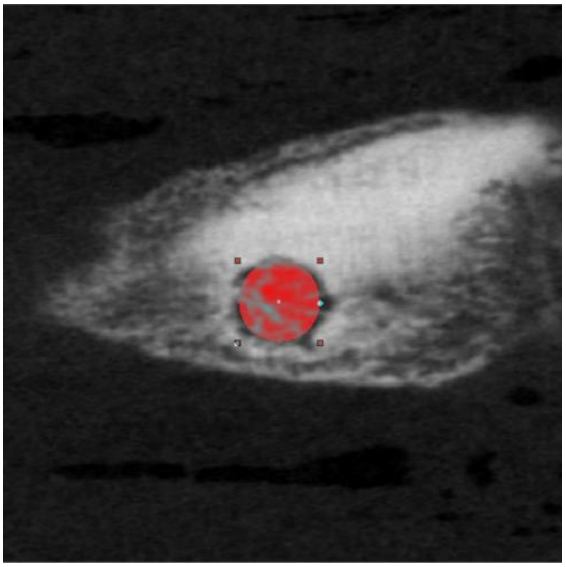

Fig. 6: Top view of cylindrical ROI (modified after Schall et al. 2020 Suppl. Figure 3, 113).

Images were rotated as shown above (left picture) and a 504 x 504 x 504 (9 µm) volume of interest (VOI) was saved for each sample. The transaxial view showed the anterior side with the proximal tibia along the right edge and the distal tibia along the left edge. The blue and green lines should cross in the center of the defect.

The top surface of the defect was selected as the highest point on the tibia where the full defect region was still visible. Quantitative analysis were performed in a cylindrical volume of interest (VOI) with diameter 0.65 mm (74 pixels) and height 0.3 mm (33 slices) that will extend from the outer surface of the tibia, through the cortical bone region. Selecting and saving elliptical regions of interest (ROI) will be done using CTAn. Three dimensional images from the region of interest (ROI) were constructed using CTvol software. An adaptive threshold (using the mean maximum and minimum pixel intensity values of the surrounding 10 pixels) was used to identify trabecular bone (40).

Three-dimensional histology and Digital Volumetric Imaging (DVI)

Resolution Sciences developed Digital Volumetric Imaging (DVI), a micro-imaging platform technology that eliminates the need for glass slide mounted tissue sections. DVI directly images the cut surface of a specimen and electronically captures a high-resolution picture of the embedded sample. A series of cuts and images are captured throughout the sample that can be reconstructed back to a 3D sample.

Ten week-old Prkg1 Control and Prkg1 OB-KO male mice underwent tibial monocortical defect surgery as described above in Methods. Labelling was performed by i.p. injection of alizarin red complexone (50 mg/kg) and calcein green (25mg/kg) at 7 and 2 d before euthanasia. Tibiae were fixed in 10% neutral buffered formalin overnight, scanned for micro-CT, processed in 5% aqueous potassium hydroxide for 4 days as described above in Methods. The samples were transferred to 50% Ethanol and stored at room temperature for further analysis. Samples were trimmed to 2 mm x 2 mm x 2 mm blocks containing native of regenerating bone and a depth (z) extending to ~3 mm (full thickness), processed without staining, dehydrated in graded ethanol series (50, 70, 100, 100%) and xylene, embedded with modified Spurr resin opacifier (20% Sudan Black) and imaged with a fluorescence microscope with G-2A and B-2A filters at 4x and 10x. Articular cartilage was stained and imaged to localize cell nuclei within the 3-D cartilage

block using digital volumetric imaging as described (76). The embedded sample was mounted onto a translation stage assembly, which drew the sample over a diamond edge knife, removed the section with vacuum, then repositioned the block face in its original location, in the field of view and imaged with a Nikon E600 microscope with a 10x Plan Apochcromat objective (NA 0.45). Images were acquired at 0.89 μm^3/voxel resolution with a field of view 1.8 x 1.8 mm^2 using a black and white digital camera [Kodak Megaplus 10bit Model 4.2i]. A series of 3500 x 0.88 µm sections were imaged starting within the central portion of the tibial shaft cutting towards the proximal tibia. The central tibia was inserted in the tapered portion of the medium DVI mold (2 x 2 mm) because the geometry of the central tibia was smaller in diameter than the proximal tibia. The tibial shaft was scanned at 4x at 5s (gain=12) at both colour channels. The defect was identified at 4x and resumed scanning at 10x (Red exposure 5s gain=12, Green exposure 3s gain=12). From the 3-D data, summary slides showing cross-sections of the 3-D histology were generated, as well as fly-through movies showing the all cross-sectional frames that were imaged from the serial sectioning, in multiple orientations.

Statistical Analyses

Graph Pad Prism 5 was used for two-tailed Student t-test with Welch´s correction (to compare two groups) or one-way ANOVA with Bonferroni post-test analysis (to compare more than two groups); $p<0.05$ was considered significant. Graphs represent mean ± SD as described in Figure legends.

RESULTS

3.1 Col1a1-Cre efficiently deletes PKG1 from osteoblasts in mice carrying PKG1 floxed allels: Generation and Characterization of osteoblast-specific prkg1 knockout mice

The exact role of PKG1 for bone development and regeneration *in vivo* has not yet been investigated due to the severity of the phenotype of global PKG1 KO mice. Therefore, to delineate the *in vivo* actions of PKG1 in osteoblasts, I generated osteoblast-specific Prkg1 knockout mice by interbreeding of Col1a1-Cre+ transgenic mice heterozygous for a floxed prkg1 locus (Col1CRE+; *prkg1* fl/+) with mice homozygous for the floxed *prkg1* locus (*prkg1* fl/fl). The LoxP sites flanked exon 2 of the prkg1 locus (Fig. 1C); exon 2 is common to both splice variants of PKG1 (PKG1 α and 1β), and excision of this exon causes a frameshift with premature stop codon. Mice were genotyped by PCR analysis of genomic DNA derived from tail biopsies to identify Control (Prkg1 Ctrl, genotype *prkg1* fl/fl) and Prkg1 osteoblast specific knockout (Prkg1 OB-KO, genotype Col1CRE+; *prkg1* fl/fl) mice using corresponding primer sets (described in Methods). The floxed allele was amplified to generate a 340-bp fragment compared with 244 bp for the wildtype allele (Fig. 1A). Mutant PKG1 was expressed under control of the murine 2.3 kb Col1a1 promoter, which can drive Cre expression at high levels in osteoblasts; the promoter is active in all cells of the osteoblastic lineage, starting from committed mesenchymal stem cells through mature osteocytes (77, 89). The frequency of different genotypes observed in a cohort of 4-week old mice (n=112 total) corresponded to the expected percentage for CRE-negative control mice of each gender (25% Cre-; prkg1 fl/fl or fl/+) (Fig. 1B). Interestingly, a slight imbalance in the expected Mendelian frequency (12.5%) of the osteoblast-specific knockout lineage for female (+4.5% Cre+; prkg1 fl/fl) and male (-4.5% Cre+; prkg1 fl/fl) mice was found (Fig. 1B). PCR analysis of genomic DNA extracted from multiple organs of a control and knockout mouse showed amplification of a specific, 550 bp band after homologous recombination in the knockout mouse, corresponding to the transgene-derived *prkg1* gDNA in bone, but not in other organs (Fig. 1C); this band was not detected in the non-template control. PCR

analysis of reverse-transcribed RNA extracted from multiple organs of control and knockout mice showed a significant reduction of *Prkg1* mRNA expression in bone. In contrast, wild type and transgenic mice showed similar *Prkg1* mRNA expression in kidney, lung and brain, three organs with the highest endogenous *Prkg1* mRNA expression (78) (Fig. 1D). Primary osteoblasts (POBs) were isolated from Prkg1 Ctrl and Prkg1 OB-KO mice and RNA was analysed by qRT-PCR using primers specific for exon 1/2 normalized to 18S; the amount of PKG1 protein was assessed by Western blotting of whole cell lysates using an anti-PKG 1 antibody. *Prkg1* mRNA and protein expression were reduced by > 75% in transgenic compared to control POBs (Fig. 1E, F). Importantly, *Prkg2* mRNA expression was the same in bones (Fig. 3E) and POBs (Fig. 1E) from Prkg1 OB-KO transgenic mice. Immunohistochemical staining of bone sections for PKG1 showed a stronger signal in bone-lining osteoblasts in the Prkg1 Control compared to Prkg1 OB-KO mice (Fig. 1G); PKG2 was unchanged in the bone sections isolated from the same mice (Fig. 1H). However, staining of endogenous PKG1 in megakaryocytes was similar between transgenic and control animals (Fig. 1G). Efficient CRE-mediated knockout of PKG1 was also confirmed in *in vitro* experiments with POBs isolated from mice (C57Bl/6) homozygous for floxed prkg1 alleles (Prkg1 fl/fl) which were infected with adenovirus expressing control (GFP) or CRE recombinase (Cre) (shown in Fig. 5 and described below).

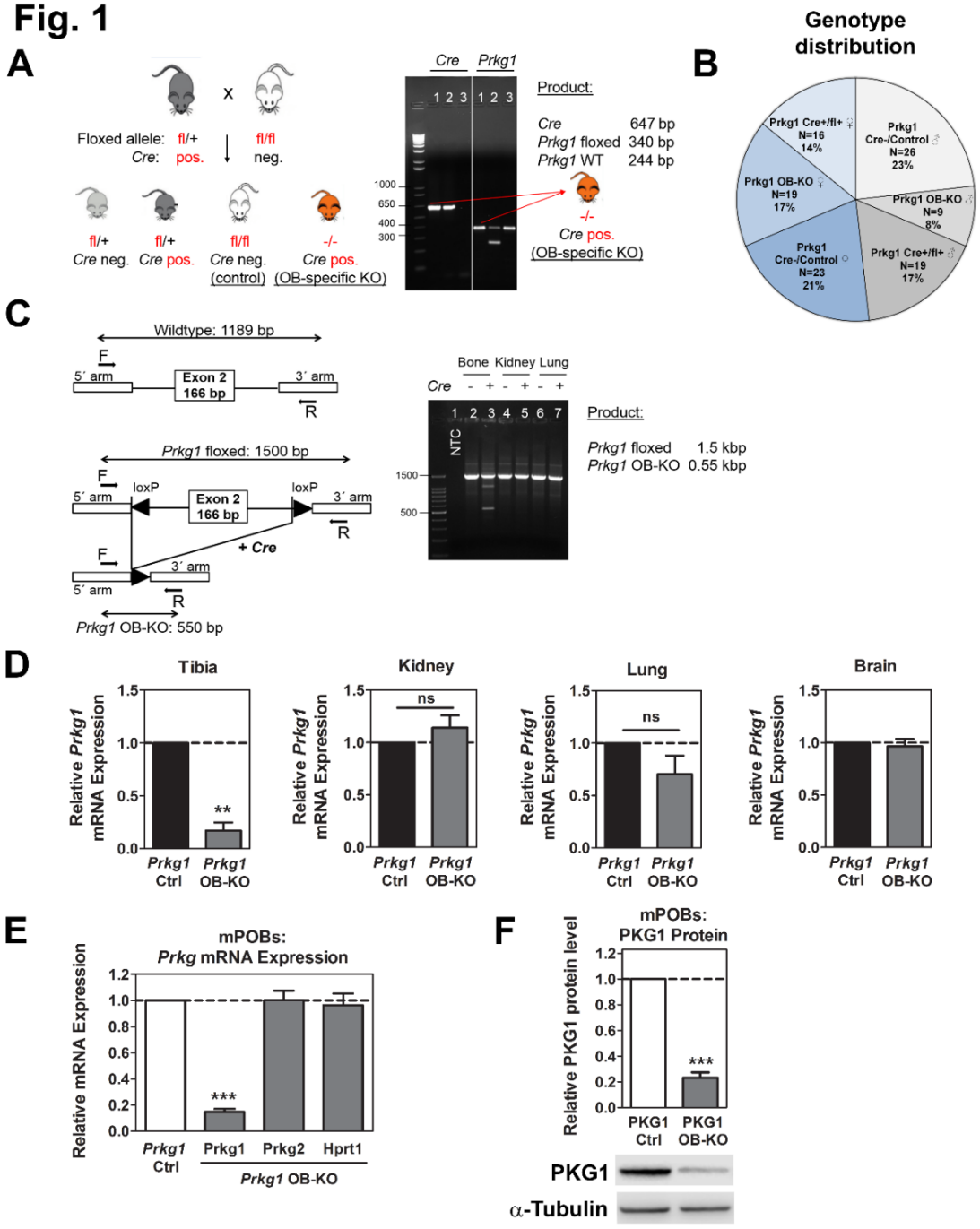
Fig. 1
A
Floxed allele: fl/+ fl/fl
Cre: pos. neg.
fl/+ Cre neg.
fl/+ Cre pos.
fl/fl Cre neg. (control)
-/- Cre pos. (OB-specific KO)
Cre Prkg1
1 2 3 1 2 3
1000
650
400
300
Product:
Cre 647 bp
Prkg1 floxed 340 bp
Prkg1 WT 244 bp
-/-
Cre pos. (OB-specific KO)
B
Genotype distribution
Prkg1 Cre+/fl+ ♀ N=16 14%
Prkg1 Cre-/Control ♂ N=26 23%
Prkg1 OB-KO ♀ N=19 17%
Prkg1 OB-KO ♂ N=9 8%
Prkg1 Cre-/Control ♀ N=23 21%
Prkg1 Cre+/fl+ ♂ N=19 17%
C
Wildtype: 1189 bp
5´ arm
Exon 2 166 bp
3´ arm
Prkg1 floxed: 1500 bp
loxP
+ Cre
Prkg1 OB-KO: 550 bp
Bone Kidney Lung
Cre - + - + - +
1 2 3 4 5 6 7
NTC
1500
500
Product:
Prkg1 floxed 1.5 kbp
Prkg1 OB-KO 0.55 kbp
D
Tibia
Kidney
Lung
Brain
Relative Prkg1 mRNA Expression
ns
**
Prkg1 Ctrl
Prkg1 OB-KO
E
mPOBs: Prkg mRNA Expression
Relative mRNA Expression
***
Prkg1 Ctrl
Prkg1
Prkg2
Hprt1
Prkg1 OB-KO
F
mPOBs: PKG1 Protein
Relative PKG1 protein level
PKG1 Ctrl
PKG1 OB-KO
PKG1
α-Tubulin

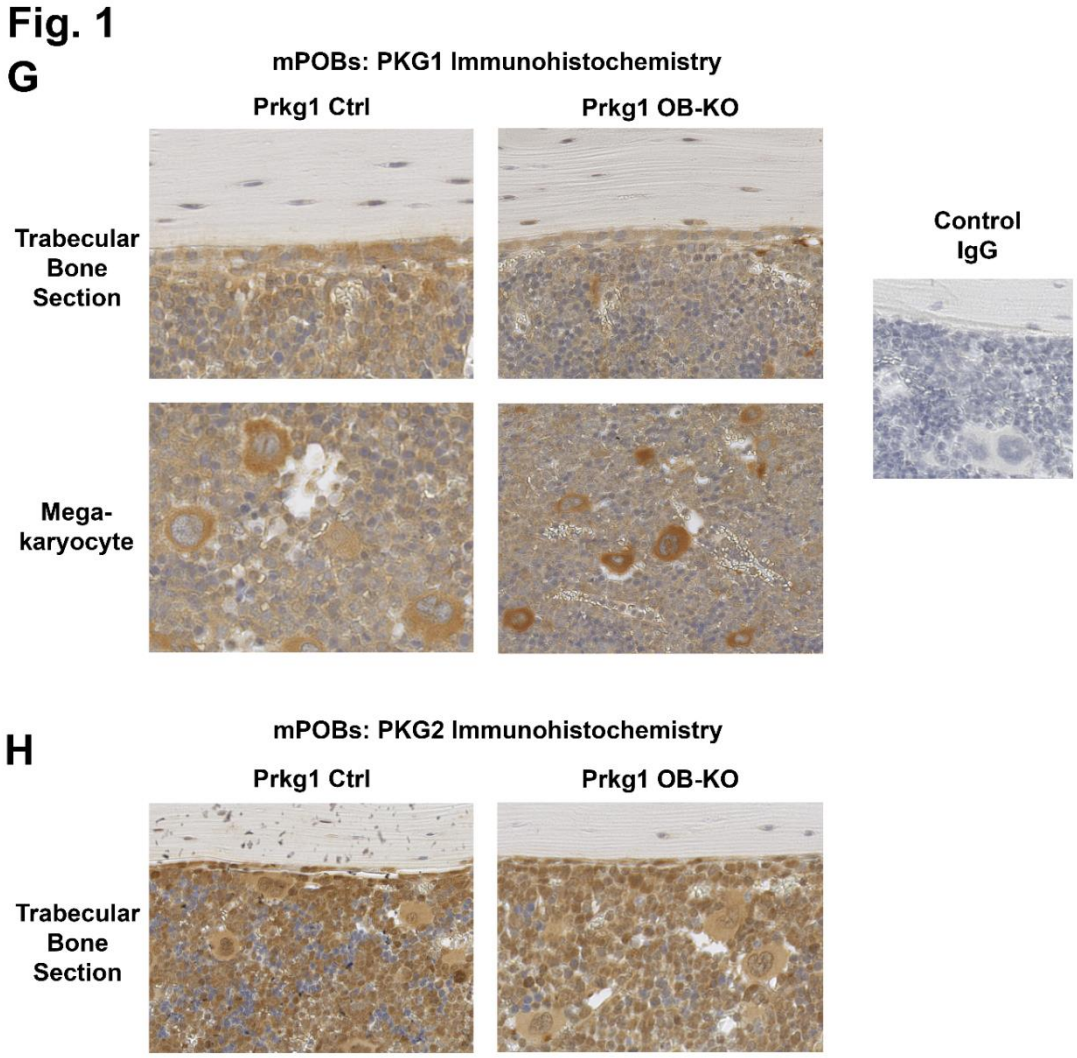

<u>Fig.1:</u> Col1a1-Cre efficiently deletes PKG1 from osteoblasts in mice carrying PKG1 floxed allels: Generation and Characterization of osteoblast-specific prkg1 knockout mice (modified after Schall et al. 2020 Figure 1 and Suppl. Figure 1, 113). **(A)** Osteoblast-specific Prkg1 knockout mice were generated by interbreeding of Col1a1-Cre+ transgenic mice heterozygous for the floxed prkg1 locus (Col1CRE+; *prkg1* fl/+) with mice homozygous for the floxed *prkg1* locus (*prkg1* fl/fl). Mice were genotyped by PCR analysis of genomic DNA derived from tail biopsies to identify Control (Prkg1 Ctrl, genotype *prkg1* fl/fl) and Prkg1 osteoblast specific knockout (Prkg1 OB-KO, genotype Col1CRE+; *prkg1* fl/fl) mice. **(B)** Frequency of different genotypes observed in a cohort of 4-week old mice (n=112 total); males in grey, females in blue. The expected percentage for each genotype in each gender was 25% Cre-; prkg1 fl/fl, fl/+, 12.5% Cre+; prkg1 fl/+ and 12.5% Cre+;prkg1 fl/fl. **(C)** The location and orientation of PCR primers flanking

exon II before and after homologous recombination is shown by arrows. Primers F and R produce a 1189-bp PCR amplicon on the prkg1 fl/fl locus before and a 550-bp PCR amplicon after homologous recombination. Genomic DNA was extracted from the indicated organs of a wildtype and knockout mouse. **(D)** RNA was extracted from bone, kidney, lung and brain of Prkg1 Ctrl (Cre-; prkg1 fl/fl) and Prkg1 OB-KO (Cre+; prkg1 fl/fl) mice, and *Prkg1* mRNA was quantified by qRT-PCR using primers for exon 2/3. Data were normalized to 18S and calculated according to the ΔΔCt method, assigning the mean of the Prkg1 Ctrl group a value of one. Data are means ± SEM from n=5 mice per genotype for all indicated organs (**p<0.01). **(E,F)** Primary osteoblasts (POBs) were isolated from Prkg1 Ctrl and Prkg1 OB-KO mice and RNA was analysed by qRT-PCR using primers specific for exon 1/2 normalized to 18S (E) or the amount of PKG1 protein was assessed by Western blotting of whole cell lysates using an anti-PKG I antibody, with tubulin serving as a loading control and blots quantified by densitometry scanning (F). *Hprt1* was normalized to 18S. Data represent means ± SEM of three independent experiments; ***p<0.001. **(G,H)** Immunohistochemical staining for PKG1 (G) and PKG2 (H) in tibial sections from Prkg1 Ctrl and Prkg1 OB-KO mice; top panels show osteoblasts on trabecular surfaces, bottom panels show megakaryocytes, which served as a positive control. G and H are representative of bones from three mice per genotype. Same time for substrate development, but slightly darker staining overall for the OB-KO samples.

3.2 Mice with osteoblast-specific deletion of PKG1 show no significant changes in bone microarchitecture

Col1a1-CRE-positive, osteoblast-specific *prkg1* knockout mice (PKG1 OB-KO mice, genotype Col1a1-CRE+, Prkg1f/f) were indistinguishable from their control littermates (genotype Col1a1-CRE-, Prkg1f/f) at birth, and showed no obvious skeletal abnormalities at eight weeks of age. Both groups had similar body weights and tibial lengths (Fig. 2A, B). Micro-computed tomography (micro-CT) analysis of tibial bone microarchitecture revealed that eight week-old male and female PKG1 OB-KO and control mice had no apparent differences in trabecular microarchitecture (Fig. 2E, F). Cortical parameters (cortical bone area fraction, cross-sectional thickness and tissue mineral density) were also the same in PKG1 OB-KO and control mice of both genders (Fig. 2G, H).

Fig. 2

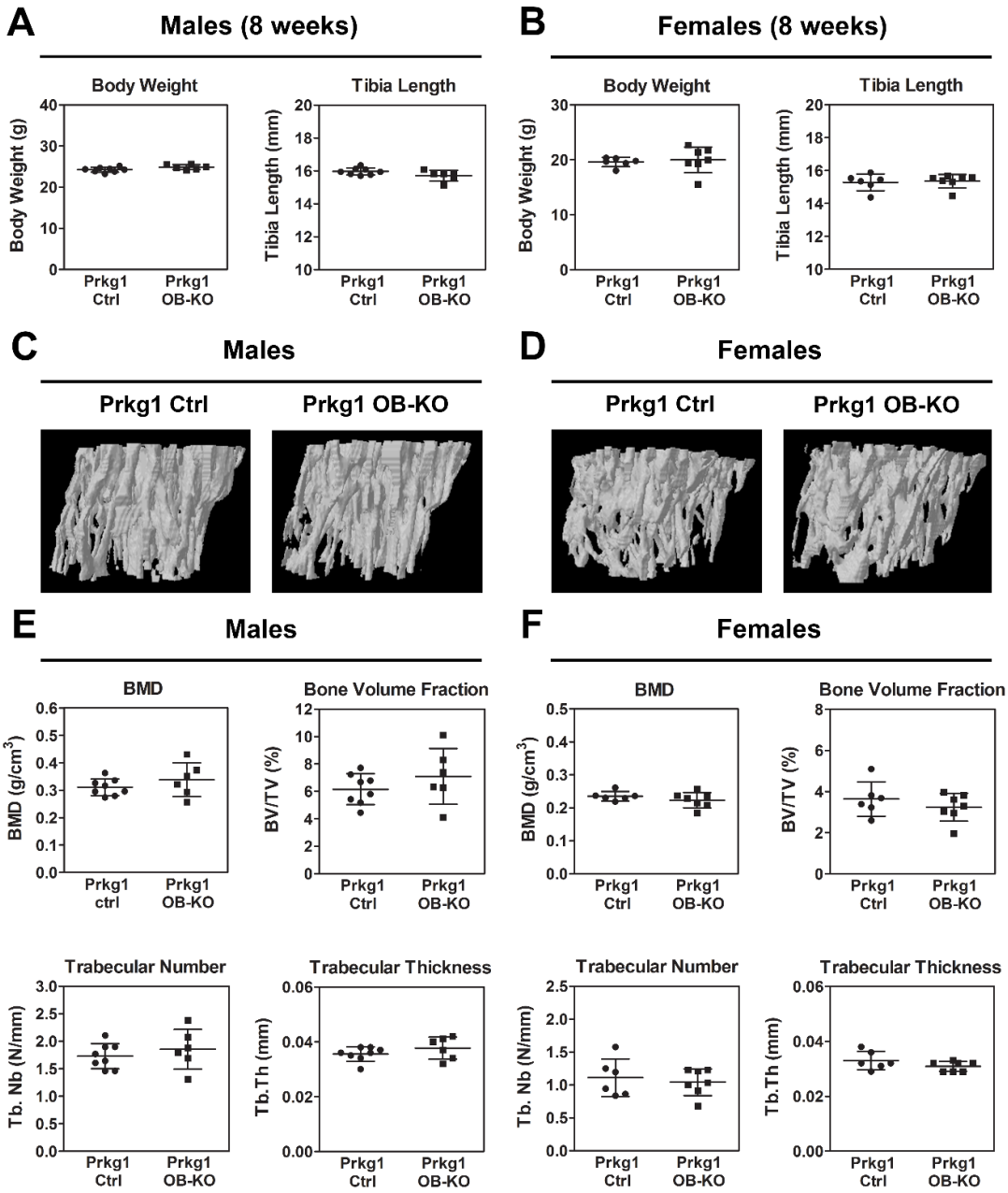
A
Males (8 weeks)
Body Weight
Body Weight (g)
Tibia Length
Tibia Length (mm)
Prkg1 Ctrl
Prkg1 OB-KO
B
Females (8 weeks)
C
Males
Prkg1 Ctrl
Prkg1 OB-KO
D
Females
E
Males
BMD
BMD (g/cm3)
Bone Volume Fraction
BV/TV (%)
Trabecular Number
Tb. Nb (N/mm)
Trabecular Thickness
Tb.Th (mm)
F
Females

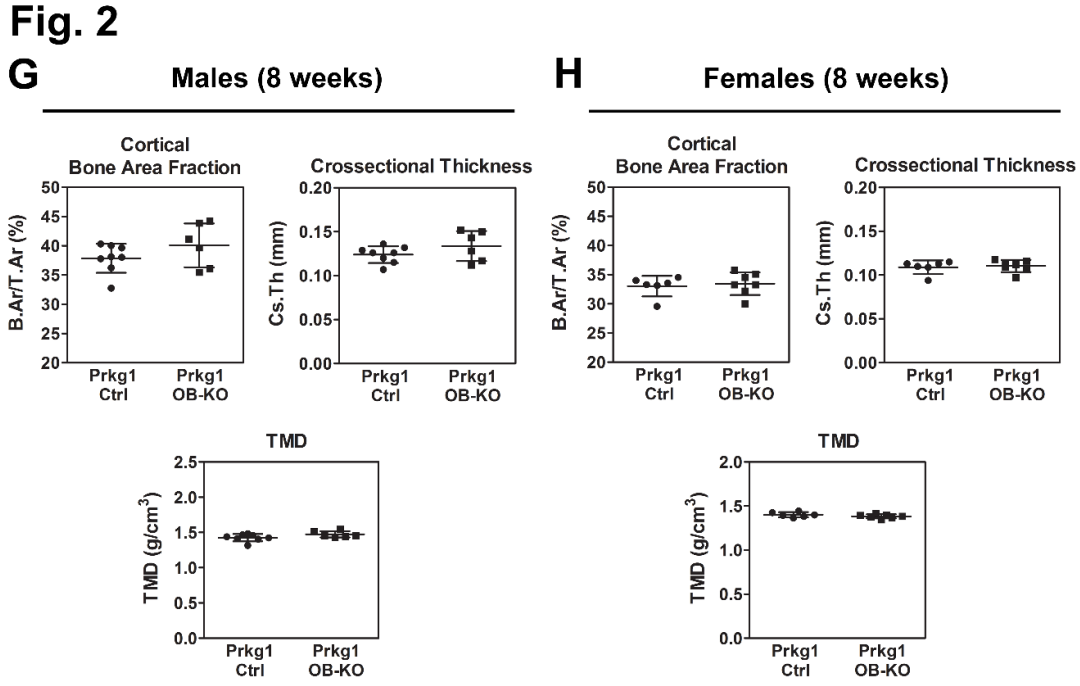

Fig. 2: Mice with osteoblast-specific deletion of PKG1 show no significant changes in bone microarchitecture (modified after Schall et al. 2020 Suppl. Figure 2, 113). Male **(A,C,E)** and female **(B,D,F)** osteoblast-specific Prkg1 knockout (Prkg1 OB-KO, genotype: CRE+;Prkg1 fl/fl) mice and their control litter mates (Prkg1 Ctrl, genotype: CRE-; Prkg1 fl/fl) were analysed at eight weeks of age. **(A,B)** Body weight and tibia length are shown for each gender. **(C,D)** Tibiae were analysed by micro-CT, with three-dimensional reconstruction of the trabecular bone at the proximal tibia below the growth plate shown. **(E,F)** Trabecular bone mineral density (BMD), trabecular bone volume fraction (BV/TV), trabecular number (Tb.N), and trabecular thickness (Tb.Th) were measured by micro-CT at the proximal tibia as described in Methods. **(G,H)** Cortical bone area fraction, cross-sectional thickness and tissue mineral density were measured by micro-CT at the mid-tibia in male (G) and female (H) mice as described in Methods. Data represent means ± SD (males: n=8 Prkg1 Ctrl and n=6 Prkg1 OB-KO; females: n=6 Prkg1 Ctrl and n=7 Prkg1 OB-KO).

3.3 Osteoblast-specific PKG1 knockout mice show decreased bone formation and altered osteoblastic-, BMP- and VEGF- gene expression

Consistent with the normal bone micro-architecture of Prkg1 OB-KO tibiae, no difference in the number of osteoblasts (Fig. 3B) and no change in osteoclast numbers on trabecular surfaces (Fig. 3C) between Prkg1 OB-KO and their control littermates was found. These results confirm lack of biologically-significant Col1a1-Cre PKG1 transgene expression in growth plate chondroblasts, and are in keeping with absent Col1a1 promoter activity in the chondroblastic lineage (79, 80, 89).

To determine the effect of osteoblast-specific deletion of Prkg1 on bone formation parameters, histomorphometric measurements in the distal tibiae after alizarin red complexone and calcein green double-labeling were performed (described in Methods). Twelve week-old Prkg1 OB-KO mice showed only a trend towards lower trabecular mineralizing surface (MS/BS, p=0.09), but significantly decreased mineral apposition rate (MAR, -29%), and bone formation rate (BFR, -48 %) compared to their wild type littermates (Fig. 3D). These results suggest decreased osteoblast activity. Next, the expression of Prkg-, osteoblast- and osteoclast-related genes in tibial shafts of control and Prkg1 OB-KO mice was examined (growth plates and bone marrow were removed and only tibial shafts were flash-frozen and analysed as described in Methods). Compared to control tibiae, Prkg1 mRNA expression was decreased by >80%, while *Prkg2* mRNA expression was unchanged (Fig. 3E). Alkaline phosphatase (*Alpl*) and osteocalcin (*Bglap*) mRNA expression was decreased by 38% and 42% in PKG1-deficient tibiae, respectively (Fig. 3F). Expression of the osteoclast regulators receptor of activated nuclear factor-Kb ligand (RANKL; gene name *Tnfsf11*) was unchanged while osteoprotegerin (OPG; gene name *Tnfrsf11b*) significantly increased in PKG1-deficient tibiae (Fig. 3G). The RANKL/OPG ratio was stable (Fig. 3H). *In vitro*, cGMP-dependent kinase 1 binds to the bone morphogenic protein (BMP) receptor-1 and enhances BMP-2 signaling via Smad-1/5 in C2C12 cells (81). BMP-2 plays an important role in the development and maintenance of bone and cartilage; it enhances differentiation of osteogenic precursor cells and the therapeutic use of recombinant BMP proteins is under investigation in human clinical trials for craniofacial deformities, fracture healing, and spine fusion (82,

83). Furthermore, BMP-2 is a potent inducer of bone formation through its stimulation of osteoblast differentiation (84). Angiogenesis is closely associated with bone regeneration and remodeling, and angiogenic factors like vascular endothelial growth factor A (VEGF-A are produced by osteoblasts and regulate osteoclast and osteoblast activity) (85). In addition, blood vessels serve as a way of transporting circulating osteoblast (86) and osteoclast precursors (87) to sites undergoing active remodeling. Regulation of BMP production and VEGF-induced angiogenesis during fracture healing are incompletely (66, 88) understood. Therefore, the effect of PKG1 deficiency on the expression of Bmp-2/ Bmp-4 and Vegfa mRNAs in osteoblasts (Fig. 3, Fig. 4 and Fig. 5) and bones (Fig. 3) from control and Prkg1 OB-KO mice were investigated. Compared to control tibiae, mRNA expression of *Bmp2* and *-4* and *Vegfa* was significantly decreased by 35.8%, 42.6% and 40.8%, respectively (Fig. 3I). Consistent with the results in bones (Fig. 3I), osteoblasts from Prkg1 OB-KO had *Bmp2*, *Bmp4* and *Vegfa* mRNA concentrations that were reduced by 82.2%, 55.5% and 47.0%, respectively, compared to control osteoblasts (Fig. 3J). However, expression of the housekeeping gene *Hprt* was unchanged. Immunohistochemical staining of bone sections for BMP-2 /BMP-4 showed a stronger signal in bone-lining osteoblasts in control compared to Prkg1 OB-KO mice (Fig. 3K). The decrease in BMP2/4 expression in PKG1-deficient osteoblasts confirming reduced BMP production by PKG-1 deficient cells of the osteoblastic lineage. Decreased phosphorylation of Smad 1/5/9 in *Prkg1* OB-KO osteoblasts and PKG1-deficient regenerating bone was found (described later and shown in Fig. 4H and Fig. 8B).

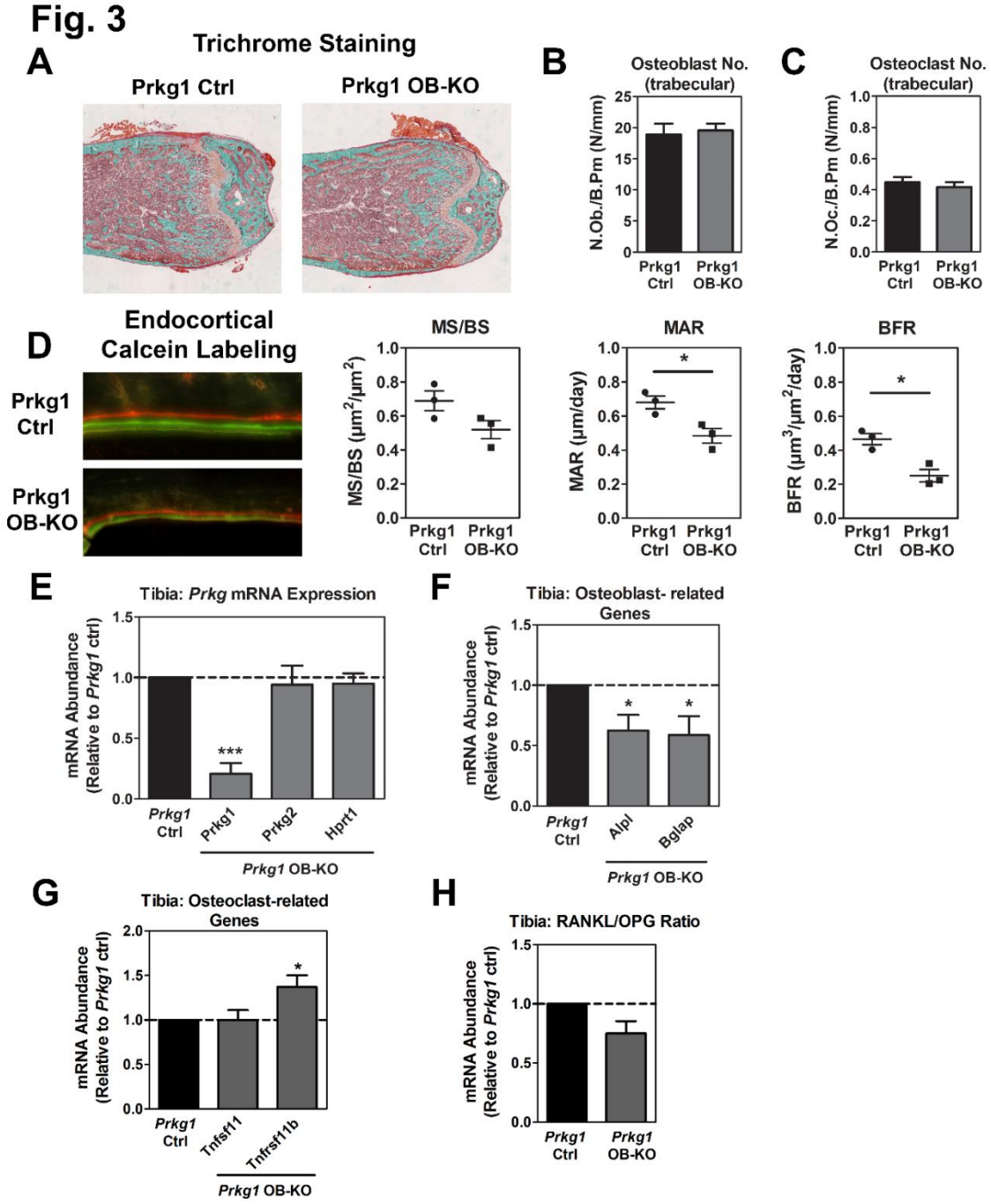
Fig. 3
A
Trichrome Staining
Prkg1 Ctrl
Prkg1 OB-KO
B
Osteoblast No. (trabecular)
N.Ob./B.Pm (N/mm)
Prkg1 Ctrl
Prkg1 OB-KO
C
Osteoclast No. (trabecular)
N.Oc./B.Pm (N/mm)
D
Endocortical Calcein Labeling
Prkg1 Ctrl
Prkg1 OB-KO
MS/BS
MS/BS (μm²/μm²)
MAR
MAR (μm/day)
BFR
BFR (μm³/μm²/day)
E
Tibia: Prkg mRNA Expression
mRNA Abundance (Relative to Prkg1 ctrl)
Prkg1 Ctrl
Prkg1
Prkg2
Hprt1
Prkg1 OB-KO
F
Tibia: Osteoblast- related Genes
Alpl
Bglap
G
Tibia: Osteoclast-related Genes
Tnfsf11
Tnfrsf11b
H
Tibia: RANKL/OPG Ratio

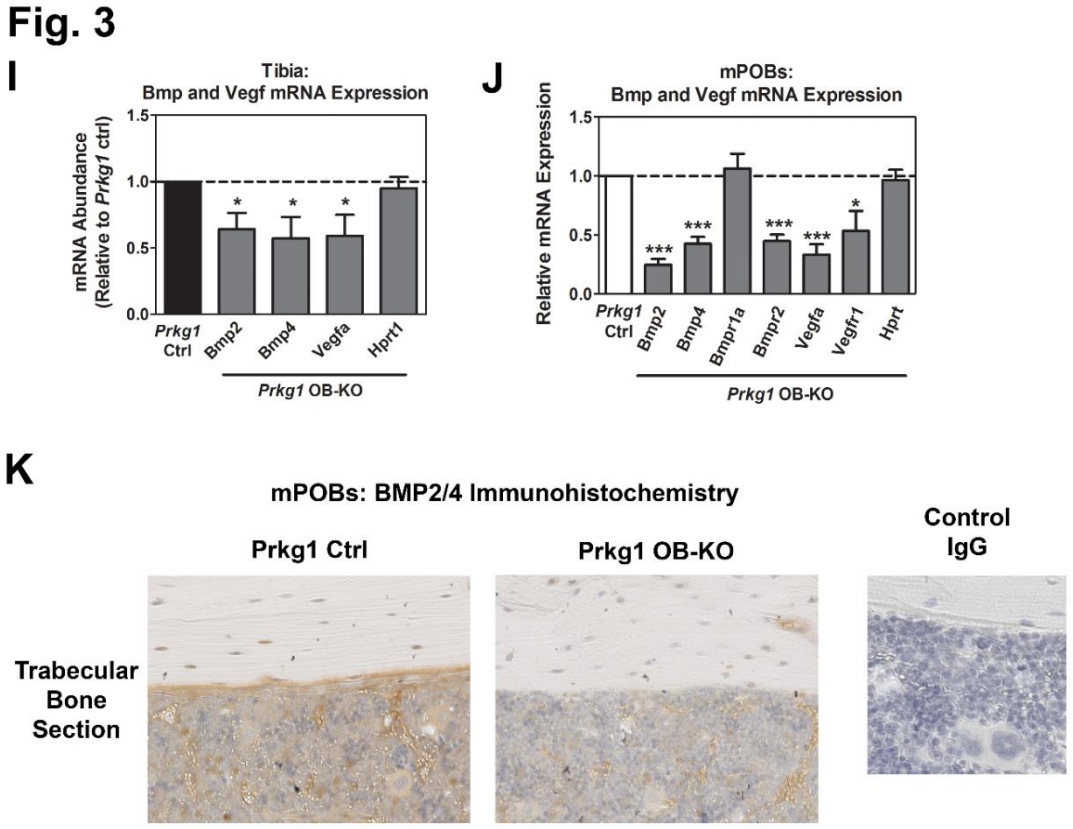

<u>Fig. 3:</u> Osteoblast-specific PKG1 knockout mice show decreased bone formation and altered osteoblastic-, BMP- and VEGF- gene expression (modified after Schall et al. 2020 Figure 1 and 3, 113). **(A)** Trichrome staining of tibial sections were analysed in 12 week-old mice. **(B,C)** Osteoblasts (B) and Osteoclasts (C) were counted on trabecular surfaces in the proximal tibia as described in Methods. Panels show means ± SEM of n=4 Prkg1 Ctrl and n=4 Prkg1 OB-KO mice. **(D)** Twelve week-old mice received alizarin complexone injection 7 days and calcein injection 2 days prior to euthanasia, and endocortical labeling was assessed by fluorescence microscopy (89). Mineralizing surfaces (MS/BS), mineral apposition rates (MAR), and bone formation rates (BFR) were measured at endocortical surfaces. Panels show means ± SEM of n=3 Prkg1 Ctrl and n=3 Prkg1 OB-KO mice; (by two-sided t-test). **(E-I)** RNA was extracted from tibial shafts, and the relative abundance of PKG-, Osteoblast-, RANKL-/Osteoclast- and BMP-/VEGF-related transcripts was quantified by qRT-PCR and normalized to two housekeeping genes (18S, *Hprt1*) (89). Data were calculated according to the ΔΔCt method, with the mean of the Prkg1 Ctrl group for each gene assigned a value of one. *Hprt1* was normalized to 18S. Gene names: *Prkg1* (cGMP-dependent protein kinase 1),

Alpl (alkaline phosphatase), *Bglap* (osteocalcin), *Tnfsf11* (RANKL), *Tnfrsf11b* (osteoprotegerin), *Bmp2/4* (bone morphogenetic protein 2/4), *Vegfa* (vascular endothelial growth factor A) and *Hprt1* (hypoxanthine phosphoribosyltransferase 1). Data represent means ± SEM from n=6 mice per genotype. *p<0.05, **p<0.01 and ***p<0.001 for the comparison between Prkg1 Ctrl and Prkg1 OB-KO mice (by two-sided t-test). **(J)** RNA was extracted from undifferentiated POBs, and the relative abundance of BMP- and VEGF-related transcripts was quantified by qRT-PCR. Gene names: *Bmpr1a* (bone morphogenetic protein receptor, type IA), *Bmpr2* (Bone morphogenetic protein receptor type II) and *Vegfr* (Vascular Endothelial Growth Factor Receptor). POBs were isolated from eight week-old osteoblast-specific Prkg1 knockout (Prkg1 OB-KO n=3) and control (Prkg1 fl/fl n=3) mice. Data represent means ± SEM. *p<0.05, **p<0.01 and ***p<0.001 for the comparison between Prkg1 Ctrl and Prkg1 OB-KO POBs (by two-sided t-test). **(K)** Immunohistochemical staining for BMP2/4 in tibial sections from Prkg1 Ctrl and Prkg1 OB-KO mice; panels show osteoblasts on trabecular surfaces. Fig.K is representative of bones from three mice per genotype.

3.4 PKG1-deficient osteoblasts show decreased apoptotic resistance, impaired BMP/Smad signaling, an altered oxidative stress response and reduced differentiation capacity

To investigate the effects of PKG1 deficiency on various osteoblast functions, I isolated primary osteoblasts from the long bones of Prkg1 OB-KO mice and control mice. As described above, in Fig. 1E and 1F, Prkg1 mRNA and PKG1 protein were reduced by 85.4% and 76.7% in osteoblasts from Prkg1 OB-KO mice compared to osteoblasts from control mice.

NO-releasing and cGMP-elevating agents protect osteoblasts from apoptosis induced by serum starvation or DNA-damaging agents, and these effects require cooperation between PKG1 and PKG2 (15). Moreover, the pro-survival effects of estradiol in osteoblasts and osteocytes are mediated by NO/cGMP (15, 89). Consistent with these data, control POBs showed enhanced survival after prolonged serum starvation in the presence of 100 µM 8-pCPT-cGMP or 100 nM estradiol (E2), while PKG1-deficient osteoblasts showed decreased apoptotic resistance with more cells staining positive for cleaved caspase-3 in the absence or presence of cGMP or estradiol (this difference reached significance only in the presence of cGMP or estradiol, as shown in Fig. 4A). The group of Dr. Pilz has shown previously *in vitro*, that PKG2 activity is required for shear- and cGMP-induced osteoblast proliferation (29). Consistent with PKG2-specific regulation of osteoblast proliferation, PKG1-deficient osteoblasts showed similar bromodeoxyuridine (BrdU) uptake into replicating DNA after treatment with 100 µM 8-pCPT-cGMP as control osteoblasts. Treatment with 20% FBS served as a positive control, (Fig. 4B).

To examine osteoblast differentiation, POBs from control and Prkg1 OB-KO mice were plated at high density, and switched to differentiation medium after reaching confluency (89). Differentiated POBs from PKG1 OB-KO mice expressed lower amounts of mRNA encoding alkaline phosphatase *(Alpl)*, osteocalcin (*bglap*) and osteoblastic transcription factor (*Runx2)* compared to wild type POBs, while expression of *Col1a1* and *Hprt1* was unchanged (Fig. 4D). Alkaline phosphatase activity was reduced in differentiated PKG1-deficient POBs compared to control cells (Fig. 4C).

The group of Dr. Pilz has shown previously *in vitro*, that pharmacologic activation of the NO/cGMP/PKG signaling cascade increases Wnt signaling and expression of Wnt-related genes in POBs, and that this does not occur in *prkg2*-deficient POBs (22, 37, 89). Therefore, the expression of Wnt-related genes in undifferentiated POBs of control and Prkg1 OB-KO transgenic mice was examined. mRNA expression of β-catenin (*ctnnb1*), and the Wnt co-receptor low-density lipoprotein receptor-related protein-5 (*lrp5*) was significantly decreased in PKG1-deficient osteoblasts (Fig. 4G). These findings are similar to those in PKG2-deficient cells, suggesting that *ctnnb1* and *lrp5* are regulated by cGMP via both PKG1 and PKG2.

Next, the expression of *Bmp*- and *Vegf*- mRNAs in undifferentiated serum-starved osteoblasts of control and *Prkg1* OB-KO mice with treatment of 100 µM 8-CPT-cGMP for 24 hours was investigated. 8-CPT-cGMP increased *Bmp2/4* and *Bmpr2* mRNA expression in control osteoblasts, but not in *Prkg1* OB-KO osteoblasts (Fig. 4E). Treating control osteoblasts with 8-CPT-cGMP for 2 h increased both *Vegfa* and *Vegfr1* mRNA expression, with no effect in PKG1-deficient osteoblasts (Fig. 4F). Thus, in osteoblasts, *Vegfa* and *Vegfr1* expression is regulated by cGMP/PKG1, and PKG1 is required for basal expression of both growth factors and receptor (113). *In vitro*, PKG1 is required for BMP-induced Smad signaling in C2C12 myoblasts (81). Consistent with this report, Smad phosphorylation in response to 1 nM BMP-2 was reduced in osteoblasts from Prkg1 OB-KO mice compared to control osteoblasts (Fig. 4H).

Oxidative stress contributes to bone loss associated with aging, estrogen deficiency, and diabetes, and cGMP-elevating agents increase the expression of antioxidant genes in diabetic osteoblasts (56). Treatment of cells with H_2O_2 causes oxidative stress and leads to increased phosphorylation of the stress-activated protein kinases SAPK/JNK-1/2 (90). Primary osteoblasts from control and Prkg1 OB-KO mice showed similar levels of basal SPK/JNK phosphorylation and showed a two- to three-fold increase in phosphorylation after treatment with 300 µM H_2O_2 for 10 min. Interestingly, when cells were pre-treated with 100 µM 8-pCPT-cGMP for 24 h to activate PKG, H_2O_2-induced SAPK/JNK phosphorylation was prevented in control osteoblasts, but cGMP had no effect in Prkg1 OB-KO osteoblasts (Fig. 4I). These results suggest that PKG1 has anti-oxidant properties in osteoblasts.

Fig. 4

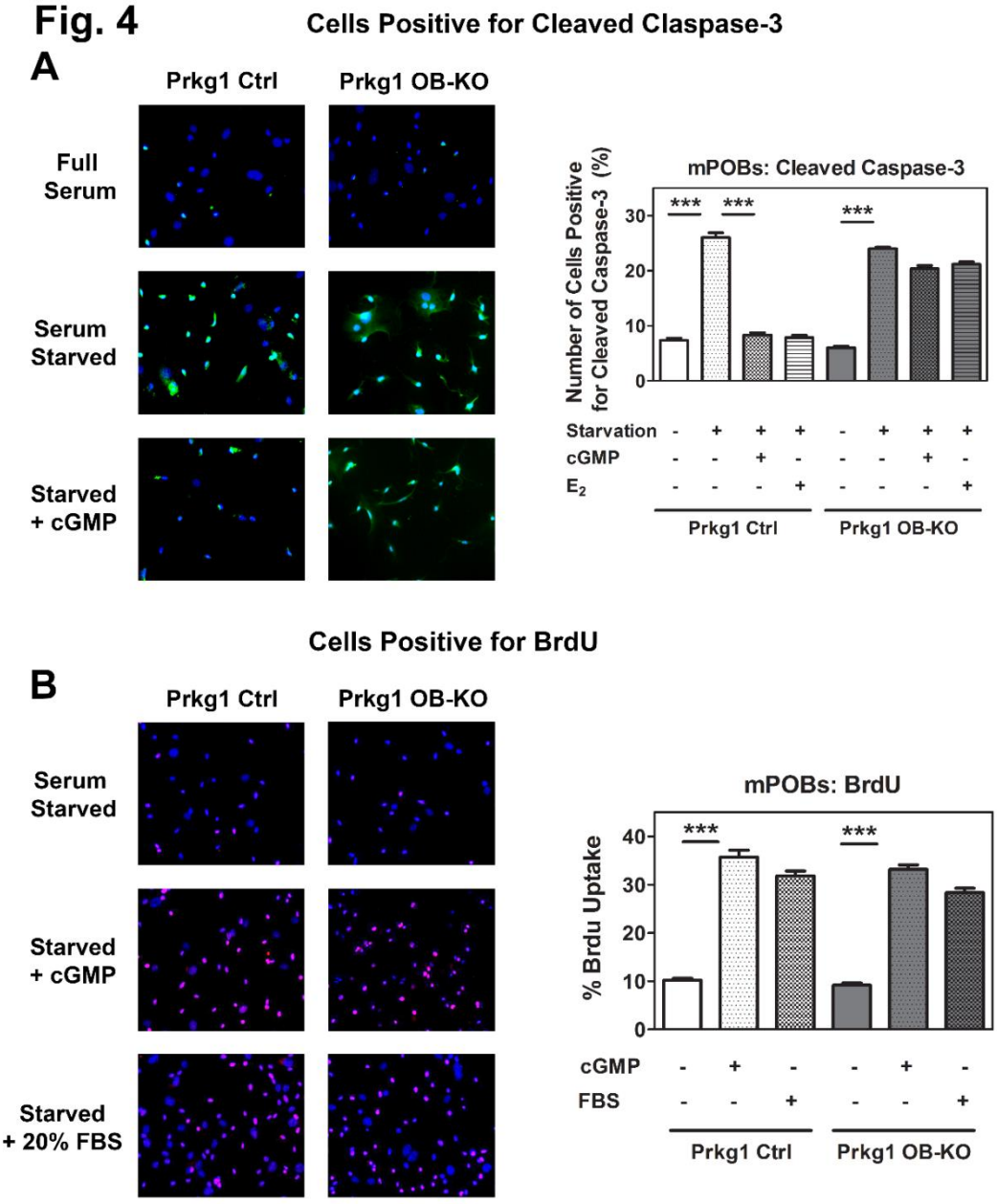
A
Cells Positive for Cleaved Claspase-3
Prkg1 Ctrl
Prkg1 OB-KO
Full Serum
Serum Starved
Starved + cGMP
mPOBs: Cleaved Caspase-3
Number of Cells Positive for Cleaved Caspase-3 (%)
***
***
***
Starvation
cGMP
E2
Prkg1 Ctrl
Prkg1 OB-KO
B
Cells Positive for BrdU
Prkg1 Ctrl
Prkg1 OB-KO
Serum Starved
Starved + cGMP
Starved + 20% FBS
mPOBs: BrdU
% Brdu Uptake
***
***
cGMP
FBS
Prkg1 Ctrl
Prkg1 OB-KO

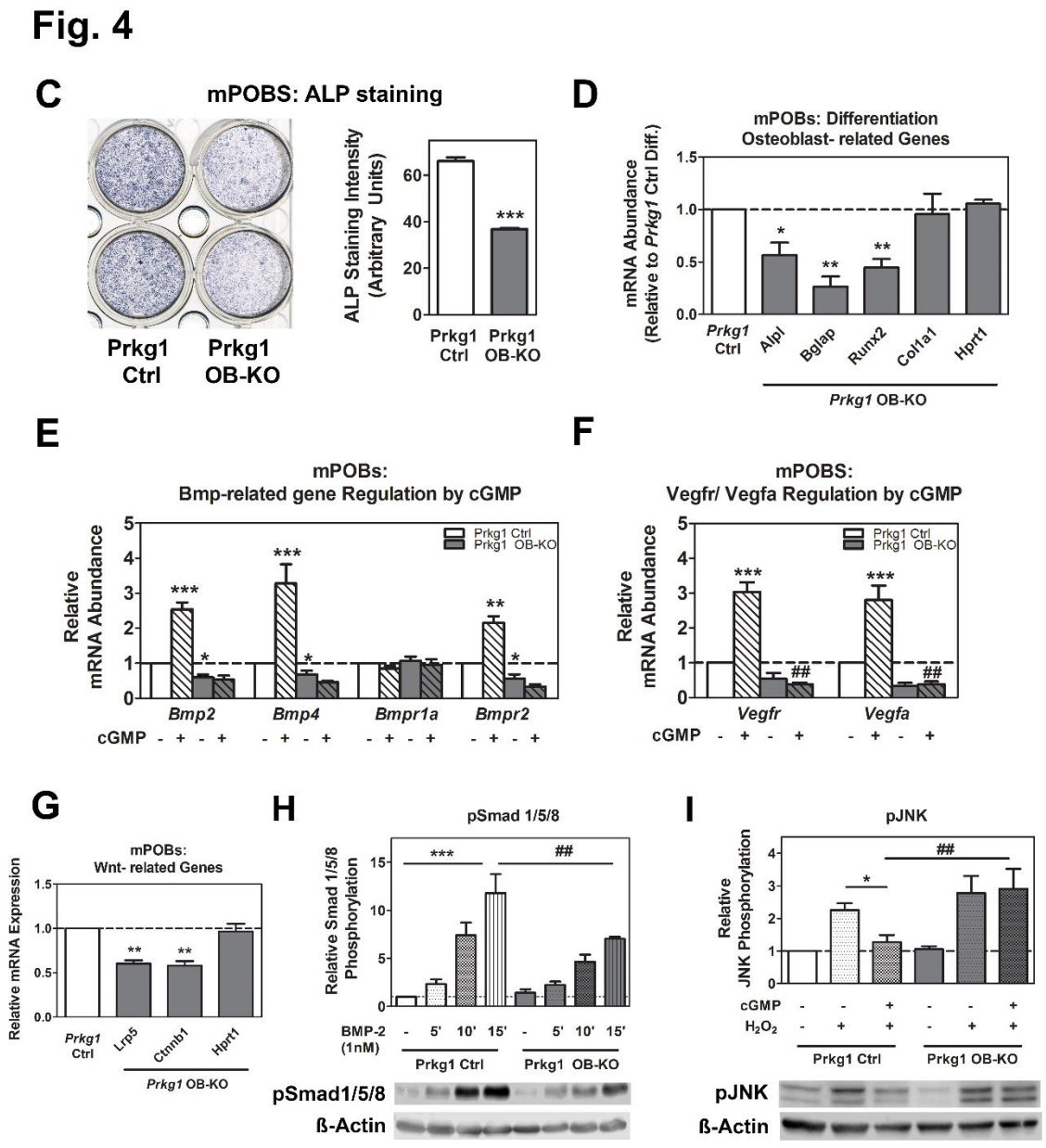

<u>Fig. 4:</u> PKG1-deficient osteoblasts show decreased apoptotic resistance, impaired BMP/Smad signalling, an altered oxidative stress response and reduced differentiation capacity (modified after Schall et al. 2020 Figure 3, 4 and 5, 113). POBs were isolated from eight week-old osteoblast-specific Prkg1 knockout (Prkg1 OB-KO n=3) and control (Prkg1 fl/fl n=3) mice. **(A)** POBs were serum-starved with 0.1% BSA for 24 h or kept in normal growth medium; apoptosis was detected by immunofluorescence staining for cleaved caspase-3 (green, nuclei counterstained with

Hoechst 33342). The percentage of cells staining positive for cleaved caspase-3 is shown, with >200 cells analysed per condition (means ± SEM of three independent experiments; ***p<0.001 for indicated comparisons) (89). **(B)** POBs were serum-starved with 0.5% FBS for 24 h, treated with either 100 µM 8-pCPT-cGMP (cGMP) or 20% FBS for 1 h, and then labeled with 200 µM BrdU for 16 h. BrdU incorporation into DNA was detected by immunofluorescence, with >200 cells analysed per condition. (mean of three experiments ± SEM; ***p<0.001 for indicated comparisons). **(C,D)** POBs were plated at high density and switched to differentiation medium after reaching confluency. After 14 d, cells were stained for ALP activity (C) and the relative mRNA abundance of *Alpl* (Alkaline phosphatase), *Bglap* (Osteocalcin), *Runx2* (Runt-related transcription factor 2) and *Col1a1* (collagen type I alpha) was quantified by qRT-PCR and normalized to two different housekeeping genes (18S, *Hprt1*). Data were calculated according to the ΔΔCt method, with the mean of the Prkg1 fl/fl group for each gene assigned a value of one. *Hprt1* was normalized to 18S. **(E-F)** POBs from control and Prkg1 OB-KO mice were cultured in medium containing 0.5% FBS for 24 h prior to receiving 100 µM 8-CPT-cGMP (cross-hatched bars) for 24 h. Vegf- and Bmp- related mRNAs were quantified and normalized to the mean level of untreated control cells (n=3 independent experiments). (E-F) Experiments performed by Hema Kalyanaraman. **(G)** Wnt-specific genes *Lrp5* and *Ctnnb1* was measured by qRT-PCR in control (white bar) and Prkg1 OB-KO mice (grey bars) and normalized as described in panel C. **(H)** POBs were serum-starved and treated with 1 nM BMP-2 for 5, 10 or 15 min. Western blots of cell extracts were analysed with a phospho-specific antibody for Smad1/5/8(pSer$^{463/465(426/428}$); β-actin served as a loading control. Panel G, H: Bar graphs summarize results from three independent experiments; means ± SEM; *p<0.05, **p/$^{\#\#}$p<0.01 and ***p<0.001 for indicated comparisons). **(I)** Serum-deprived POBs were treated with 100 µM 8-pCPTcGMP (+cGMP) for 24 h and then exposed to 300 µM H_2O_2 for 10 min. Western blots of cell extracts were analysed with a phospho-specific antibody for SAPK/JNK(pThr^{183} /pTyr^{185}); β-actin served as a loading control.

3.5 Cre-mediated deletion of Prkg1 in mPOBs from Prkg1 fl/fl mice

In order to further analyze effects of cGMP/PKG1 signaling pathway, I used early osteoblasts from long bones of homozygous *Prkg1* fl/fl mice to study the effect of PKG1 knockout after infection with adenovirus expressing Cre recombinase; infection with virus expressing green fluorescent protein (GFP) served as a control. This approach has the advantage that I could use a single cell preparation from *Prkg1* fl/fl mice to study the effect of CRE-mediated PKG1 knock-down and avoid possible variations between different primary osteoblast preparations. *Prkg1* mRNA expression and PKG1 protein were reduced by > 80% and > 60%, respectively, in CRE virus-treated compared to control virus-treated POBs. (Fig. 5A, B). The knock-down efficiency was similar to results obtained in bones and primary osteoblasts isolated from Prkg1 OB-KO and control mice (compare to Fig. 1D, E, F).

Differentiated POBs infected with adenovirus expressing GFP (Control) or Cre recombinase showed similar ALP activity after 14 d of differentiation (Fig. 5C) and mRNA expression of osteoblast-related genes was unchanged (Fig. 5D). This result differs from the result obtained with osteoblasts isolated from Prkg1 OB-KO mice (Fig. 4C and Fig.4D) and suggests differences in POB preparations or differences in the basal degree of differentiation of POBs isolated from Prkg1 OB-KO mice *versus* Prkg1 fl/fl mice.

However, when POBs from Prkg1 fl/fl mice were cultivated in differentiation medium with 1% FBS and were treated with 10 nM BMP-2 for 6 days, alkaline phosphatase (*Alpl*) mRNA expression increased by > 10-fold in cells infected with control virus, but only 5-fold in cells infected with CRE virus (Fig. 5D). These results are in agreement with our findings in osteoblasts from Prkg1 OB-KO mice, which showed decreased Smad phosphorylation in response to BMP-2 (Fig.4H).

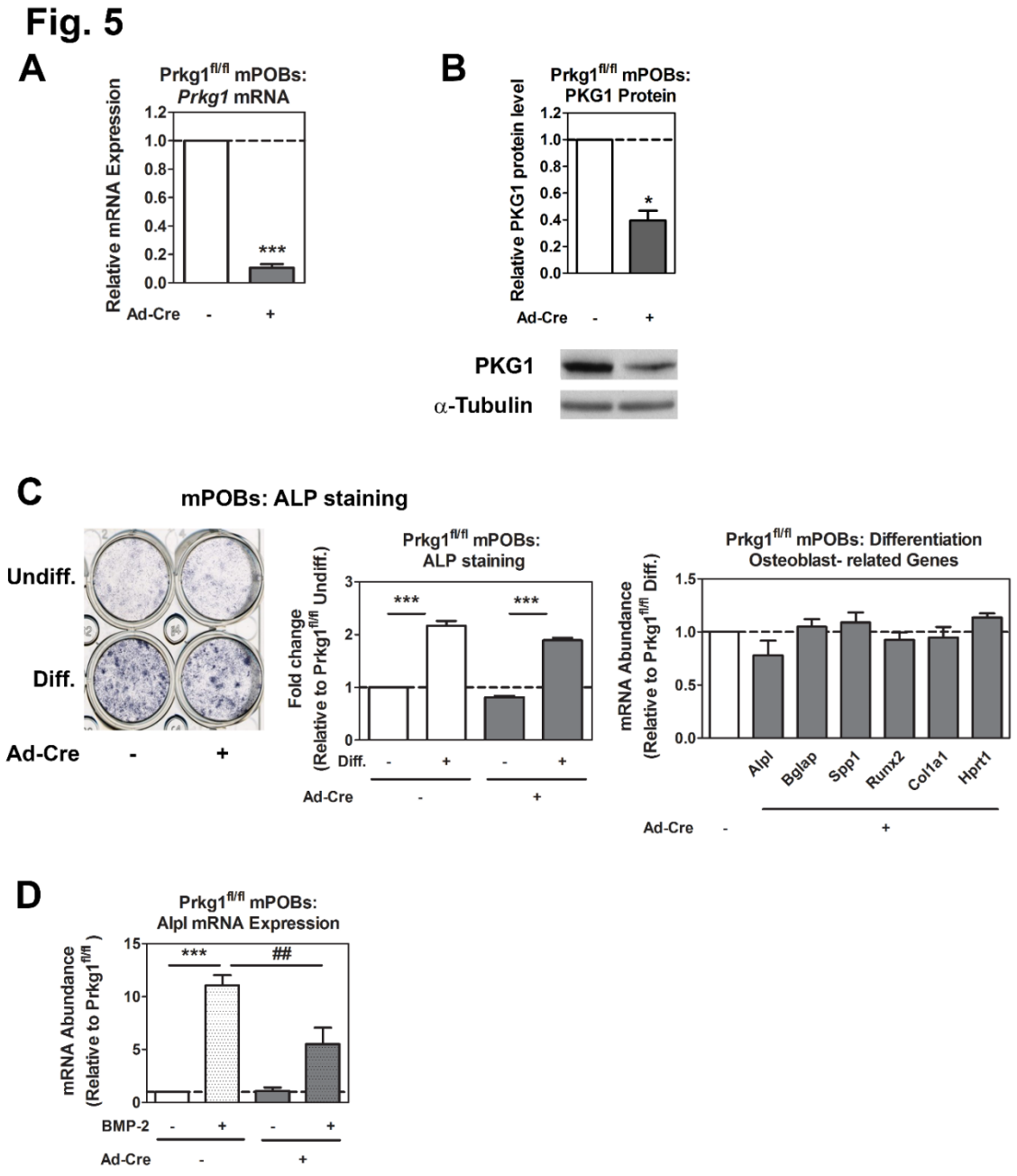

<u>Fig. 5:</u> Adenoviral Cre expression-mediated deletion of Prkg1 in mPOBs from Prkg1 fl/fl mice. *In vitro* knockout of Prkg1 in long bone murine primary osteoblasts using Adenovirus-Cre treatment. POBs isolated from mice homozygous for Prkg1 alleles flanked by loxP sites ("floxed" Prkg1 fl/fl) were infected with adenovirus expressing GFP (Control) or Cre recombinase (Cre) for 48 h (22). **(A,B)** Knockdown efficiency of Prkg1 was analysed by quantifying the relative amount of Prkg1 mRNA using qRT-PCR with a primer specific for exon 1/2 (A) and by Western blotting with a PKG1-specific antibody,

with tubulin serving as a loading control (B). **(C)** *In vitro* osteoblastic differentiation studies of POBs isolated from Prkg1 fl/fl mice and infected with control or Ad-Cre virus. Confluent murine POB (mPOB) cultures were induced to differentiate using 0.3 mM L-ascorbic acid (AA) and 5 mM β-glycerophosphate (ß-GP). Alkaline phosphatase (ALP) activity was assessed after 14 days by colorimetric assay (left panel). RNA was extracted from differentiated POBs, and the relative mRNA abundance of osteoblast-related genes was quantified by qRT-PCR and normalized to 18S as housekeeping gene. *Hprt1* was normalized to 18S (right panel). **(D)** BMP-2 induced *Alpl* gene expression. Prkg1 fl/fl mPOBs infected with control or Cre-virus for 48 hours were cultured in medium containing 0.5% FBS for 24 h prior to receiving 1 nM BMP-2 for 24 h. Data represent means ± SEM from three independent experiments; *$p<0.05$, **p/$^{\#\#}p<0.05$ and ***$p<0.01$ for the indicated comparisons.

3.6 PKG1-deficient bone marrow stromal cells show altered basal differentiation and reduced *Alpl* mRNA expression in response to BMP-2

To examine the role of PKG1 in osteoblast progenitors, I cultured bone marrow stromal cells (BMSCs) from control and Prkg1 OB-KO mice in osteoblastic differentiation medium. BMCSs isolated from Prkg1 OB-KO mice formed less alkaline phosphatase positive colonies in osteoblastic differentiation medium than BMSCs from control Prkg1 fl/fl mice, suggesting reduced differentiation capacity of PKG1-deficient osteoblast precursors (Figure 6A) (113). I found the same number and size of colonies staining positive for Alizarin Red staining of mineralizing colonies (Fig. 6B). Previous workers studied effects of BMP-2 on osteoblastic differentiation of bone marrow-derived stromal cell lines and found BMP-2 stimulated ALP activity in ST2 cells (91). I isolated BMSCs from Prkg1 Control and Prkg1 OB-KO mice, switched them to osteoblastic differentiation medium containing 3% FBS, and treated them with 10 nM BMP-2 for 7 days (Fig. 6C). In the presence of BMP, control BMSCs showed a two-fold higher *Alpl* mRNA expression compared to cells cultured in the absence of BMP; in contrast, BMP did not stimulate ALP mRNA expression in BMSCs from Prkg1 OB-KO mice. Thus, BMP signaling in BMSCs was dependent on PKG1, similar to results found in POBs.

Fig. 6

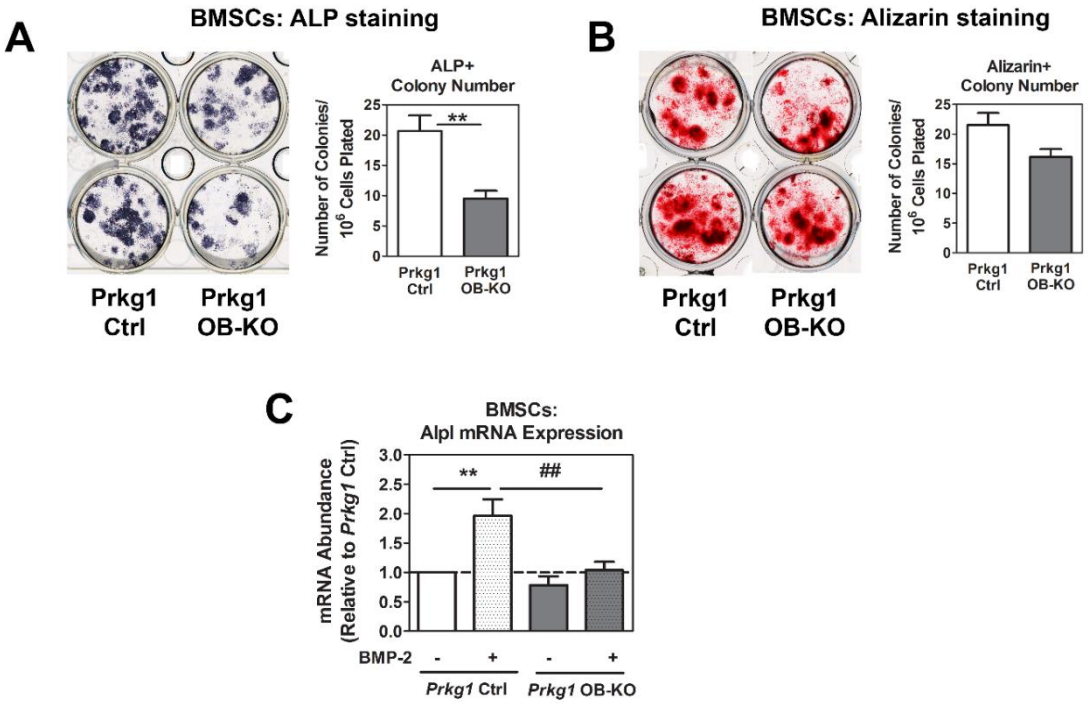

Fig. 6: PKG1-deficient bone marrow stromal cells show altered basal differentiation and reduced *Alpl* mRNA expression in response to BMP-2 (modified after Schall et al. 2020 Figure 3 and Suppl. Figure 4, 113). BMSCs were isolated from eight week-old Prkg1 knockout (Prkg1 OB-KO n=3) and control (Prkg1 Ctrl n=3) mice. **(A,B)** Bone marrow mononuclear cells were plated at 4 x 10^5 cells/cm^2, and adherent stromal cells (BMSCs) were switched to osteoblastic differentiation medium for 14 d (A) or 21 d (B). BMSC colonies were stained for alkaline phosphatase activity after 14 d (A), and mineralization was assessed by Alizarin Red staining after 21 d (B). **(C)** BMSCs were switched to osteoblastic differentiation medium containing 3% FBS, and some cells received 10 nM BMP-2 for 7 d. The relative mRNA abundance of *Alpl* was quantified by qRT-PCR. Data were calculated according to the ΔΔCt method, with the mean of the Prkg1 fl/fl group for each gene assigned a value of one. Data represent means ± SEM; *p<0.05 and **p/$^{\#\#}$p<0.01 for the indicated comparisons.

3.7 PKG1 is required for bone regeneration in male mice

Bone regeneration after an injury such as a fracture involves formation of a hematoma at the site of injury with generation of growth factors and cytokines; this leads to an inflammatory response necessary for recruitment of mesenchymal stem cells (65). These cells proliferate and differentiate to chondroblasts/cytes and form cartilage (endochondral phase of bone formation). The cartilage mineralizes and mechanically stabilizes the fracture site, but is later removed by the action of osteoclasts and replaced by bone. Cells along the periosteum differentiate into osteoblasts to produce the new bone; transition from cartilage to bone is linked to increased angiogenesis and requires vascular endothelial growth factor (VEGF) produced by osteoblasts (66). Growth factors most important for fracture healing include Wnts, bone morphogenic proteins (BMPs), and VEGF; (88) osteoblast production of all three factors is increased by cGMP, and signaling downstream of the corresponding receptors involves NO/cGMP either directly or indirectly, via positive cross-talk with NO/cGMP/PKG (4). Since bone fracture models in mice are difficult to standardize and associated with prolonged discomfort to the animals, I studied bone regeneration in an alternative model, using a 0.8 mm burr hole placed in the anterior tibial cortex of Prkg1 OB-KO and control mice. The well-defined small bone defect was set under anesthesia, and male mice (Fig. 7) or female mice (Fig. 10) were euthanized 10 days later to examine bone regeneration in the injured tibia by (a) micro-CT analysis, (b) immunohistochemistry and (c) histomorphometry of the regenerating bone. I investigated bone regeneration in male and female Prkg1 Control and Prkg1 OB-KO mice and randomized another cohort of female Prkg1 Control and Prkg1 OB-KO mice to receive (a) vehicle or (b) cinaciguat for eight consecutive days after surgery (Fig. 10).

Micro-CT was used to quantify the newly formed bone in the defect at this stage. Lateral views of the 3D reconstruction of injured tibia showed less mineralized tissue in 10 d old bone defects of Prkg1-deficient male mice (Prkg1 OB-KO), than of controls (Fig. 7B). In Prkg1 OB-KO male mice, trabecular bone volume (BV/TV, -35.2%) and bone mineral density (BMD, -20%) was decreased in the defect hole region (Fig. 7C) and mineralized bone in defects of Prkg1 OB-KO mice showed increased trabecular separation (Tb.Sp, +38%) and decreased trabecular number (Tb.N, -30%); however,

trabecular thickness (Tb.Th) was not significantly altered (Fig. 7C). Longitudinal paraffin sections of right tibiae (5 µm) were cut through the hole region and stained with Masson Trichrome. An area of 200 µm x 500 µm between the two cortical bone ends (CB) was analysed (a 0.1 mm^2 "region of interest" marked by the black rectangle). Collagen content (% of hole region stained by Aniline blue) and the number of osteoblasts was decreased by 38% and 17%, respectively, in this region of interest (an area of 0.1 mm^2) (Fig. 7D).

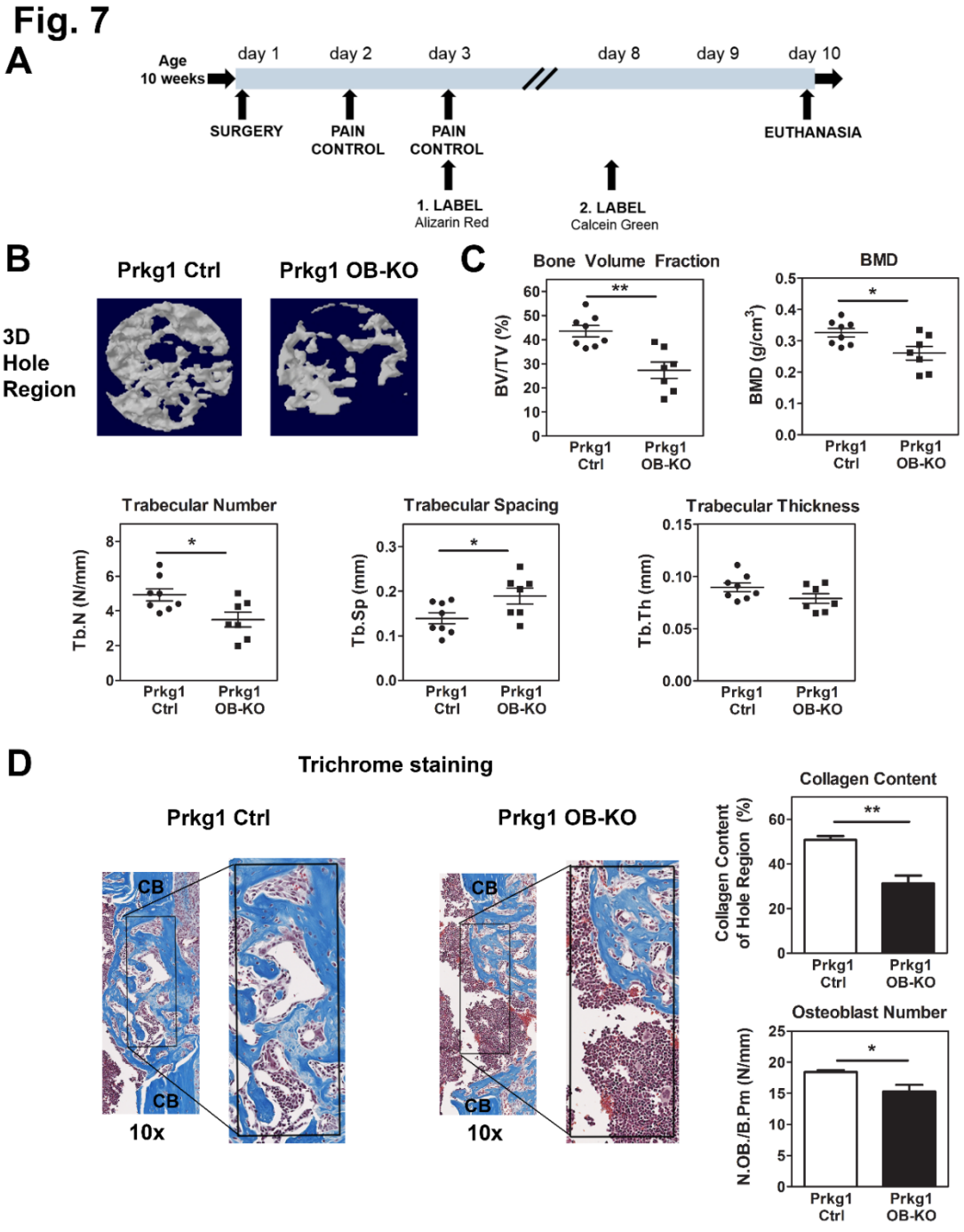

Fig. 7: PKG1 is required for bone regeneration in male mice (modified after Schall et al. 2020 Figure 2, 113). **(A)** Time line of *in vivo* experiments examining bone regeneration in a monocortical defect model. Ten-week-old male mice were placed under general anesthesia by i.p. injection of 100 mg/kg ketamine and 10 mg/kg xylazine. The lateral aspect of right tibia was exposed, carefully cleared of overlying soft tissues and a monocortical osseous hole (0.8 mm diameter) was created on the anterior surface of the tibia using a round burr attached to a dental drill (66). After surgery, mice received s.c. injection of 0.05–0.1 mg/kg buprenorphine for analgesia. Mice received alizarin complexone injection 7 days and calcein injection 2 days prior to euthanasia. **(B)** 3D reconstruction of mineralized bone formed in hole region imaged by micro-CT. **(C)** 3D structural parameters — trabecular bone volume fraction (BV/TV), bone mineral density (BMD), trabecular number (Tb.N), trabecular spacing (Tb.Sp), and trabecular thickness (Tb.Th) — of mineralized bone formed in the hole region was analysed by micro-CT as described in Methods; Prkg1 Ctrl n=8, Prkg1 OB-KO n=7. **(D)** Fixed tibiae were decalcified in 0.5 M EDTA (pH 8.0) for 7 days and embedded in paraffin. Longitudinal sections (5 µm) were cut through the hole region and stained with Trichrome. An area of 200 µm x 500 µm between the two cortical bone ends (CB) was analysed (a 0.1 mm^2 "region of interest" marked by the black rectangle). Collagen content (% of hole region stained by Aniline blue) was measured using ImageJ (upper panel). Osteoblasts attached to newly formed bone were counted in the hole region (lower panel). Panel (C) shows means ± SD; *$p<0.05$ and **$p<0.01$ for the indicated pair-wise comparisons by Student´s *t* test (with similar results by Wilcoxon rank-sum test). Panel (D) shows means ± SEM of Prkg1 Ctrl n=5 and Prkg1 OB-KO n=6 mice; *$p<0.05$ and **$p<0.01$ for the indicated comparisons by two-sided t-test. Black rectangle: hole region, 200 µm x 500 µm.

3.8 PKG1 in osteoblasts regulates capillary density, BMP-dependent Smad phosphorylation and osteoclast number in regenerating bone

Immunostaining at postsurgery day 10 (PSD10) was performed on longitudinal tibial sections (5 μm) of the hole region. Sections were incubated with primary antibodies against CD31 and pSmad1/5/9, stained with an HRP-coupled secondary antibody and DAPI substrate. At PSD10, micro blood vessel (capillary) density, calculated based on the number of anti-CD31-positive cell clusters in the defect hole region, was reduced by 60% in Prkg1 OB-KO mice compared with control Prkg1 littermates (Fig. 8A). Single CD31 immunoreactive endothelial cells and clusters separate from other microvessels (red arrow heads) were counted as individual capillaries. To examine BMP signaling in the regenerating bone, I also assessed the number of phospho-Smad1/5/9-positive cells in the hole region (area 0.1 mm^2). Brown cells/nuclei, indicated by red arrows, represent cells/nuclei stained with a phosphor-Smad1/5/9 (Ser 463/465/467)-specific antibody (Fig. 8B). The number of pSmad1/5/9+ osteoblastic cells was lower by 33% in defects of Prkg1 OB-KO mice compared to Prkg1 Control mice (Fig. 8B).

Osteoclasts were detected by staining for tartrate-resistant acid phosphatase (TRAP; TRAP+ osteoclasts are red/brown-stained multinucleated cells indicated by red arrow heads). Relatively few TRAP+ osteoclasts were recruited into the defects, and the number of osteoclasts was decreased by 42% in Prkg1 OB-KO mice compared to control mice (Fig. 8C). The differences in the numbers of CD31+, pSmad1/5/9+ and tartrate-resistant acid phosphatase–positive (TRAP+) cells between the two different genotypes (Fig. 8 A-C) suggest that the impaired bone repair in Prkg1 OB-KO mice at PSD10 is likely caused by a reduced angiogenic response, impaired BMP/pSmad1/5/9+ signaling and decreased osteoclast recruitment.

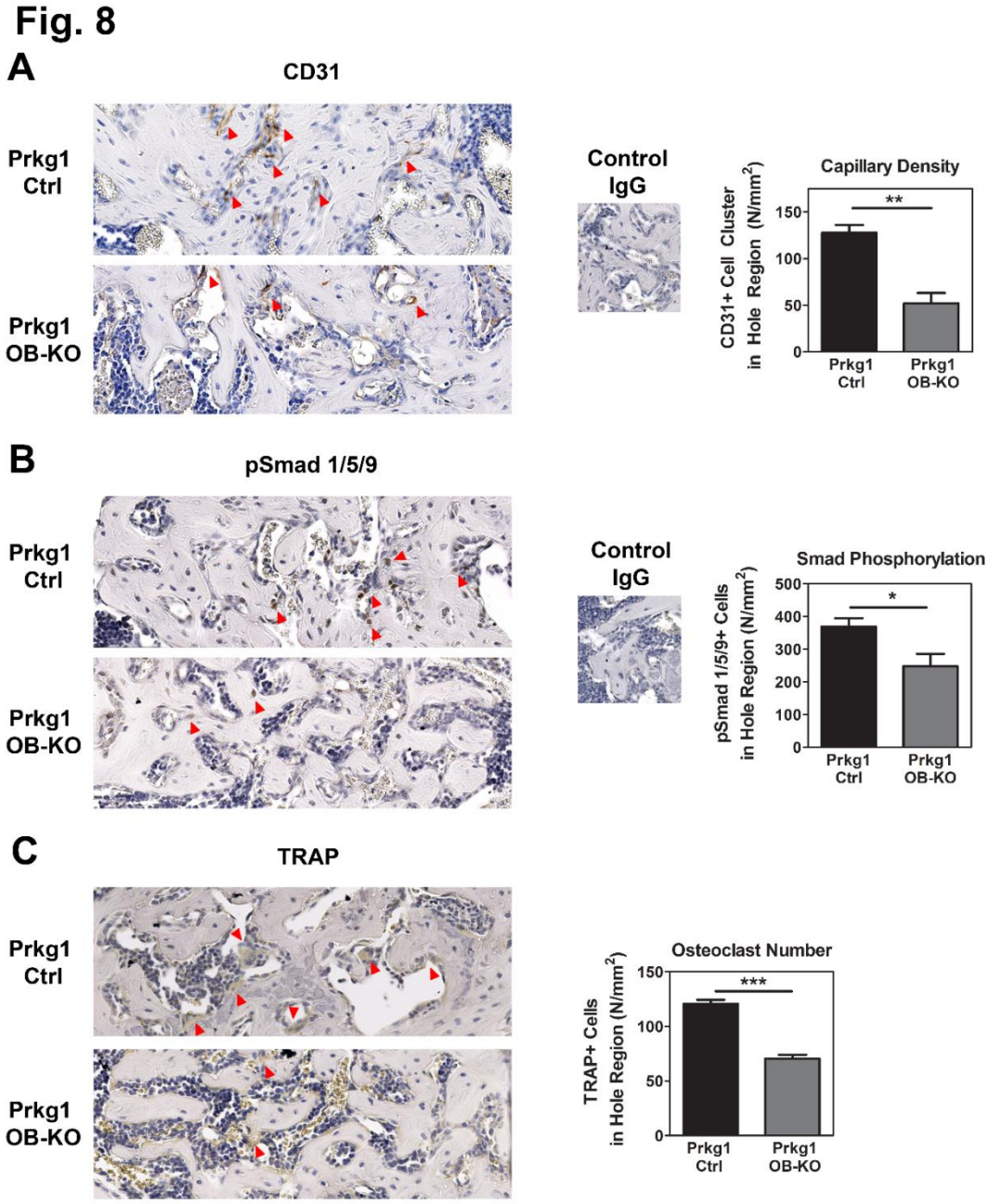

Fig. 8: PKG1 in osteoblasts regulates capillary density, BMP- dependent Smad phosphorylation and osteoclast number in regenerating bone (modified after Schall et al. 2020 Figure 2 and 4, 113). Immunostaining was performed on longitudinal tibial sections (5 µm) of the hole region. Sections were incubated with primary antibodies against CD31 and pSmad1/5/9, stained with an HRP-coupled secondary antibody and DAPI substrate. **(A)** Blood vessel (capillary) density was calculated based on anti-CD31 staining. Single CD31 immunoreactive endothelial cells and clusters separate from other

microvessels (red arrow heads) were counted as individual capillaries. The total number of microvessels in the hole region (as defined in Fig. 6D, area 0.1 mm^2) was counted to calculate capillary density (N/mm^2). **(B)** Brown cells/nuclei, indicated by red arrows, represent cells/nuclei stained with a phosphor-Smad1/5/9 (Ser 463/465/467)-specific antibody. The number of phospho-Smad1/5/9 positive cells was counted in the hole region (area 0.1 mm^2). **(C)** A commercial TRAP staining kit (Sigma) was used to detect osteoclasts (red/brown-stained multinucleated cells indicated by red arrow heads) as described in manufacturer's instructions. Panel (A-C) shows means ± SEM of Prkg1 Ctrl n=4 and Prkg1 OB-KO n=5 mice; *p<0.05, **p<0.01 and ***p<0.001 for the indicated comparisons by two-sided t-test.

3.9 Osteoblast-specific PKG1 knockout mice show a different bone formation pattern and a reduced volume of regenerating bone in the monocortical defect model

10-week old male Prkg1 Ctrl and Prkg1 OB-KO mice underwent tibial monocortical defect surgery under general anesthesia. Seven and two days before sacrifice, mice underwent i.p. injection of Alizarin Red complexone and Calcein Green, respectively, to label newly synthesized bone. Ten days post-surgery, murine tibia were isolated, formalin-fixed, KOH-treated, and trimmed to 2mm x 2mm x 2mm blocks containing the hole region with regenerating bone. Samples were dehydrated and embedded in modified Spurr resin (20% Sudan Black) prior to 3-D imaging at 10x with Digital Volumetric Imaging (DVI) (described in Methods). The first image (z1) in panels A, B shows the tibial crosssection at the top of the defect, the following images (z101 – z901) show the progress inside the hole region every hundred slices to the distal part of the tibia (z=depth). Osteoblast-specific PKG1 knockout mice showed a different bone formation pattern e.g. less calcein and amplex red incorporation into newly formed bone in the hole region and covering the surrounding cortex, a reduced volume of regenerating bone and less osteoblast activity in the monocortical defect model (Fig. 9 B, z301-z701).

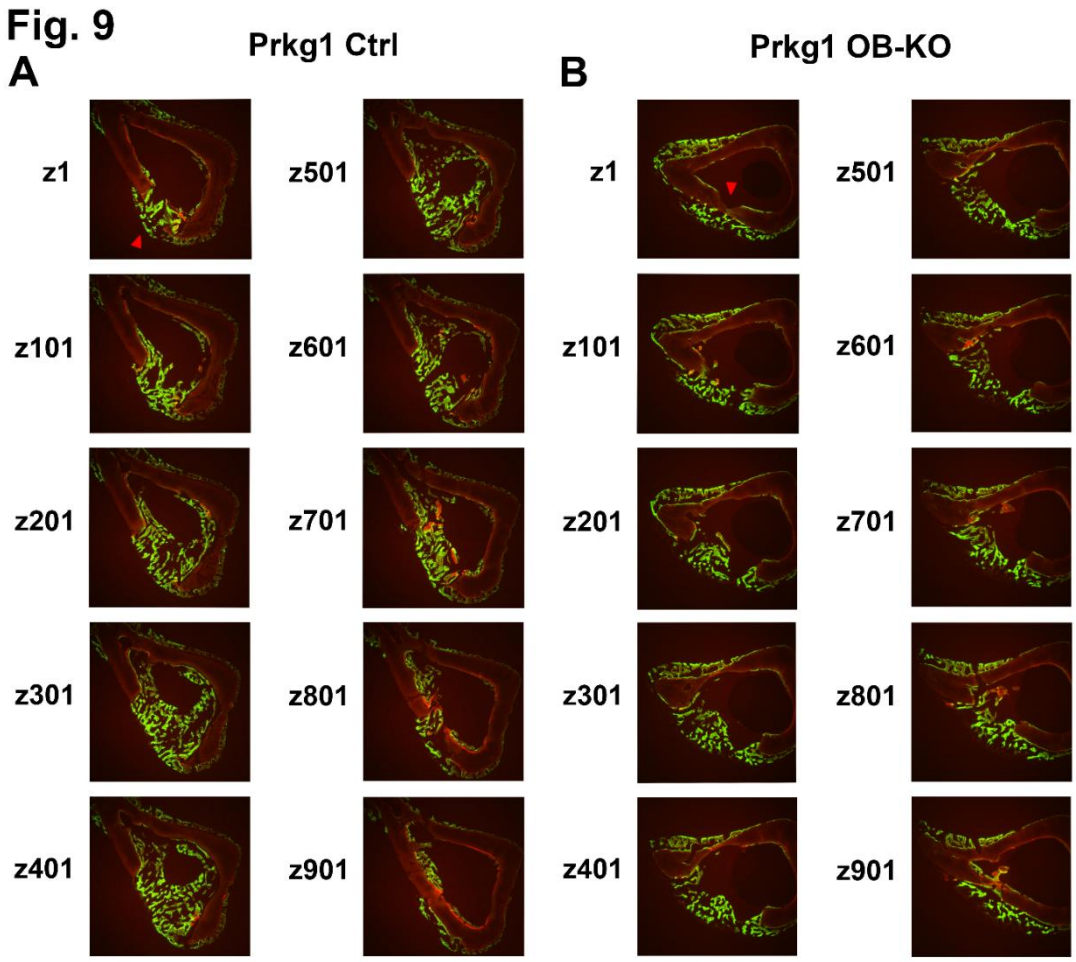

Fig. 9: Osteoblast specific PKG1 knockout mice show a different bone formation pattern and a reduced volume of regenerating bone in the monocortical defect model. Digital Volumetric Imaging (DVI), directly images the cut surface of a specimen and electronically captures a high-resolution picture. A series of cuts and images are captured that can be reconstructed to a 3D sample. **(A,B)** 10-week old male Prkg1 Ctrl and Prkg1 OB-KO mice underwent tibial monocortical defect surgery under general anesthesia. Seven and two days before sacrifice, mice underwent i.p. injection of Alizarin Red complexone and Calcein Green, respectively, to label newly synthesized bone. Ten days post-surgery, murine tibia were isolated, formalin-fixed, KOH-treated, and trimmed to 2mm x 2mm x 2mm blocks containing the hole region with regenerating bone. Samples were dehydrated and embedded in modified Spurr resin (20% Sudan Black) prior to imaging at 10x with DVI. From the 3-D data, summary slides with selected cross-sections of the 3-D histology are shown. A series of 3500 x 0.88 µm sections were imaged starting within the central portion of the tibial shaft cutting towards the distal tibia. The first image (z1) in panels A, B shows the tibial crosssection at the top of the

defect, the following images (z101 – z901) show the progress inside the hole region every hundred slices to the distal part of the tibia (z=depth). Hole region indicated by red arrow heads.

3.10 Cinaciguat enhances bone regeneration in female control mice (Prkg1 Ctrl), but not in the osteoblast-specific Prkg1 knockout mice

The group of Dr. Pilz showed previously, that the NO/cGMP/PKG pathway mediates some of the anabolic effects of estrogens in osteoblasts and osteocytes, leading me to hypothesize that cGMP-elevating agents may have bone-protective effects (40, 92). Cinaciguat, a prototype of a novel class of soluble guanylate cyclase activators, was tested in a monocortical defect mouse model for bone regeneration. I investigated general bone regeneration in female Prkg1 Control and Prkg1 OB-KO mice and randomized another cohort of female Prkg1 Control and Prkg1 OB-KO mice to receive (a) vehicle or (b) cinaciguat for eight consecutive days after surgery (Fig. 10). Micro-CT was used to quantify the newly formed bone in the defect at this stage. Lateral views of the 3D reconstruction of injured tibia showed a trend to less mineralized tissue in defects of Prkg1-deficient female mice (Prkg1 OB-KO), than of controls (Fig. 10B). In Prkg1 OB-KO female mice, trabecular bone volume and bone mineral density was not altered in the defect hole region (Fig. 10C), while cinaciguat treatment significantly improved bone microarchitecture in regenerating bone of female control mice (Prkg1 Ctrl) as seen in the 3D lateral view (Fig. 10D) and trabecular bone volume and bone mineral density changes by 33% and 10%, respectively (Fig. 10E).

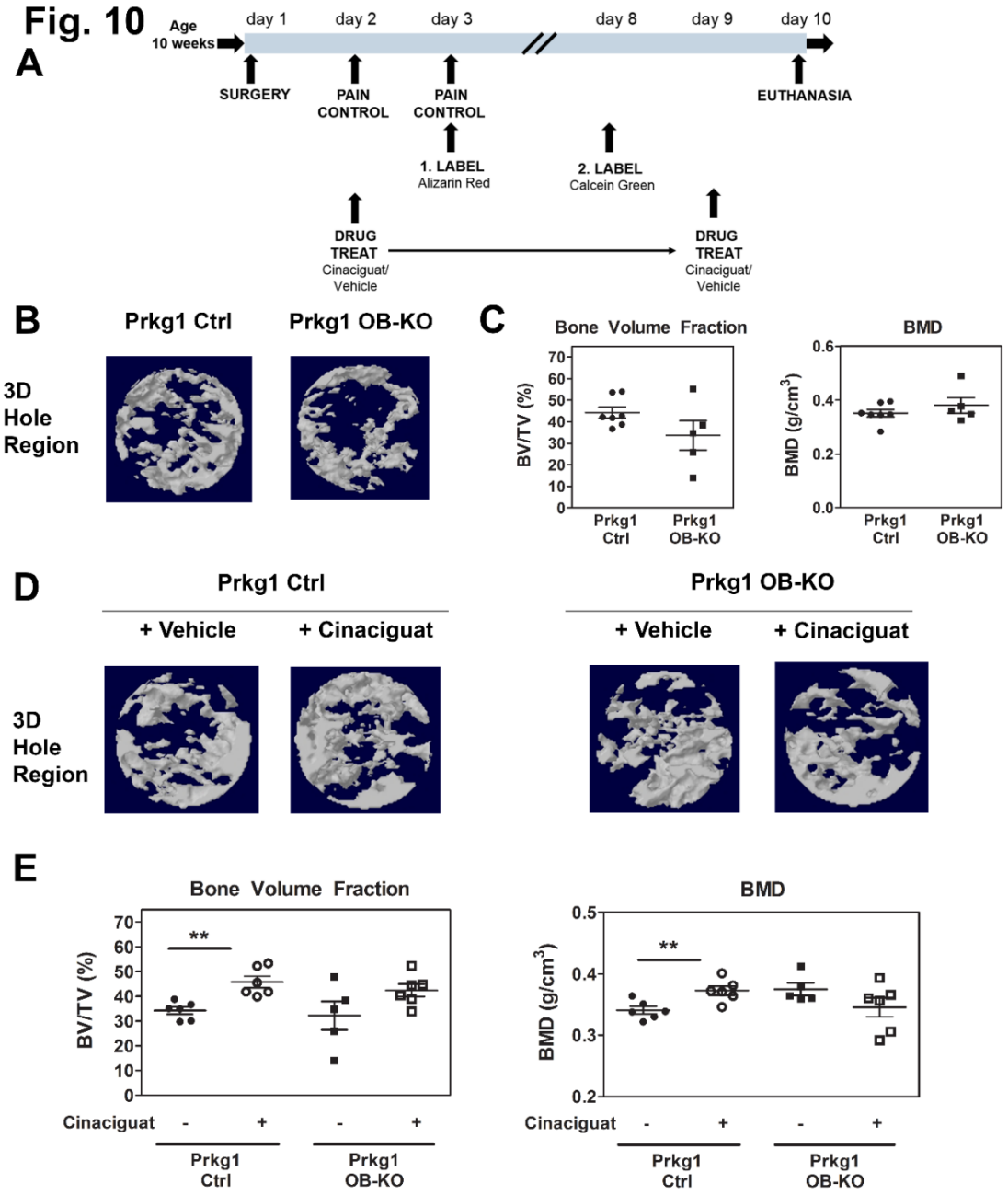

<u>Fig. 10:</u> Cinaciguat enhances bone regeneration in female control mice (Prkg1 Ctrl), but not in the osteoblast-specific Prkg1 knockout mice (modified after Schall et al. 2020 Suppl. Figure 5, 113). **(A)** Time line of the experiment. Ten-week-old female mice were placed under general anesthesia, and a monocortical osseous hole was created on the anterior surface of the tibia as described in Fig. 6. Starting the day after surgery, the mice were injected into the peritoneal cavity with vehicle (0.1% DMSO in 0.9% NaCl) or Cinaciguat (10 µg/kg/d in 0.1% DMSO) for 8 d. Mice received alizarin complexone

injection 7 d and calcein injection 2 d prior to euthanasia. **(B,D)** 3D reconstruction of mineralized bone formed in hole region by micro-CT. **(C,E)** 3D structural parameters — trabecular bone volume fraction (BV/TV) and bone mineral density (BMD) — of mineralized bone formed in hole region was analysed by micro-CT in untreated female mice (C) and female mice treated with either vehicle or cinaciguat (E). For Panel B-C, Prkg1 Ctrl n=7, Prkg1 OB-KO n=5; for panel D-E, Prkg1 Ctrl vehicle-treated n=6, Prkg1 Ctrl cinaciguat-treated n=6, Prkg1 OB-KO vehicle-treated n=5 and Prkg1 OB-KO cinaciguat-treated n=6. Panel (C,E) shows means ± SD; *$p<0.05$ and **$p<0.01$ for the indicated pair-wise comparisons by Student´s *t* test (with similar results by Wilcoxon rank-sum test).

DISCUSSION

4.1 A novel Osteoblast-specific Prkg1 Knockout Mouse

Global *Prkg1* knockout mice have a significant reduced lifespan with defects in the relaxation of vascular and visceral smooth muscle cells, disturbed platelets and red blood cells, which limits the availability of adult mice (32, 96).

To circumvent the problems of global Prkg1 knockout, a novel tissue-specific Prkg1 knockout mouse was designed by crossing mice carrying floxed Prkg1 alleles with transgenic mice expressing CRE recombinase under the control of a 2.3-kb type I collagen promoter *(Col1a1-Cre)*. The latter promoter drives Cre expression at high levels in osteoblasts throughout their differentiation, starting after embryonic day 14.5 (77). Specific and efficient knockout of PKG1 in osteoblasts isolated from Prkg1-OB-KO mice was confirmed, with similar decreases found in bones from these mice. Tissue-specific deletion of the transgene was shown, and *Prkg1* mRNA expression and PKG1 protein levels were decreased by >80% in knockout compared to control POBs. PCR analysis of genomic DNA extracted from multiple organs of control and knockout mice showed amplification of a specific product after homologous recombination in the knockout mouse, in bone, but not in other organs. Slight imbalances in the expected Mendelian ratio for PKG1-osteoblast specific male (-4.5%) and female (+4.5%) knockout mice were observed. Germline recombination has been reported in transgenic mice expressing Cre recombinase under the control of the 2.3 kb and 3.6 kb rat *Col1a1* promoter (93). Therefore Col1a1-Cre might be active in germ cells of PKG1 knockout mice with, e.g. influencing sperm activity or gender determining pathways. Immunohistochemical staining for PKG1 and PKG2 in tibial sections showed loss of PKG1 expression in lining osteoblasts in Prkg1 OB-KO mice, with unchanged PKG2 expression in the same mice.

The exact role of PKG1 for bone development and regeneration *in vivo* has never been investigated due to severity of the phenotype of global PKG1 knockout mice. Global PKG1 deletion in mice show no overt skeletal abnormalities, but the mice have severe gastrointestinal dysmotility with many of the mice dying at the time of weaning, and the surviving animals suffering from malnutrition (34). Young (Eight week-old) osteoblast-

specific Prkg1 knockout mice had normal body weights, tibial length and growth plate architecture, and normal trabecular and cortical bone micro-architecture with no gender-specific differences, consistent with specificity of the 2.3 kb fragment of the murine Col1a1 promoter for cells of the osteoblastic lineage (89, 93). In contrast, *Prkg2* osteoblast-specific knockout mice show decreased trabecular bone volumes in males, but not in females (unpublished data). Expression of an osteoblast-specific $prkg2^{RQ}$ transgene in male mice, produced increased trabecular bone volumes and bone mineral density at two, three, and six months of age, whereas this phenotype was not evident in two month-old female mice, and at 6 months, only about 20-30% of transgenic females had higher trabecular bone volume and BMD than their wild type littermates (89).

Reduced osteoblast activity was observed, as reflected by decreased bone formation rates and decreased expression of *Bmp2/4* and *Vegf*, and altered osteoblastic gene expression in tibiae of Prkg1 OB-KO mice compared to control mice (113). Although these deficiencies were not sufficient to affect bone microarchitecture under basal, non-stressed condition, they did impair bone healing after drill-hole injury that stimulates a stable bone fracture (113). Analysis of the bone phenotype of older Prkg1 OB-KO mice may be of particular interest for future studies. The changes in bone formation rates were modest compared to those measured in mice with transgenic overexpression of PKG2 (showed increase of >200%) (89). No decrease in the number of osteoblasts in Prkg1 OB-KO mice was found, suggesting that the decreased bone formation rates were from decreased osteoblast activity rather than number. Previous studies have shown that PKG2 rather than PKG1 controls osteoblast proliferation, confirmed in this study by showing normal proliferative activity of POBs from Prkg1 OB-KO mice. A decrease in osteoblastic gene expression and a trend to lower RANKL/OPG ratio was observed, without detectable changes in the number of osteoclasts under basal conditions.

Next, the effect of PKG1 deficiency on osteoblast apoptosis and differentiation was investigated. Previously Marathe et al., showed the importance of PKG1 and PKG2 in mediating the anti-apoptotic effects of estrogens in osteoblasts (15). Consistent with these results, PKG1-deficient osteoblasts show the same degree of apoptosis after serum starvation as control osteoblasts, but only control cells, and not PKG1-deficient cells, are protected from apoptosis by cGMP or estradiol treatment. My hypothesis was, that PKG1 deficiency might influence osteoblast differentiation, since others have reported that

cGMP-elevating agents can enhance differentiation of calvarial osteoblasts (mice/rat) and MC3T3-E1 cells (25), as shown by increased alkaline phosphatase activity. A reduction in *Bglap, Alpl* and *Runx2* mRNA expression in PKG1-deficient compared to control osteoblasts was found, and PKG1-deficient osteoblasts showed less staining capacity for alkaline phosphatase activity. The group of Dr. Pilz has previously shown, that pharmacologic or genetic activation of the NO/cGMP/PKG signaling cascade increases ß-catenin signaling and expression of Wnt-related genes in POBs (22, 37). A significant decrease of these genes in Prkg1 OB-KO osteoblasts was also found, suggesting that PKG1 is involved in regulating Lrp5/ß-catenin mRNA.

Previous workers have shown cross-talk between NO/cGMP/PKG signaling and signaling downstream of BMP and VEGF receptors. Moreover, BMP-2 and BMP-4 were shown to favour angiogenesis by stimulating the secretion of VEGF in osteoblasts (94). During bone formation and fracture healing there is a close cooperation between endothelial cells and osteoblasts. Osteogenic factors, such as BMP-2, are released from sprouting blood vessels, to promote osteoblast differentiation and mineralization, and in turn, maturing osteoblasts generate angiogenic factors, such as VEGF, to further support angiogenesis (107, 114-116). Specifically, VEGF binding to its receptors increases NO synthesis and activates PKG-pathways (95) and in turn treatment of smooth muscle and other cells with NO donors increases VEGF mRNA expression. PKG1 was identified as a downstream effector of VEGFR2 in endothelial cells (95). The described results show that VEGF and BMP production in osteoblasts are regulated by PKG1. Induction of VEGF-A and VEGF-R mRNA by CPT-cGMP or Cinaciguat treatment in control osteoblasts was shown, but not in the Prkg1 OB-KO cells. Similarly, BMP-2/4 and BMPR2 were upregulated by Cinaciguat or cGMP, while BMPR1 stayed stable. PKG1 deficiency also affects BMP signaling downstream of BMPR2 and PKG1 is required for maximal Smad phosphorylation in myoblasts (C2C12 cells) (81). Consistent with these findings in C2C12 cells, reduced Smad phosphorylation in response to BMP treatment in PKG1-deficient osteoblasts was shown. The decrease in BMP2/4 ligand mRNA expression might be caused, in part, by a feedback loop of Smads regulating the BMP promotors. BMP-2 is known to enhance osteoblastic differentiation of BMSCs (97). Following, effects of BMP in osteoblasts and bone marrow stromal cells were investigated. Reduced osteoblastic differentiation potential was found, shown by the lower number of colonies staining positive for ALP activity, whereas the same intensity

for Alizarin red staining of mineralizing colonies. The osteogenic phenotype in control osteoblasts and BMSCs was significantly increased by BMP-2 treatment.

4.2 PKG1 requirement for bone regeneration

Since the basal skeletal phenotype of Prkg1 OB-KO mice was mild, the role of PKG1 in a bone regeneration model was examined, using a monocortical defect. Bone fracture models in mice are difficult to standardize and associated with prolonged discomfort to the animals, a tibial monocortical defect model was used instead, as a simplified model of stable fractures. Bone healing after such an injury occurs predominantly via primary ossification with direct differentiation of mesenchymal progenitor cells into osteoblasts (66). I hypothesized that defective NO/cGMP/PKG signaling in osteoblast-specific *Prkg1* knockout mice might impair fracture healing and vasculargenesis because of reduced BMP- and VEGF-signaling. Moreover, increasing cGMP generation with cinaciguat might enhance bone regeneration in Prkg1 Control mice by increasing BMP- and VEGF-production by osteoblasts. The regulation of bone regeneration by PKG1 likely involves VEGF- and BMP-signaling, as both of these pathways are required for bone healing and were impaired in *Prkg1* OB-KO mice. Based on various animal studies and pre-clinical trials, clinical studies have been performed to demonstrate the efficiacy of BMPs in accelerating bone regeneration and fracture healing. Implantation of recombinant rhBMP-2 in a collagen sponge of non-union fractures led to a significantly higher union rate, improved wound healing and reduced infection rate (98). Previous studies have also documented the importance of NO/cGMP/PKG1 signaling for VEGF production and angiogenesis. PKG1 mediates the generation of new vessels through local expansion of mature endothelial cells and increases tube formation downstream of VEGF (95, 96). BMP-2/4 may act synergistically with VEGF to enhance bone regeneration (108, 109). *Prkg1* OB-KO mice expressed less *Vegfa* and *Vegfr1* mRNA than control mice in bones and primary osteoblasts - PKG1 was required for cGMP stimulation of *Vegfa* and *Vegfr1* mRNA expression in osteoblasts (113).

Ischemia-induced angiogenesis is severely impaired in soluble guanylate cyclase- or PKG1-deficient mice, suggesting a role of cGMP-elevating agents on angiogenesis (96, 102, 103). Consistent with these data, decreased capillary density in regenerating bone in *Prkg1* OB-KO mice compared to control litter mates was found, correlating with decreased *Vegfa* and *Vegfr1* mRNA expression by PKG1-deficient osteoblasts (113). Osteoblast-derived VEGF is critical in driving angiogenesis in healing long bones, and

plays a crucial role in the coupling of angiogenesis and osteogenesis (104, 105). The reduced *Vegfa/Vegfr1* expression in *Prkg1* OB-KO mice likely contributed to the decreased healing of bone defects.

Expression of BMP-2/4 and BMP receptor-2 is induced during fracture repair, and mice lacking the ability to produce BMP fail to heal fractures (106, 107). Conditional global BMP-2 and BMP-4 knockout mice display low turnover bone loss and impaired bone regeneration (110). In the described results, cGMP stimulated *Bmp-2/4* and *Bmpr-2* mRNA expression in POBs in a PKG1-dependent fashion, and *Bmp-2/4* mRNA and protein expression were reduced in bones and osteoblasts from *Prkg1* OB-KO mice. In addition to reduced BMP synthesis, evidence for impaired Smad-1/5/8 signaling downstream of the BMP receptor was found, with decreased Smad phosphorylation in BMP-2 treated PKG1-deficient osteoblasts, as well as in uninjured and regenerating bones from *Prkg1* OB-KO mice (113). These data are consistent with previous reports of cross-talk between cGMP/PKG1 and BMP receptor signaling, with PKG1 enhancing BMP receptor-2 phosphorylation of Smads, and stimulating Smad-dependent transcription via regulation of a nuclear co-factor (81). A novel mechanism whereby BMP signaling was upregulated by cGMP-elevating agents was identified.

I developed a surgical technique in the group of Dr. Pilz following Hu and Olsen, 2016 (66) analysing regenerated bone defects at post surgery day 10 by micro CT (µCT) and by histological examination (in cooperation with the µCT and Histocore facility). In the present study, PKG1 in osteoblastic cells was identified to be critical for angiogenesis/ osteogenesis coupling during repair of small bone defects. Multiple steps in the repair process require osteoblast-derived Prkg1. First, the results show a dramatic decrease in newly formed bone in the drilled hole for male osteoblast specific PKG1 knockout mice, as reflected in decreased bone parameters like BMD, TbN, TbSp, with the biggest effect on the bone volume revealed by µCT analysis. Second, after histological examination of the wound area, decreased collagen content, osteoblast and osteoclast number were found in regenerating bone. Third, these data demonstrate an important role of PKG1 in osteoblasts regulating capillary density, and BMP-dependent Smad phosphorylation in the regenerating bone.

Bone regeneration involves two mechanisms: the de novo formation of vessels (vasculargenesis) and the sprouting and growth of new vessels from pre-existing ones

(angiogenesis) (111). Neovascularization is important for recruitment of osteoblasts and osteoclasts and bone repair requires osteogenic cells to reach to the sites that need to be rebuilt. A failure of osteoblasts contributes to impaired fracture repair. The presence of blood vessels is absolutely required for bone formation (112). PKG1 in osteoblasts appears to be important for the attraction of new blood vessels into the wound. By using 3D imaging with Digital Volumetric Imaging (DVI) different osteoblast activity was documented by staining of newly formed bone, showing reduced volume of regenerating bone in the monocortical defect model in *Prkg1* OB-KO mice.

The NO/cGMP/PKG pathway mediates some of the anabolic effects of estrogens in osteoblasts leading me to hypothesize that cGMP elevating agents may have bone-protective effects (40). In fact, cinaciguat treatment enhanced bone regeneration in female control mice. It should be taken into consideration from the present study that the trend towards lower bone volume for the female Prkg1 osteoblast-specific knockout mice may be due to a variable estrogen cycle leading to variable cGMP production, and more variable regenerating bone volumes. This would be consistent with studies of Ramdani et al., 2018 reporting higher NO_x and cGMP serum concentrations in female mice compared to male mice. In summary, these data demonstrate that osteoblast-derived PKG1 plays a key role in angiogenesis and bone formation at bone repair sites.

The presented results in PKG1 osteoblast-specific knockout mice, using a stable fracture healing model, suggest that the positive effects of cGMP on primary ossification processes during bone regeneration are mediated by PKG1 via regulation of VEGF and BMP signaling. cGMP-elevating agents are in clinical use, including NO-generating nitrates, phosphodiesterase-5 inhibitors, and the stimulator of soluble guanylate cyclase, riociguat (113). The following studies indicate the enhancement of cGMP-elevating agents in fracture healing via primary and secondary ossification: (i) systemic inhibition of NO synthase reduces callus formation and bone regeneration in an open fracture model (reversable by local administration of an NO donor) (43), (ii) treatment with sildenafil increases intracellular cGMP concentrations, accelerates fracture healing and increases biomechanical strength in a mice femur fracture model (71) and (iii) mice with increased production of C-type natriuretic peptide show accelerated fracture healing in an open and stabilized femur fracture model (70). These agents could represent a novel treatment paradigm for patients with impaired fracture healing, especially in situations where

impaired healing is associated with reduced angiogenesis, such as in the elderly and in diabetic patients (68).

In future studies, modulation of PKG1 activity may be of particular interest to enhance the effects of BMPs on bone repair. In case of a relatively small defect, a single cinaciguat- or cGMP-loaded slow-release scaffold could be used to stimulate bone repair. In case of a larger defect, cGMP-elevating agents could be combined with BMP treatment. Currently, local drug delivery that enhances fracture healing in clinical trials includes BMP-2 and statins, which modulate VEGF expression in osteoblasts (66). The goal would be to replace tissue transplantation with implantation of constructs that stimulate endogenous regeneration and repair (112). There is an increased interest of acellular biomaterial-based delivery of pro-osteogenic drugs for bone regeneration (112). The relationship between growth factors, bone forming progenitor cells and scaffolds are important components of procedures to stimulate bone regeneration and should therefore be considered for treatment of osteoporotic and other fractures (69).

SUMMARY

Cyclic guanosine monophosphat (cGMP) mediates physiological effects of nitric oxide and natriuretic peptides on different processes, including bone formation. Osteoporotic bone loss, the most common metabolic bone disease affecting humans, is becoming major problem due to an ageing population, and osteoporotic fractures cause significant morbidity and mortality in the elderly. Novel therapies for osteoporosis and fracture healing are needed, and cGMP modulating substances could be a novel approach. cGMP activates three major downstream receptors in the cell: phosphodiesterases (PDEs) that hydrolyze cGMP, cyclic nucleotide-gated channels and cGMP-dependent protein kinases (protein kinase G, PKG1 and PKG2), which in turn regulate the function of downstream proteins by phosphorylation of serine/threonine residues. Using osteogenic cell models and knockout mice, we recently demonstrated involvement of PKG 2 in skeletal maintenance and the response of osteoblasts to mechanical loading. The role of PKG1 in skeletal maintenance and bone repair was studied by generating mice with osteoblast-specific knockout of type 1 PKG (*Prkg1* OB-KO). These mice have normal osteoblast and osteoclast numbers, and PKG1-deficient osteoblasts proliferate normally *in vitro*. Prkg1 OB-KO mice showed normal bone micro-architecture under basal conditions, even though decreased bone formation rates and osteoblastic marker gene expression. However, bone regeneration in a mono-cortical defect model was severely reduced in *Prkg1* OB-KO mice compared to control litter mates, and the knockout mice exhibit decreased capillary density and evidence of reduced BMP signaling in the region of the bone defect. PKG1 was required for cGMP-stimulated expression of these genes, and for BMP-induced Smad phosphorylation in osteoblasts, shown by primary osteoblasts and tibiae of Prkg1 OB-KO mice containing less transcripts encoding bone morphogenic protein (BMP) -2/4, vascular endothelial growth factor (VEGF)-a, and their receptors BMPR2 and VEGFR1. The results in Prkg1 OB-KO mice suggest that the positive effects of cGMP on bone regeneration are mediated by PKG1 via regulation of VEGF and BMP signaling. These agents could represent a novel treatment paradigm for patients with impaired fracture healing, especially in situations where impaired healing is associated with reduced angiogenesis.

REFERENCES

1. Kobayashi,T., and Kronenberg,H.M. 2014. Overview of skeletal development. Methods Mol. Biol. 1130:3-12.
2. Miep H.Helfrich, Stuart H. Ralston, 2012. Bone Research Protocols, Springer Link.
3. Dallas,S.L., Prideaux,M., and Bonewald,L.F. 2013. The osteocyte: an endocrine cell ... and more. Endocr. Rev. 34:658-690.
4. Kalyanaraman,H., Ramdani,G., and Pilz,R.B. 2016. Targeting NO signaling for the treatment of osteoporosis. Current Medicinal Chemistry 23:1-8.
5. Wimalawansa,S.J. 2010. Nitric oxide and bone. Ann. N. Y. Acad. Sci 1192:391-403.
6. Klein-Nulend,J., van Oers,R.F., Bakker,A.D., and Bacabac,R.G. 2014. Nitric oxide signaling in mechanical adaptation of bone. Osteoporos. Int. 25:1427-1437.
7. van't Hof,R.J., and Ralston,S.H. 2001. Nitric oxide and bone. Immunology 103:255-261.
8. Helfrich,M.H., Evans,D.E., Grabowski,P.S., Pollock,J.S., Ohshima,H., and Ralston,S.H. 1997. Expression of nitric oxide synthase isoforms in bone and bone cell cultures. J. Bone Miner. Res. 12:1108-1115.
9. Basso,N., and Heersche,J.N. 2006. Effects of hind limb unloading and reloading on nitric oxide synthase expression and apoptosis of osteocytes and chondrocytes. Bone 39:807-814.
10. Zheng,H., Yu,X., Collin-Osdoby,P., and Osdoby,P. 2006. RANKL stimulates inducible nitric-oxide synthase expression and nitric oxide production in developing osteoclasts. An autocrine negative feedback mechanism triggered by RANKL-induced interferon-beta via NF-kappaB that restrains osteoclastogenesis and bone resorption. J. Biol. Chem. 281:15809-15820.
11. Brandi,M.L., Hukkanen,M., Umeda,T., Moradi-Bidhendi,N., Bianchi,S., Gross,S.S., Polak,J.M., and MacIntyre,I. 1995. Bidirectional regulation of

osteoclast function by nitric oxide synthase isoforms. Proc. Natl. Acad. Sci. U. S. A 92:2954-2958.

12. Rangaswami,H., Marathe,N., Zhuang,S., Chen,Y., Yeh,J.C., Frangos,J.A., Boss,G.R., and Pilz,R.B. 2009. Type II cGMP-dependent protein kinase mediates osteoblast mechanotransduction. J. Biol. Chem. 284:14796-14808.

13. Russell,K.S., Haynes,M.P., Sinha,D., Clerisme,E., and Bender,J.R. 2000. Human vascular endothelial cells contain membrane binding sites for estradiol, which mediate rapid intracellular signaling. Proc. Natl. Acad. Sci. U. S. A 97:5930-5935.

14. O'Shaughnessy,M.C., Polak,J.M., Afzal,F., Hukkanen,M.V., Huang,P., MacIntyre,I., and Buttery,L.D. 2000. Nitric oxide mediates 17beta-estradiol-stimulated human and rodent osteoblast proliferation and differentiation. Biochem. Biophys. Res. Commun. 277:604-610.

15. Marathe,N., Rangaswami,H., Zhuang,S., Boss,G.R., and Pilz,R.B. 2012. Pro-survival Effects of 17beta-Estradiol on Osteocytes Are Mediated by Nitric Oxide/cGMP via Differential Actions of cGMP-dependent Protein Kinases I and II. J. Biol. Chem. 287:978-988.

16. Kalyanaraman,H., Schwappacher,R., Joshua,J., Zhuang,S., Scott,B.T., Klos,M., Casteel,D.E., Frangos,J.A., Dillmann,W., Boss,G.R. et al 2014. Nongenomic thyroid hormone signaling occurs through a plasma membrane-localized receptor. Sci. Signal. 7:ra48.

17. van't Hof,R.J., Macphee,J., Libouban,H., Helfrich,M.H., and Ralston,S.H. 2004. Regulation of bone mass and bone turnover by neuronal nitric oxide synthase. Endocrinology 145:5068-5074.

18. Jung,J.Y., Lin,A.C., Ramos,L.M., Faddis,B.T., and Chole,R.A. 2003. Nitric oxide synthase I mediates osteoclast activity in vitro and in vivo. J. Cell Biochem. 89:613-621.

19. Watanuki,M., Sakai,A., Sakata,T., Tsurukami,H., Miwa,M., Uchida,Y., Watanabe,K., Ikeda,K., and Nakamura,T. 2002. Role of inducible nitric oxide synthase in skeletal adaptation to acute increases in mechanical loading. J. Bone Miner. Res. 17:1015-1025.

20. Yan,Q., Feng,Q., and Beier,F. 2010. Endothelial nitric oxide synthase deficiency in mice results in reduced chondrocyte proliferation and endochondral bone growth. Arthritis Rheum. 62:2013-2022.

21. Aguirre,J., Buttery,L., O'Shaughnessy,M., Afzal,F., de Marticorena,I.F., Hukkanen,M., Huang,P., Maclntyre,I., and Polak,J. 2001. Endothelial nitric oxide synthase gene-deficient mice demonstrate marked retardation in postnatal bone formation, reduced bone volume, and defects in osteoblast maturation and activity. Am. J. Pathol. 158:247-257.

22. Kalyanaraman,H., Ramdani,G., Joshua,J., Schall,N., Boss,G.R., Cory,E., Sah,R.L., Casteel,D.E., and Pilz,R.B. 2017. A Novel, Direct NO Donor Regulates Osteoblast and Osteoclast Functions and Increases Bone Mass in Ovariectomized Mice. J. Bone Miner. Res. 32:46-59.

23. Otsuka,E., Hirano,K., Matsushita,S., Inoue,A., Hirose,S., Yamaguchi,A., and Hagiwara,H. 1998. Effects of nitric oxide from exogenous nitric oxide donors on osteoblastic metabolism. Eur. J. Pharmacol. 349:345-350.

24. Dong,S.S., Williams,J.P., Jordan,S.E., Cornwell,T., and Blair,H.C. 1999. Nitric oxide regulation of cGMP production in osteoclasts. J. Cell Biochem. 73:478-487.

25. Hagiwara,H., Inoue,A., Yamaguchi,A., Yokose,S., Furuya,M., Tanaka,S., and Hirose,S. 1996. cGMP produced in response to ANP and CNP regulates proliferation and differentiation of osteoblastic cells. Am. J. Physiol. 270:C1311-C1318.

26. Miura,K., Namba,N., Fujiwara,M., Ohata,Y., Ishida,H., Kitaoka,T., Kubota,T., Hirai,H., Higuchi,C., Tsumaki,N. et al 2012. An overgrowth disorder associated with excessive production of cGMP due to a gain-of-function mutation of the natriuretic peptide receptor 2 gene. PLoS. ONE. 7:e42180.

27. Bocciardi,R., Giorda,R., Buttgereit,J., Gimelli,S., Divizia,M.T., Beri,S., Garofalo,S., Tavella,S., Lerone,M., Zuffardi,O. et al 2007. Overexpression of the C-type natriuretic peptide (CNP) is associated with overgrowth and bone anomalies in an individual with balanced t(2;7) translocation. Hum. Mutat. 28:724-731.

28. Francis,S.H., Busch,J.L., Corbin,J.D., and Sibley,D. 2010. cGMP-dependent protein kinases and cGMP phosphodiesterases in nitric oxide and cGMP action. Pharmacol. Rev. 62:525-563.

29. Rangaswami,H., Schwappacher,R., Marathe,N., Zhuang,S., Casteel,D.E., Haas,B., Chen,Y., Pfeifer,A., Kato,H., Shattil,S. et al 2010. Cyclic GMP and protein kinase G control a Src-containing mechanosome in osteoblasts. Sci. Signal. 3:ra91.

30. Yaroslavskiy,B.B., Zhang,Y., Kalla,S.E., Garcia,P., V, Sharrow,A.C., Li,Y., Zaidi,M., Wu,C., and Blair,H.C. 2005. NO-dependent osteoclast motility: reliance on cGMP-dependent protein kinase I and VASP. J. Cell Sci. 118:5479-5487.

31. Yaroslavskiy,B.B., Turkova,I., Wang,Y., Robinson,L.J., and Blair,H.C. 2010. Functional osteoclast attachment requires inositol-1,4,5-trisphosphate receptor-associated cGMP-dependent kinase substrate. Lab Invest 90:1533-1542.

32. Pfeifer,A., Klatt,P., Massberg,S., Ny,L., Sausbier,M., Hirneib,C., Wang,G.-X., Korth,M., Aszòdi,A., Andersson,K.-E. et al 1998. Defective smooth muscle regulation in cGMP kinase I-deficient mice. EMBO J. 17:3045-3051.

33. Weber,S., Bernhard,D., Lukowski,R., Weinmeister,P., Worner,R., Wegener,J.W., Valtcheva,N., Feil,S., Schlossmann,J., Hofmann,F. et al 2007. Rescue of cGMP Kinase I Knockout Mice by Smooth Muscle Specific Expression of Either Isozyme. Circ. Res.

34. Pfeifer,A., Aszòdi,A., Seidler,U., Ruth,P., Hofmann,F., and Fässler,R. 1996. Intestinal secretory defects and dwarfism in mice lacking cGMP-dependent protein kinase II. Science 274:2082-2086.

35. Bonnet,C., Andrieux,J., Beri-Dexheimer,M., Leheup,B., Boute,O., Manouvrier,S., Delobel,B., Copin,H., Receveur,A., Mathieu,M. et al 2010. Microdeletion at chromosome 4q21 defines a new emerging syndrome with marked growth restriction, mental retardation and absent or severely delayed speech. J. Med. Genet. 47:377-384.

36. Mancini,L., Moradi-Bidhendi,N., Becherini,L., Martineti,V., and MacIntyre,I. 2000. The biphasic effects of nitric oxide in primary rat osteoblasts are cGMP dependent. Biochem. Biophys. Res. Commun. 274:477-481.

37. Rangaswami,H., Schwappacher,R., Tran,T., Chan,G.C., Zhuang,S., Boss,G.R., and Pilz,R.B. 2012. Protein Kinase G and Focal Adhesion Kinase Converge on Src/Akt/beta-Catenin Signaling Module in Osteoblast Mechanotransduction. J. Biol. Chem. 287:21509-21519.

38. Hikiji,H., Shin,W.S., Oida,S., Takato,T., Koizumi,T., and Toyo-oka,T. 1997. Direct action of nitric oxide on osteoblastic differentiation. FEBS Lett. 410:238-242.

39. Lin,I.C., Smartt,J.M., Jr., Nah,H.D., Ischiropoulos,H., and Kirschner,R.E. 2008. Nitric oxide stimulates proliferation and differentiation of fetal calvarial osteoblasts and dural cells. Plast. Reconstr. Surg. 121:1554-1566.

40. Joshua,J., Schwaerzer,G.K., Kalyanaraman,H., Cory,E., Sah,R.S., Li,M., Vaida,F., Boss,G.R., and Pilz,R.B. 2014. Soluble guanylate cyclase as a novel treatment target for osteoporosis. Endocrinology 155:4720-4730.

41. Turner,C.H., Owan,I., Jacob,D.S., McClintock,R., and Peacock,M. 1997. Effects of nitric oxide synthase inhibitors on bone formation in rats. Bone 21:487-490.

42. Homer,B.L., Morton,D., Bagi,C.M., Warneke,J.A., Andresen,C.J., Whiteley,L.O., Morris,D.L., and Tones,M.A. 2015. Oral administration of soluble guanylate cyclase agonists to rats results in osteoclastic bone resorption and remodeling with new bone formation in the appendicular and axial skeleton. Toxicol. Pathol. 43:411-423.

43. Diwan,A.D., Wang,M.X., Jang,D., Zhu,W., and Murrell,G.A. 2000. Nitric oxide modulates fracture healing. J. Bone Miner. Res. 15:342-351.

44. Khosla,S., Melton,L.J., III, and Riggs,B.L. 2011. The unitary model for estrogen deficiency and the pathogenesis of osteoporosis: is a revision needed? J. Bone Miner. Res. 26:441-451.

45. Samuels,A., Perry,M.J., Gibson,R.L., Colley,S., and Tobias,J.H. 2001. Role of endothelial nitric oxide synthase in estrogen-induced osteogenesis. Bone 29:24-29.

46. Hukkanen,M., Platts,L.A., Lawes,T., Girgis,S.I., Konttinen,Y.T., Goodship,A.E., MacIntyre,I., and Polak,J.M. 2003. Effect of nitric oxide donor nitroglycerin on

bone mineral density in a rat model of estrogen deficiency-induced osteopenia. Bone 32:142-149.

47. Thomas,G.R., DiFabio,J.M., Gori,T., and Parker,J.D. 2007. Once daily therapy with isosorbide-5-mononitrate causes endothelial dysfunction in humans: evidence of a free-radical-mediated mechanism. J. Am. Coll. Cardiol. 49:1289-1295.

48. Parker,J.D. 2004. Nitrate tolerance, oxidative stress, and mitochondrial function: another worrisome chapter on the effects of organic nitrates. J. Clin. Invest 113:352-354.

49. Broderick,K.E., Alvarez,L., Balasubramanian,M., Belke,D.D., Makino,A., Chan,A., Woods,V.L., Jr., Dillmann,W.H., Sharma,V.S., Pilz,R.B. et al 2007. Nitrosyl-cobinamide, a new and direct nitric oxide-releasing drug effective in vivo. Exp. Biol. Med. (Maywood.) 232:1432-1440.

50. Hayashi,T., Ito,I., Kano,H., Endo,H., and Iguchi,A. 2000. Estriol (E3) replacement improves endothelial function and bone mineral density in very elderly women. J. Gerontol. A Biol. Sci. Med. Sci. 55:B183-B190.

51. Rosselli,M., Imthurn,B., Keller,P.J., Jackson,E.K., and Dubey,R.K. 1995. Circulating nitric oxide (nitrite/nitrate) levels in postmenopausal women substituted with 17 beta-estradiol and norethisterone acetate. A two-year follow-up study. Hypertension 25:848-853.

52. Wimalawansa,S.J. 2000. Nitroglycerin therapy is as efficacious as standard estrogen replacement therapy (Premarin) in prevention of oophorectomy-induced bone loss: a human pilot clinical study. J. Bone Miner. Res. 15:2240-2244.

53. Nabhan,A.F., and Rabie,N.H. 2008. Isosorbide mononitrate versus alendronate for postmenopausal osteoporosis. Int. J. Gynaecol. Obstet. 103:213-216.

54. Manolagas,S.C. 2010. From estrogen-centric to aging and oxidative stress: a revised perspective of the pathogenesis of osteoporosis. Endocr. Rev. 31:266-300.

55. Schmidt,H.H., Schmidt,P.M., and Stasch,J.P. 2009. NO- and haem-independent soluble guanylate cyclase activators. Handb. Exp. Pharmacol.309-339.

56. Kalyanaraman,H., Schwaerzer,G., Ramdani,G., Castillo,F., Scott,B.T., Dillmann,W., Sah,R.L., Casteel,D.E., and Pilz,R.B. 2018. Protein Kinase G

Activation Reverses Oxidative Stress and Restores Osteoblast Function and Bone Formation in Male Mice With Type 1 Diabetes. Diabetes 2018 Apr;67(4):607-623.

57. Singh,M., Singh,P., Singh,S., Juneja,P.K., and Kaur,T. 2014. A susceptibility haplotype within the endothelial nitric oxide synthase gene influences bone mineral density in hypertensive women. J. Bone Miner. Metab 32:580-587.

58. Cho,K., Demissie,S., Dupuis,J., Cupples,L.A., Kathiresan,S., Beck,T.J., Karasik,D., and Kiel,D.P. 2008. Polymorphisms in the endothelial nitric oxide synthase gene and bone density/ultrasound and geometry in humans. Bone 42:53-60.

59. Bartels,C.F., Bukulmez,H., Padayatti,P., Rhee,D.K., van Ravenswaaij-Arts,C., Pauli,R.M., Mundlos,S., Chitayat,D., Shih,L.Y., Al-Gazali,L.I. et al 2004. Mutations in the transmembrane natriuretic peptide receptor NPR-B impair skeletal growth and cause acromesomelic dysplasia, type Maroteaux. Am. J. Hum. Genet. 75:27-34.

60. Wang,W., Song,M.H., Miura,K., Fujiwara,M., Nawa,N., Ohata,Y., Kitaoka,T., Kubota,T., Namba,N., Jin,D.K. et al 2016. Acromesomelic dysplasia, type maroteaux caused by novel loss-of-function mutations of the NPR2 gene: Three case reports. Am. J. Med Genet. A 170A:426-434.

61. Lipska,B.S., Brzeskwiniewicz,M., Wierzba,J., Morzuchi,L., Piotrowski,A., and Limon,J. 2011. 8.6Mb interstitial deletion of chromosome 4q13.3q21.23 in a boy with cognitive impairment, short stature, hearing loss, skeletal abnormalities and facial dysmorphism. Genet. Couns. 22:353-363.

62. Miura,K., Kim,O.H., Lee,H.R., Namba,N., Michigami,T., Yoo,W.J., Choi,I.H., Ozono,K., and Cho,T.J. 2014. Overgrowth syndrome associated with a gain-of-function mutation of the natriuretic peptide receptor 2 (NPR2) gene. Am. J. Med Genet. A 164A:156-163.

63. Fazzalari, N. L. (2011) Bone fracture and bone fracture repair. Osteoporos Int 22, 2003-2006.

64. Gerstenfeld LC, Alkhiary YM, Krall EA, Nicholls FH, Stapleton SN, Fitch JL et al (2006) Three-dimensional reconstruction of fracture callus morphogenesis. J Histochem Cytochem 54:1215–1228.

65. Jiao H, Xiao E, Graves DT. Diabetes and its effect on bone and fracture healing. Cur Osteoporos Rep 2015;13:327-35.

66. Hu K, Olsen BR. Osteoblast-derived VEGF regulates osteoblast differentiation and bone formation during bone repair. J Clin Invest 2016;126:509-26.

67. Cho TJ, Gerstenfeld LC, Einhorn TA (2002) Differential temporal expression of members of the transforming growth factor beta superfamily during murine fracture healing. J Bone Miner Res 17:513–520.

68. Lim JC, Ko K, Mattos M, Fang M, Zhang C, Feinberg D, et al. TNFa contributes to diabetes impaired angiogenesis in fracture healing. Bone 2017;99:26-38.

69. Hu K, Olsen BR. The roles of vascular endothelial growth factor in bone repair and regeneration. Bone. 2016 Oct;91:30-8.

70. Kondo E, Yasoda A, Fujii T, Nakao K, Yamashita Y, Ueda-Sakane Y, Kanamoto N, Miura M, Arai H, Mukoyama M, Inagaki N, Nakao K. Increased bone turnover and possible accelerated fracture healing in a murine model with an increased circulating C-type natriuretic peptide. Endocrinology 2015;156:2518-29.

71. Histing, T., Marciniak, K., Scheuer, C., Garcia, P., Holstein, J. H., Klein, M., Matthys, R., Pohlemann, T., and Menger, M. D. (2011) Sildenafil accelerates fracture healing in mice. J. Orthop. Res 29, 867-873.

72. Haas, B., Mayer, P., Jennissen, K., Scholz, D., Berriel, D. M., Bloch, W., Herzig, S., Fassler, R., and Pfeifer, A. (2009) Protein kinase G controls brown fat cell differentiation and mitochondrial biogenesis. Sci. Signal 2, ra78.

73. He, Y. X., Zhang, G., Pan, X. H., Liu, Z., Zheng, L. Z., Chan, C. W., Lee, K. M., Cao, Y. P., Li, G., Wei, L., Hung, L. K., Leung, K. S., and Qin, L. (2011) Impaired bone healing pattern in mice with ovariectomy-induced osteoporosis: A drill-hole defect model. Bone 48, 1388-1400.

74. Dempster DW, Compston JE, Drezner MK, Glorieux FH, Kanis JA, Malluche H, et al. Standardized nomenclature, symbols, and units for bone histomorphometry: a 2012 update of the report of the ASBMR Histomorphometry Nomenclature Committee. J Bone Miner Res. 2013;28(1):2-17.

75. Porter A, Irwin R, Miller J, Horan DJ, Robling AG, and McCabe LR. Quick and inexpensive paraffin-embedding method for dynamic bone formation analyses. Sci Rep. 2017;7:42505.

76. Kyle D. Jadin, Won C. Bae, Barbara L. Schumacher, and Robert L. Sah. 3-D Imaging of Chondrocytes in Articular Cartilage: Growth-Associated Changes in Cell Organization. Biomaterials. 2007 Jan; 28(2): 230–239.

77. Wook-Young Baek, Min-A Lee, Ji Won Jung, Shin-Yoon Kim, Haruhiko Akiyama, Benoit de Crombrugghe, and Jung-Eun Kim. Positive regulation of adult bone formation by osteoblast-specific transcription factor osterix. JBMR Volume 24, Number 6, 2009.

78. https://www.ncbi.nlm.nih.gov/gene/19091

79. Kalajzic,I., Kalajzic,Z., Kaliterna,M., Gronowicz,G., Clark,S.H., Lichtler,A.C., and Rowe,D. 2002. Use of type I collagen green fluorescent protein transgenes to identify subpopulations of cells at different stages of the osteoblast lineage. J. Bone Miner. Res. 17:15- 25.

80. Dacquin,R., Starbuck,M., Schinke,T., and Karsenty,G. 2002. Mouse a1(I)-collagen promoter is the best known promoter to drive efficient Cre recombinase expression in osteoblast. Dev. Dyn. 224:245-251.

81. Schwappacher, R., Weiske, J., Heining, E., Ezerski, V., Marom, B., Henis, Y. I., Huber, O., and Knaus, P. (2009) Novel crosstalk to BMP signalling: cGMP-dependent kinase I modulates BMP receptor and Smad activity. EMBO J 28, 1537-1550.

82. Luu HH, Song WX, Luo X et al. Distinct roles of bone morphogenetic proteins in osteogenic differentiation of mesenchymal stem cells. J Orthop Res 2007; 25: 665–677.

83. Razzouk S, Sarkis R. BMP-2: biological challenges to its clinical use. N Y State Dent J 2012; 78: 37–39.

84. Reddi, A. H. 1998. Role of morphogenetic proteins in skeletal tissue engineering and regeneration. Nat. Biotechnol. 16:247–252.

85. Brandi ML, Collin-Osdoby P. Vascular biology and the skeleton. J Bone Miner Res. 2006; 21:183–92.

86. Eghbali-Fatourechi GZ, Lamsam J, Fraser D, Nagel D, Riggs BL, Khosla S. Circulating osteoblast-lineage cells in humans.[see comment]. N Engl J Med. 2005;352:1959–66.

87. Kassem M, Risteli L, Mosekilde L, Melsen F, Eriksen EF. Formation of osteoblast-like cells from human mononuclear bone marrow cultures. APMIS. 1991;99:269–74.

88. Majidinia M, Yousefi B. The roles of signaling pathways in bone repair and regeneration. J Cell Physiol. 2018 Apr;233(4):2937-2948.

89. Ramdani G, Schall N, Kalyanaraman H, Wahwah N, Moheize S, Lee JJ, et al. cGMP-dependent protein kinase-2 regulates bone mass and prevents diabetic bone loss. J Endocrinol. 2018;238(3):203-19.

90. Kamata H, Honda S, Maeda S, Chang L, Hirata H, Karin M. Reactive oxygen species promote TNFalpha-induced death and sustained JNK activation by inhibiting MAP kinase phosphatases.Cell. 2005 Mar 11;120(5):649-61.

91. Yamaguchi A, Ishizuya T, Kintou N, Wada Y, Katagiri T, Wozney JM, Rosen V, Yoshiki S. Effects of BMP-2, BMP-4, and BMP-6 on osteoblastic differentiation of bone marrow-derived stromal cell lines, ST2 and MC3T3-G2/PA6. Biochem Biophys Res Commun. 1996 Mar 18;220(2):366-71.

92. Joshua J, Kalyanaraman H, Marathe N, Pilz RB. Nitric oxide as a mediator of estrogen effects in osteocytes. Vitam Horm. 2014;96:247-63.

93. Cochrane RL, Clark SH, Harris A, Kream BE. Rearrangement of a conditional allele regardless of inheritance of a Cre recombinase transgene. Genesis. 2007;45:17–20.

94. Deckers MM, van Bezooijen RL, van der Horst G, Hoogendam J, van Der Bent C, Papapoulos SE, Löwik CW. Bone morphogenic protein stimulate angiogenesis through osteoblast-derived vascular endothelial growth factor. Endocrinology. 2002 Apr;143(4):1545-53.

95. Koika V, Zhou Z, Vasileiadis I, Roussos C, Finetti F, Monti M, Morbidelli L, Papapetropoulos A. PKG-I inhibition attenuates vascular endothelial growth factor-stimulated angiogenesis. Vascul Pharmacol. 2010 Nov-Dec;53(5-6):215-22.

96. Aicher A, Heeschen C, Feil S, Hofmann F, Mendelsohn ME, Feil R, Dimmeler S. cGMP-dependent protein kinase I is crucial for angiogenesis and postnatal vasculogenesis. PLoS One. 2009;4(3):e4879.

97. Sun J, Li J, Li C, and Yu Y. Role of bone morphogenetic protein-2 in osteogenic differentiation of mesenchymal stem cells. Mol Med Rep. 2015 Sep; 12(3): 4230–4237.

98. Lissenberg-Thunnissen SN1, de Gorter DJ, Sier CF, Schipper IB. Use and efficacy of bone morphogenetic proteins in fracture healing. Int Orthop. 2011 Sep;35(9):1271-80.

99. Ziche, M., and Morbidelli, L. (2000) Nitric oxide and angiogenesis. J. Neurooncol 50, 139-148.

100. Jozkowicz, A., Dulak, J., Nigisch, A., Funovics, P., Weigel, G., Polterauer, P., Huk, I., and Malinski, T. (2004) Involvement of nitric oxide in angiogenic activities of vascular endothelial growth factor isoforms. Growth Factors 22, 19-28.

101. Kawasaki, K., Smith, R. S., Jr., Hsieh, C. M., Sun, J., Chao, J., and Liao, J. K. (2003) Activation of the phosphatidylinositol 3-kinase/protein kinase Akt pathway mediates nitric oxide-induced endothelial cell migration and angiogenesis. Mol. Cell Biol 23, 5726-5737.

102. Sahara, M., Sata, M., Morita, T., Nakajima, T., Hirata, Y., and Nagai, R. (2010) A phosphodiesterase-5 inhibitor vardenafil enhances angiogenesis through a protein kinase G-dependent hypoxia-inducible factor-1/vascular endothelial growth factor pathway. Arterioscler Thromb Vasc Biol 30, 1315-1324.

103. Bettaga, N., Jager, R., Dunnes, S., Groneberg, D., and Friebe, A. (2015) Cell-specific impact of nitric oxide-dependent guanylyl cyclase on arteriogenesis and angiogenesis in mice. Angiogenesis 18, 245-254.

104. Hu, K., and Olsen, B. R. (2017) Vascular endothelial growth factor control mechanisms in skeletal growth and repair. Dev Dyn 246, 227-234.

105. Maes, C., and Clemens, T. L. (2014) Angiogenic-osteogenic coupling: the endothelial perspective. Bonekey Rep 3, 578.

106. Onishi, T., Ishidou, Y., Nagamine, T., Yone, K., Imamura, T., Kato, M., Sampath, T. K., ten Dijke, P., and Sakou, T. (1998) Distinct and overlapping patterns of localization of bone morphogenetic protein (BMP) family members and a BMP type II receptor during fracture healing in rats. Bone 22, 605-612.

107. Tsuji, K., Bandyopadhyay, A., Harfe, B. D., Cox, K., Kakar, S., Gerstenfeld, L., Einhorn, T., Tabin, C. J., and Rosen, V. (2006) BMP2 activity, although dispensable for bone formation, is required for the initiation of fracture healing. Nat Genet 38, 1424-1429.

108. Dai, J., Li, L., Jiang, C., Wang, C., Chen, H., and Chai, Y. (2015) Bone Morphogenetic Protein for the Healing of Tibial Fracture: A Meta-Analysis of Randomized Controlled Trials. PLoS One 10, e0141670.

109. Peng, H., Usas, A., Olshanski, A., Ho, A. M., Gearhart, B., Cooper, G. M., and Huard, J. (2005) VEGF improves, whereas sFlt1 inhibits, BMP2-induced bone formation and bone healing through modulation of angiogenesis. J Bone Miner Res 20, 2017-2027.

110. Khan MP, Khan K, Yadav PS, Singh AK, Nag A, Prasahar P, et al. BMP signaling is required for adult skeletal homeostasis and mediates bone anabolic action of parathyroid hormone. Bone. 2016;92:132-44.

111. Carmeliet P, Jain RK. Molecular mechanisms and clinical applications of angiogenesis. Nature. 2011 May 19;473(7347):298-307.

112. Sarita R. Shah, Caroline A. Werlang, F. Kurtis Kasper, and Antonios G. Mikos. Novel Applications of Statins for bone regeneration. Natl Sci Rev. 2015 Mar 1; 2(1): 85–99.

113. Schall N, Garcia JJ, Kalyanaraman H, Pal China S, Lee JJ, Sah RL, Pfeifer A, Pilz RB. Protein Kinase G1 regulates bone regeneration and rescues diabetic fracture healing. JCI Insight, 2020 May 07.

114. Hadjiargyrou M, and O'Keefe RJ. The convergence of fracture repair and stem cells: interplay of genes, aging, environmental factors and disease. J Bone Miner Res. 2014;29:2307-22.

115. Kim J-B, Leucht P, Lam K, Luppen C, Berge DT, Nusse R, et al. Bone regeneration is regulated by Wnt signaling. J Bone Miner Res. 2007;22:1913-22.

116. Dulak J, Jozkowicz A, Dembinska-Kiec A, Guevara I, Zdzienicka A, Zmudzinska-Grochot D, et al. Nitric oxide induces the synthesis of vascular endothelial growth factor by rat vascular smooth muscle cells. Arterioscler Thromb Vasc Biol. 2000;20(3):659-66.

117. Kalyanaraman H, Schall N, Pilz RB. Nitric oxide and cyclic GMP functions in bone. Nitric Oxide. 2018 Mar 14; 76: 62-70.

APPENDIX

LIST OF FIGURES

INTRODUCTION

MATERIALS AND METHODS

RESULTS

LIST OF TABLES

Table 1: Primers Used for Quantitative RT-PCR (modified after Schall et al. 2020, 113)

All primer pairs were tested with serially-diluted cDNAs and were intron-spanning (except the primers for 18S).

Abbrev.	Gene Name	Sense Primer (5'-3')	Anti-sense Primer (5'-3')
18S	18s Ribosomal RNA	GATCCATTGGAGG GCAAGTCT	CCAAGATCCAACT ACGAGCTTTTT
hprt	Hypoxanthine phosphoribosyl transferase	CCAGACAAGTTTG TTGTTGGAT	GCTTTGTATTTGG CTTTTCCA
alpl	Alkaline Phosphatase	TCAGGGCAATGAG GTCACATC	CACAATGCCCACG GACTTC
bglap	Osteocalcin	GAGGACCATCTTT CTGCTCAC	CCAAGGTAGCGCC GGAGTCTG
spp1	Osteopontin	CCAGGTTTCTGAT GAACAGTATCC	ACTTGACTCATGG CTGCCCTTT
col1a1	Collagen, type I, alpha 1	CTGCTGGCAAAGA TGGAGA	ACCAGGAAGACCC TGGAATC
runX2	Runt related Transcription Factor 2	GACAGAAGCTTGA TGACTCTAAACC	TCTGTAATCTGAC TCTGTCCTTGT

Abbrev.	Gene Name	Sense Primer (5'-3')	Anti-sense Primer (5'-3')
ctnnb1	β-Catenin	GACTCACGCAGTG AAGAATG	GCTGTAGCAGGTT CACTAGA
lrp5	LDL Receptor-related Protein 5	ACTCACGGGTGTC AAAGAGG	AGGGTAGTCGAGG CCAAACT
tnfsf11 *(RANKL)*	Receptor activator of nuclear factor kappa-B ligand	CAGCCATTTGCAC ACCTCAC	GTCTGTAGGTACG CTTCCCG
tnfrsf11b *(OPG)*	Osteoprotegerin	ACAGTTTGCCTGG GACCAAA	CAGGCTCTCCATC AAGGCAA
prkg1	Protein Kinase G 1 (exon 1/2)	CCTACAGGTCCTT CCACGAC	GATGATGCAGCTG TCCTTGC
prkg2	Protein Kinase G 2 (exon 3/4)	AGCTACGTCATTA AGCAGGG	TAGCCAGTTCCCC AAACGTG
bmp2	Bone Morphogenetic Protein 2	GCTAGATCTGTAC CGCAGGC	CTCCACGGCTTCT TCGTGAT
bmp4	Bone Morphogenetic Protein 4	CATCACGAAGAAC ATCTGGAGAAC	GGAGATCACCTCA TTCTCTGGG
bmpr1a	Bone morphogenetic protein receptor Type-1a	AGGTTGGTAAAGG CCGCTAT	CTGAGTCCAGGAA CCAGTGC

Abbrev.	Gene Name	Sense Primer (5'-3')	Anti-sense Primer (5'-3')
bmpr2	Bone morphogenetic protein receptor Type-2	AACTTTCCACCCC CTGACAC	TGTTCATGCTGTG AAGACCC
vegfa	Vascular Endothelial Growth Factor A	GACCCTGGCTTTA CTGCTGTA	GTGAGGTTTGATC CGCATGAT
vegfr1	Vascular endothelial growth factor receptor Type1	CGTTCCAGTCTTTC AACACC	CAGGCGAGCCATC TTTTAAC

Table 2: Antibody Sources (modified after Schall et al. 2020, 113)

Antibody	Company	Cat. #
ß-Actin (C-4) antibody-HRP-conjugate	Santa Cruz Biotechnology	sc-47778
Alpha-Tubulin	Santa Cruz Biotechnology	sc-8035
BMP-2/4	Santa Cruz Biotechnology	Sc-137087
CD31 (PECAM1)	Cell Signaling Technology	#77699
Cleaved Caspase-3	Cell Signaling Technology	#9664
Phospho-Smad 1/5/8 (Ser463/465)	Cell Signaling Technology	#9511

Antibody	Company	Cat. #
SAPK/ JNK (pThr183/ pTyr185)	Cell Signaling Technology	#9251
PKG-1 (C8A4)	Cell Signaling Technology	#3248
PKG-2	Invitrogen	PA5-15223

LIST OF ABBREVIATIONS

µA	micro ampere
µCT	micro-computed tomography
Akt	proteinkinase B
B.Ar	cross-sectional cortical bone area
B.Ar./T.Ar	cortical bone area fraction
BAD	Bcl-2-Antagonist of Cell Death
BFR	bone formation rate
BMD	bone mineral density
BMP	bone morphogenic protein
BMSC	bone marrow stromal cell
BrdU	bromodeoxyuridine
BV/TV	bone volume fraction
CD-31	cluster of differentiation 31
cDNA	complementary DNA
CNP	C-type natriuretic peptide
Col1a1-Cre	Collagen type 1- Cre recombinase
Cs.Th.	cross-sectional bone thickness
DMEM	Dulbecco's Modified Eagle's Medium
DVI	Digital Volumetric Imaging
EDTA	Ethylenediamine tetraacetic acid
Erk	extracellular receptor kinase
FBS	fetal bovine serum

FDA	Food Drug Administration
FITC	Fluorescein isothiocyanate
GC-B	guanylyl cyclase-B
GSK	glycogen synthase kinase
IRAG	inositol-1,4,5-triphosphate receptor-associated protein
JCI	Journal of Clinical Investigation
kVp	kilo volt
MAR	mineral apposition rate
MC3T3-E1	osteoblast precursor cell line derived from Mus musculus (mouse) calvaria
M-CSF	macrophage colony-stimulating factor
mPOB	murine primary osteoblast
mRNA	messenger ribonucleic acid
NBT	Nitro blue tetrazolium chloride
NO	nitric oxide
NO-Cbi	nitrosyl-cobinamide
NOS	NO-synthase
OB	osteoblast
OC	osteoclast
OPG	osteoprotegerin
OVX	ovariectomy
PKG	cGMP-dependent protein kinase
Prkg fl/fl	floxed
Prkg1 OB-KO	Protein kinase G1 osteoblast specific knockout

RANKL	receptor of activated nuclear factor-KB ligand
RT-qPCR	real-time quantitative polymerase chain reaction
SAPK/JNK	Stress-activated protein kinase/c-Jun NH(2)-terminal kinase
sGC	soluble guanylyl cyclase
Src	tyrosinkinase
T.Ar.	cross-sectional tissue area
Tb.N.	Trabecular number
Tb.Sp.	Trabecular spacing
Tb.Th.	Trabecular thickness
TMD	tissue mineral density
VASP	vasodilator-stimulated protein
VEGF	vascular endothelial growth factor
VOI	volume of interest

SCIENTIFIC CONTRIBUTION

Publications in scientific journals

1. Schall N, Garcia J, Kalyanaraman H, Pal China S, Lee JJ, Sah RL, Pfeifer A, Pilz RB.
   Protein Kinase G1 regulates bone regeneration and rescues diabetic fracture healing.
   JCI Insight; 2020 May 07. DOI: 10.1172/jci.insight.135355 .
   Impact Factor: 6.01

2. Ramdani G, Schall N, Kalyanaraman H, Wahwah N, Mohaize S, Lee JJ, Sah RL, Pfeifer A, Casteel DE, Pilz RB.
   cGMP-dependent protein kinase-2 regulates bone mass and prevents diabetic bone loss.
   J Endocrinol. 2018 Jun 18. DOI: 10.1530/JOE-18-0286.
   Impact Factor: 4.0

3. Kalyanaraman H, Schall N, Pilz RB.
   Nitric oxide and cyclic GMP functions in bone.
   Nitric Oxide. 2018 Mar 14; 76:62-70. DOI: 10.1016/j.niox.2018.03.007.
   Impact Factor: 4.18

4. Kalyanaraman H, Ramdani G, Joshua J, Schall N, Boss GR, Cory E, Sah RL, Casteel DE, Pilz RB.
   A Novel, Direct NO Donor Regulates Osteoblast and Osteoclast Functions and Increases Bone Mass in Ovariectomized Mice.
   J Bone Miner Res. 2017 Jan; 32(1):46-59. DOI: 10.1002/jbmr.2909.
   Impact Factor: 6.28